CHARACTERIZING MEMBRANE RECEPTOR SIGNALING:

NEW ROLES FOR ELECTROSTATIC RESIDUES IN EGFR REGULATION AND ACTIN IN FcεRI SIGNALING

A Thesis

Presented to the Faculty of the Graduate School

of Cornell University

In Partial Fulfillment of the Requirements for the Degree of

Doctor of Philosophy

by

Jordan David Mohr

December 2019

CHARACTERIZING MEMBRANE RECEPTOR SIGNALING: NEW ROLES FOR ELECTROSTATIC RESIDUES IN EGFR REGULATION AND ACTIN IN FcεRI SIGNALING

Jordan David Mohr, Ph. D.

Cornell University 2019

Membrane proteins play a critical role in cellular survival, function, and communication. Membrane receptors are one of the primary means by which cells interact with their extracellular environment to locate nutrients, identify threats, and communicate with other cells. This communication across the cell membrane is referred to as signal transduction and represents an immense biophysical feat that has evolved numerous transduction mechanisms. Given the importance of signal transduction, it is no surprise that defects in membrane receptor function have been linked to many disease states in humans.

The membrane receptors discussed in this work are the epidermal growth factor receptor (EGFR) and the immunoglobulin E (IgE) FcεRI immunorececptor. Dysregulation of EGFR through gain-of-function mutations has been linked to many cancers and is most commonly observed in brain, breast, and non-small cell lung cancer, while activation of FcεRI through normally benign antigens triggers the allergic response. Both of these represent cases of inappropriate receptor activation, though through differing mechanisms. Both of these receptors also serve as model receptors with broad implications to other receptors: EGFR is a model receptor tyrosine kinase while FcεRI is a model immunoreceptor that shares many similarities with B-cell and T-cell receptor signaling. Improving our understanding of these receptors also

benefits our understanding of these other systems and the pathologies associated with their dysregulation.

An earlier study of ours demonstrated that electrostatic residues in the juxtamembrane domain of EGFR play an inhibitory role by preventing spontaneous receptor activation. Prompted by this, we attempted to identify a potential mechanism for this activation. We were able to show that this mutation requires a series of conformational states consistent with an "inside-out" activation mechanism, in which these electrostatic residues prevent receptor dimerization and activation in the absence of ligand.

In another study, we showed that we could use microfabricated patterned ligand features to study protein recruitment to FcεRI clusters and quantify the effects of actin polymerization inhibitors on this recruitment. Here we expand upon that work by showing the recruitment of all the components of the Arp2/3 signaling complex in RBL-2H3 mast cells on patterned features. We also identify new roles for Arp2/3 and formins in FcεRI activation using pharmacological inhibitors. These actin-catalyzing enzymes appear to play both cooperative and differential roles in FcεRI signaling, with Arp2/3 potentially mediating complex stability while formins maintain quality control of the basal actin cytoskeleton and cellular processes. This is the first time that these roles have been investigated in detail in FcεRI signaling.

Taken together, this work extends our knowledge of juxtamembrane electrostatic residues in EGFR regulation and identifies new, differential roles for actin-polymerizing enzymes in FcεRI signaling.

BIOGRAPHICAL SKETCH

Jordan D. Mohr was born on December 10th, 1990 in York, Pennsylvania. He then moved to upstate New York where he graduated from Vestal Senior High School in 2009. He went on to Elmira College where he earned a Bachelor of Science in Biology, Chemistry, and Mathematics in 2013. While there, he discovered a passion for molecular and cellular biology through his coursework and research experiences. He was accepted to Cornell University's Pharmacology program through the Biological and Biomedical Sciences program where he joined the lab of Drs. Barbara Baird and David Holowka. While working on his thesis, Jordan realized he always had an immense passion and hobby for teaching and spent the final year of his thesis work learning modern pedagogy through the Center for Teaching Innovation's workshops and seminars and through the Discipline Based Education Research journal club on campus. As of this writing, he is hoping to pursue a career in education and education administration where he can leverage these techniques to improve student learning and start meaningful education dialogues between faculty members to improve their classrooms.

Outside the lab, Jordan enjoys playing video games, reading, cooking, and participating in, leading, and organizing student outreach programs. He spent his graduate career mastering creamy pasta sauces and has finally created the perfect alfredo sauce, which his gluten-allergic mother can never eat. He appreciates most forms of humor but has a particular fondness for exceedingly dry and sarcastic humor and those who have mastered it.

I would like to dedicate this work to my friends, family, and colleagues whom I could not have completed this without their support.

ACKNOWLEDGMENTS

I owe thanks to the many people who helped me reach this point and provided me with emotional support throughout my time here at Cornell.

First, I would like to thank my advisors Barbara and Dave, who provided guidance and much needed emotional support in my times of need. I am not very expressive, so I will express here that I always felt better after talking through my problems and fears with Barbara and Dave in our subgroups and it was an immense relief to me at the times when I needed it most. I would also like to acknowledge all my colleagues in the Baird-Holowka group over the years: Sarah Shelby, Devin Wakefield, Lily Chylek, Marcus Wilkes, Alice Wagenknecht-Wiesner, Eshan Mitra, Meraj Ramezani, Arianna Gagnon, Nirmlya Bag, and Roselynn Cordero. I would like to give special thanks to Devin Wakefield and Kirsten Bryant whose work this thesis expands upon, and to Meraj Ramezani for being such a great and loyal friend while also fabricating materials for me as fast as I could unreasonably ask for them.

I would also like to give thanks to some of my other staff and faculty mentors. I would like to thank Dr. Dave Lin at the Vet School for his support in our Fall into Science outreach program. He was always available to talk and bounce educational ideas off of and that helped me grow more than I knew at the time. I'd like to thank Dr. Cynthia Kinsland in Chemistry and Chemical Biology for being an all-around great TA boss. I learned countless valuable skills under her guidance. I'd also like to thank my committee members Rick Cerione for always being himself, as well as Hening Lin and Claire Fewtrell for their advice and our colorful committee meetings. The last shout-out in this section goes to Deb Crane, the rock who held the Department of Molecular Medicine together until her recent retirement. Deb was like a second mom to me while I was at Cornell and it was a real pleasure to swing by her office and check in with her.

I would like to thank my family, especially my sister for always checking in on me and my brother for being one of my best friends and an abundant resource of random scientific knowledge. My family and parents have always been supportive of me and my endeavors and for that I am truly grateful.

Lastly, I would like to thank my friends, both at Cornell and around the world. Your support, in whatever form it was, has helped me get to where I am today. I would like to give special thanks to Anthony Annunziata and Gabriel Sanna for their over-the-top and unsolicited support in all endeavors, and my friend and colleague Matthew Pennington for going to such great lengths to get me out of my house and the lab.

Thank you all for everything.

TABLE OF CONTENTS

LIST OF FIGURES

LIST OF ABBREVIATIONS

ADAP	Adhesion- and degranulation-promoting adaptor protein
AF488	Alexa Fluor 488
AF647	Alexa Fluor 647
Arp	Actin Regulatory Protein
BSA	Bovine serum albumin
BSS	Buffered salt solution
Cyto D	Cytochalasin D
DAG	Diacylglycerol
DNP	2,4-dinitrophenyl
DMEM	D-minimum essential medium
DMSO	Dimethylsulfoxide
DNP-cap-DPPE	1,2-dipalmitoyl-sn-glycero-3-phosphoethanolamine-N-[6-[(2,4-dinitrophenyl)amino]hexanoyl]
DOPC	1,2-dioleoyl-sn-glycero-3-phosphocholine
ECD	Extracellular Domain
EGF	Epidermal growth factor
EGFP	Enhanced green fluorescent protein
EGFR	Epidermal growth factor receptor
ERK	Extracellular signal-regulated kinase
FcεRI	High affinity IgE receptor
FRET	Fluorescence (or Förster) resonance energy transfer
GMBS	N-γ-maleimidobutyryl-oxysuccinimide ester

GPCR	G-protein coupled receptor
Grb2	Growth factor receptor-bound protein 2
IgE	Immunoglobulin E
IP3	Inositol 1,4,5-trisphosphate
ITAM	Immunoreceptor tyrosine-based activation motif
JX	Juxtamembrane
LAT	Linker for activation of T cells
Ld	Liquid disordered
LissRhod-DOPE	1,2-dioleoyl-sn-glycero-3-phosphoethanolamine-N-(lissamine rhodamine B sulfonyl)
Lo	Liquid ordered
MAPK	Mitogen activated protein kinase
mCFP	Monomeric cyan fluorescent protein
mEos	Monomeric Eos fluorescent protein
MPTS	(3-mercaptopropyl)trimethoxysilane
mTOR	Mammalian target of rapamycin
Nck	Non-catalytic region of tyrosine kinase adaptor protein
N-WASP	Neural Wiskott-Aldrich syndrome protein
PALM	Photoactivated localization microscopy
PBS	Phosphate buffered saline
PI3K	Phosphoinositide 3-kinase
PIP2	Phosphatidylinositol 4,5-bisphosphate
PKC	Protein Kinase C

PLCγ	Phospholipase Cγ
POPC	1-palmitoyl-2-oleoyl-sn-glycero-3-phosphocholine
PTPα	Protein tyrosine phosphatase α
RBL	Rat basophilic leukemia
RTK	Receptor Tyrosine Kinase
SH2	Src homology 2
SIM	Structured illumination microscopy
SLB	Supported lipid bilayer
SLP-76	SH2 domain-containing leukocyte phosphoprotein of 76 kDa, or LCP2
SMIFH2	Small molecular inhibitor of formin homology 2 domains
STED	Stimulated emission depletion
STORM	Stochastic optical reconstruction microscopy
SUV	Small unilamellar vesicle
Syk	Spleen tyrosine kinase
TIRF	Total internal reflection fluorescence
TM	Transmembrane
TKD	Tyrosine Kinase Domain
YFP	Yellow fluorescent protein
WASP	Wiskott-Aldrich syndrome protein

CHAPTER 1

INTRODUCTION

1.1 Microfabricated patterned ligand features for studying membrane receptor signaling

Overview of membrane receptor signaling

Membrane proteins, particularly membrane receptors, play a key role in transducing extracellular signals into intracellular responses[1]. These signals range from mechanical chemotaxis towards nutrients in single cells to sophisticated communication networks in multicellular organisms. In humans, defects in membrane receptor signaling can cause a variety disease states, notably cancers[2,3]. Thus, the study and understanding of membrane receptors and how they transduce these signals is an area of intense interest in cellular and molecular biology.

From a broad perspective, membrane receptor signal transduction can be broken down into a three-step process:

1. Recognition of a specific signaling molecule (binding).
2. Biophysical change in the receptor system indicating recognition (signal).
3. Transfer of the signal into the cell's signaling network (transduction).

In the first step, all receptor proteins possess some mechanism to recognize and bind to a specific set of molecules, known as their ligands. For example, the epidermal growth factor (EGF) receptor (EGFR) specifically recognizes EGF and a half dozen other molecules[4]. Ligand specificity confers precise control over receptor signaling - receptors that lose their ability to bind ligand will typically lose their ability to initiate signaling (loss-of-function) while receptors that start recognizing other molecules (or bypass ligand binding entirely) will initiate constitutive signaling (gain-of-function). These two types of mutations often serve as the molecular basis for many disease states.

In the second step, the mechanism through which a receptor signals ligand binding to the cell varies greatly among receptors. At its core, this step must represent an observable change in the membrane biology. The most common mechanism relies on intramolecular conformational changes of a single receptor to expose binding sites for other proteins, as is observed in G-protein coupled receptors (GPCRs)[4] or ligand gated ion channels[4]. However, other mechanisms for initiating signaling exist. For instance, ligand binding to EGFR induces receptor dimerization, and this intermolecular conformational change activates the enzymatic kinase domain of the receptor[5]. In the case of the immunoglobulin E (IgE) FcεRI receptor, the receptor binds an intermediate antibody to form in an inactive antibody-receptor complex. The binding of multiple antibody-receptor complexes to multivalent antigens to generate a local cluster of receptors[6] stabilizes an ordered lipid domain around the receptor cluster that initiates signaling by selectively recruiting and excluding other membrane proteins[7–10].

In the third step, all signaling pathways must transduce the local signal into a cellular response. In the simplest cases, the conformational change directly generates the cellular effect, like a ligand gated ion channel opening to initiate a neuron's action potential[4]. In more sophisticated signaling apparatuses, the receptor may drive the formation of a large signaling complex that produces secondary cytosolic messengers and activates cytosolic enzymes to transmit the signal beyond the membrane. The complexity of these signaling apparatuses allows for many opportunities to modulate the signal and produce differential outputs in different contexts. This complexity is key to understanding receptor signaling and this work serves to further our understanding of these underlying processes.

Microfabricated patterned ligand surfaces as a tool for studying membrane biology

Many powerful tools have been developed to aid in the study of membrane biology. Fluorophores in particular allow researchers to track the localization of various proteins and molecules through the use of fluorescent labeling techniques or genetically encoded fluorophores. These methods, in combination with fluorescence microscopy, represent some of the greatest achievements in the fields of cellular and molecular biology. However, these techniques are often limited by the inherent diffraction limit of microscopy techniques.

The diffraction limit is the minimal resolvable distance between two fluorophores – it depends on both the wavelength of light being observed and the refractive index of the lens capturing that light. For confocal microscopy, the diffraction limit is roughly 200 nm in the *xy*-plane and 600 nm in the *z*-plane under ideal conditions, which is to say confocal microscopy cannot distinguish fluorophores within 200 nm of each other. This poses a challenge in studying membrane signaling complexes as many systems, like FcεRI[11], create nanoclusters below the diffraction limit.

Advances in computational imaging techniques, like stochastic optical reconstruction microscopy (STORM)[12], photo-activatable localization microscopy (PALM)[13], and structured illumination microscopy (SIM)[13], have enabled researchers to surpass this limit and generate super resolution images. However, these methods require specific optical setups and significant computational resources to use. Other approaches change the illumination field to only excite a subdiffraction-limited region, like total internal reflection fluorescence (TIRF)[13] microscopy and stimulated emission depletion (STED)[13] microscopy. TIRF microscopy is particularly advantageous to studying membrane biology because it only excites fluorophores within 100-200 nm of the ventral surface, where the plasma membrane and its associated proteins are located.

Microfabrication techniques provide an alternative means of circumventing the diffraction limit. Microfabricated materials rely on the use of advanced fabrication techniques, like photolithography, to engineer nano- and microscale functional surfaces[14]. These techniques were originally developed for the semiconductor industry and have been adapted to biological techniques for use in scientific research and in commercial applications. Microfluidic devices are an example of a successfully implemented microfabricated technology, with a focus on sampling diagnostics because of their high sensitivity while using extremely small sample volumes[13]. Many groups have used microfabricated surfaces to study biological effects, for example, by using the surfaces to create artificial corrals to study diffusion dynamics or by presenting subdiffraction ligand-functionalized surfaces.

We use a variation of the latter method to create micron-scale patterned ligand features that recruit and stabilize signaling complexes beyond the diffraction limit (Figure 1.1). This can be considered an inverse of the methodology behind STORM and SIM – instead of resolving diffraction-limited information, we create a system that exists above the diffraction limit.

This system poses several notable advantages. First, the technical difficulty of this system lies in the initial fabrication of the patterns, which can be made en masse and stored for many months. It is a singular cost instead of a per-experiment cost. Second, the system is compatible with conventional biology techniques, like confocal microscopy. It does not require significant computational resources nor advanced instrumentation to evaluate. Third, the large size of the signaling complex stabilizes interactions that could be too transient or too weak to detect with other techniques. Fourth, the structured nature of the patterns allows for rapid and reliable qualitative measures of recruitment. However, microfabrication techniques often require specialized facilities and training to perform the initial fabrication.

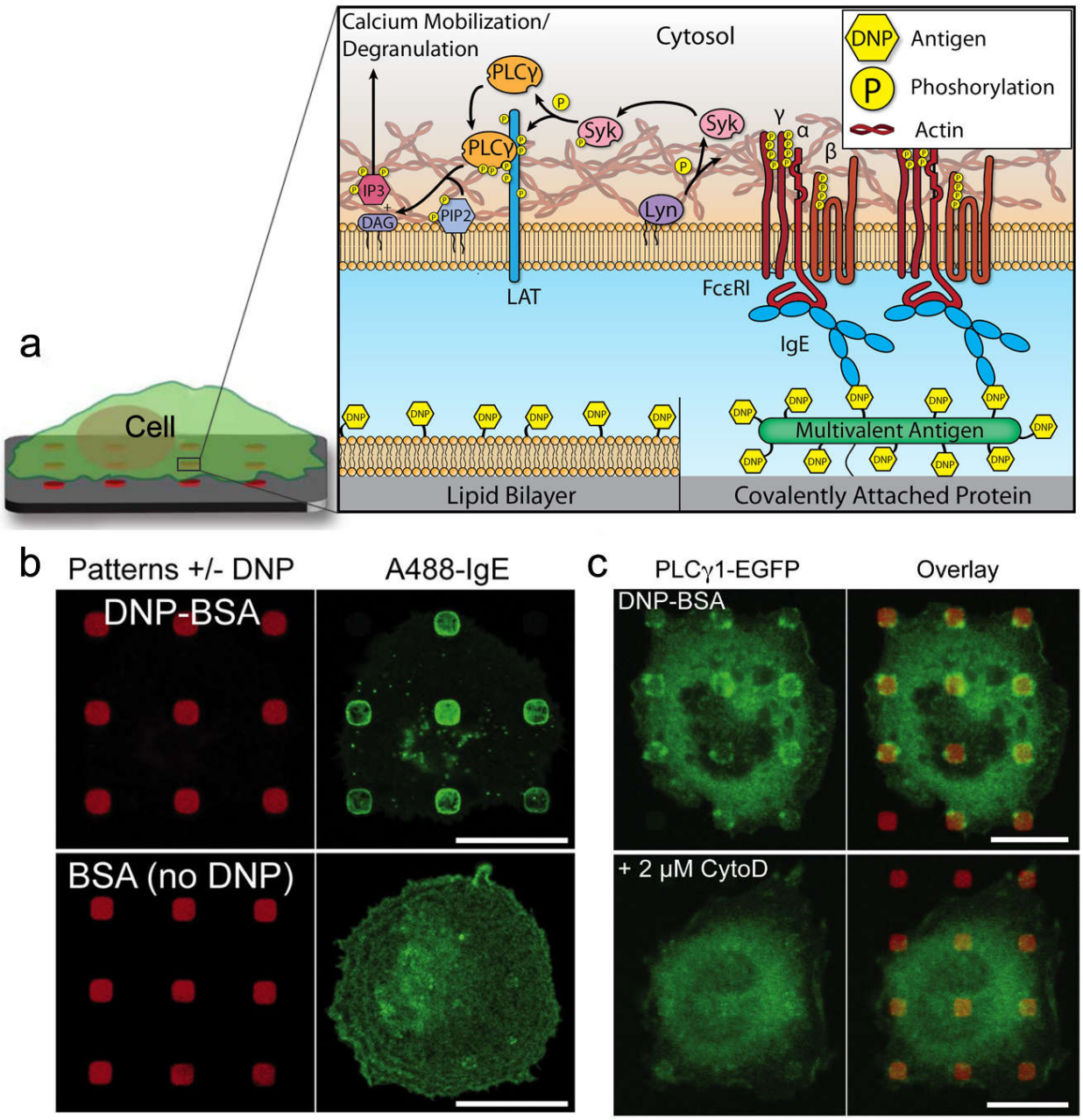

Figure 1.1[15]: Cell engaging DNP-BSA patterned ligand features. (a) representation of lipid (inlay: left) and covalent protein (inlay: right) surface presentation of antigen (DNP) and recruitment of anti-DNP IgE-FcεRI signaling components. (b) Representative images of cells demonstrating IgE recruitment is dependent on DNP antigen presentation[16]. (c) Patterned lipid surfaces can be used to study recruitment in response to pharmacological treatments, such as measuring PLCγ1 recruitment with and without Cytochalasin-D (Cyto D) treatment[16].

Microfabrication and functionalization of patterned ligand features

We fabricate our patterned ligand features using a combination of photolithography, surface functionalization, and parylene lift-off (Figure 1.2a). Briefly, glass or silicon wafers are coated with parylene, anti-reflective (AR) coating, and photoresist. A chrome mask containing the patterned features is used to expose the photoresist to directed-UV light (DUV). The UV-exposed regions of the photoresist are removed (developed) and then the underlying layers are etched to expose the glass underneath. Lastly, the wafer is stripped to remove any remaining photoresist and AR-coating, leaving only patterned ligand features etched into a layer of parylene. At this point, the patterned wafers can be stored for many months under vacuum.

The exposed glass surfaces can then be selectively functionalized while the non-reactive parylene protects the spaces between patterned features. Currently, we use two methods to functionalize these surfaces: covalent modification of proteins[17] or small unilamellar vesicle (SUV) deposition[18] (Figure 1.2b). Covalent protein modification allows us to leverage functionalized proteins and present a variety of proteins or peptides as part of the patterned ligand features. We have used this to present EGF to EGFR[19] or DNP-BSA antigen to FcεRI[16]. Additionally, the covalent modification also immobilizes the protein (figure 1.3b) and any biological factors that may interact with it, which may be desirable depending on the experiment.

Lipid modification allows for the presentation of ligand on a membrane mimetic surface. In this method, antigens are mobile and able to freely diffuse through the lipid bilayer, which is intended to mimic the surface presentation of antigens or proteins observed in many immune cell processes. This method is flexible in that the composition of the lipid bilayer is easy to tailor and biotinylated lipids allow streptavidin conjugation to the bilayer. We have previously used DNP-modified lipids to study FcεRI recruitment in RBL-2H3 mast cells[20,21].

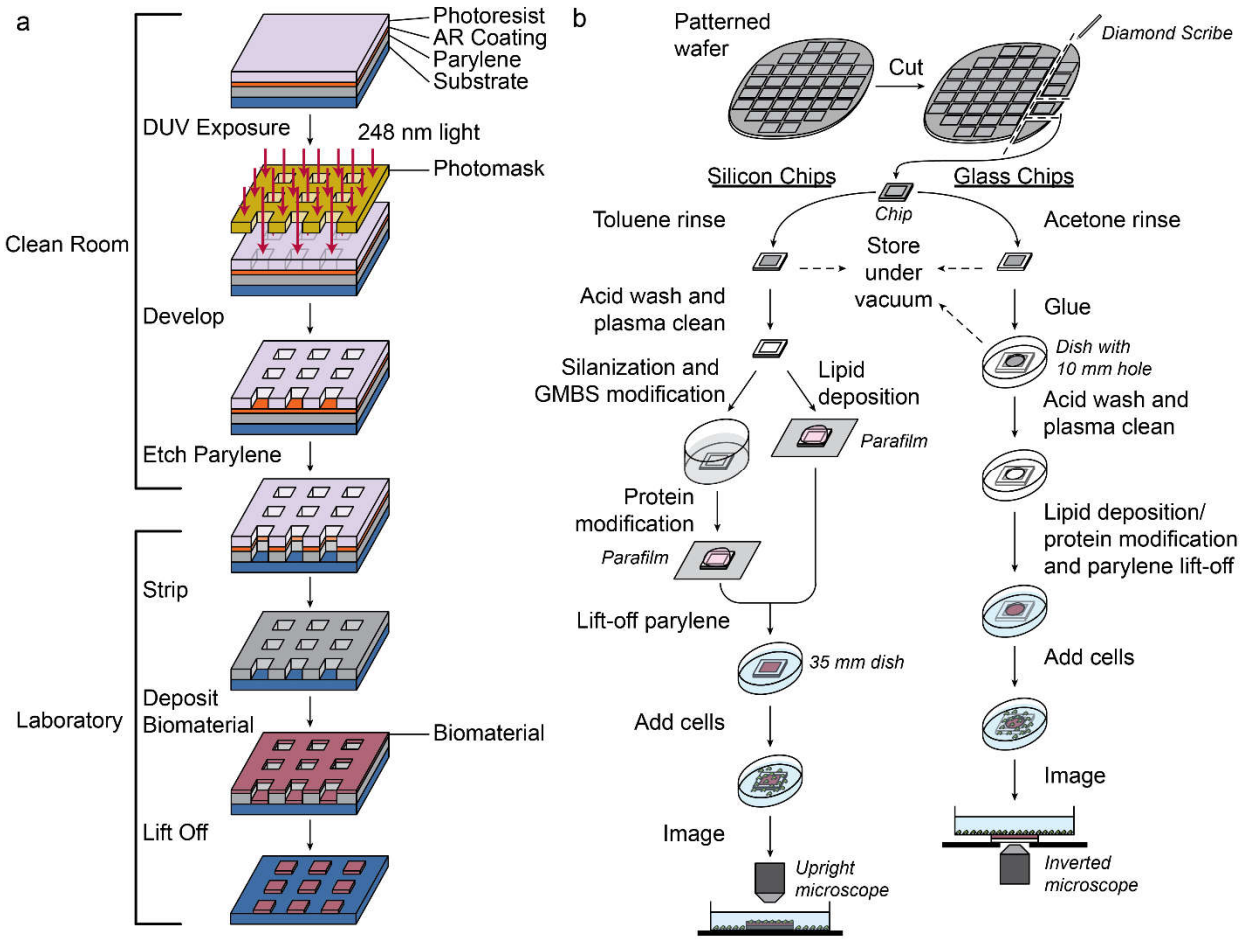

Figure 1.2[15]: Fabrication and modification scheme for patterned ligand features. (a) Patterned wafers are fabricated in a clean room and then functionalized in the lab. (b) Breakdown of lab functionalization component. Wafers containing many patterned features are separated into individual chips for functionalization and imaging. Opaque silicon chips and transparent glass chips have different chemical and optical properties resulting in slightly different cleaning and functionalization schemes. Glass chips can be imaged with inverted microscopy techniques like TIRF, while silicon is ideal for upright techniques, though we have used inverted microscopy to study inverted silicon chips[21].

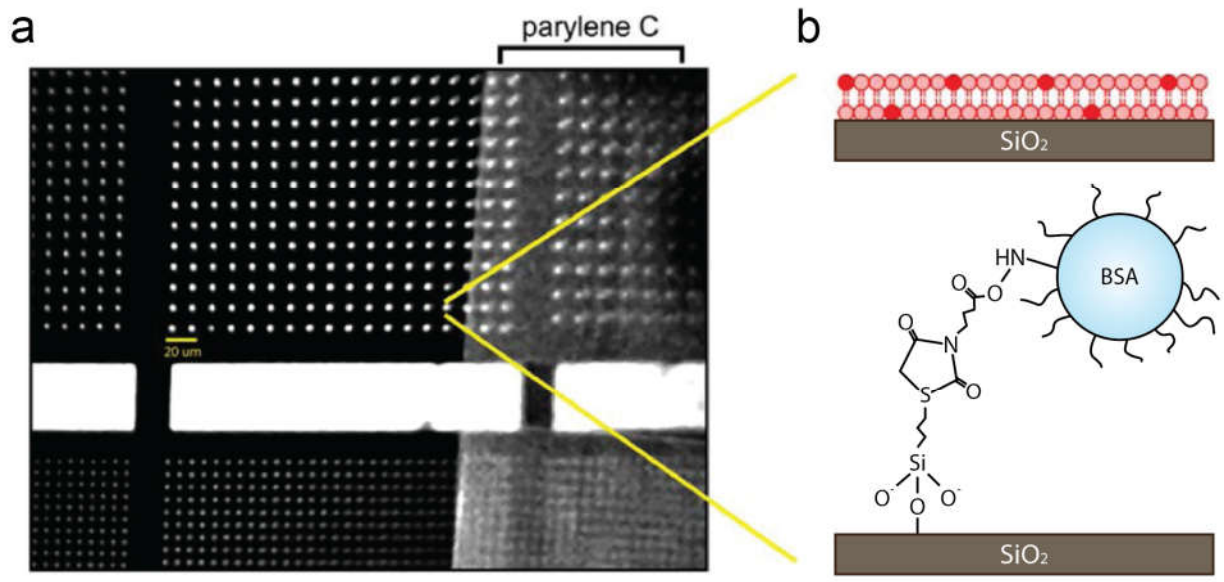

Figure 1.3[15]: Covalent attachment of protein to glass surfaces. (a) Patterned protein features with part of the parylene removed to reveal clean features. (b) Covalent attachment scheme using MPTS ((3-mercaptopropyl)trimethoxysilane) and GMBS (N-γ-maleimidobutyryl-oxysuccinimide ester) to attach a primary amine on BSA to the surface.

Ligand patterned features provide us with a valuable tool kit for studying membrane protein recruitment and can be used with conventional biology techniques to address questions that would normally lie beyond the diffraction limit or be otherwise too difficult to detect. Using this technique with quantitative techniques, we can measure protein and fluorophore recruitment to patterned features and answer novel questions concerning membrane receptor signaling.

1.2 Overview of EGF Receptor mediated signaling

The epidermal growth factor receptor (EGFR or ErbB1) is the most well-studied of the receptor tyrosine kinases. These membrane receptors govern a variety of complex signaling networks and are able to carefully tune cellular responses to a variety of ligands[22]. EGFR is a master regulator of cellular pro-survival and pro-growth signaling pathways. Gain-of-function and over-expression mutations in EGFR have been linked to many cancers[23], as cells with constitutive EGFR signaling are able to rapidly proliferate, invade neighboring tissues, and avoid apoptosis[14].

The structure of the EGFR (Fig 1.4) necessitates a novel signaling mechanism[5]. The receptor consists of an extracellular ligand binding and dimerization domain, a single transmembrane helix, a semi-helical amphipathic juxtamembrane domain (JX), a tyrosine kinase domain (TKD), and a flexible C-terminal tail. The extracellular domain can bind seven different ligands and generate modulated outputs for each ligand[24]. However, the mechanism of this transduction poses an interesting question.

Physically, the receptor must communicate across the membrane which ligand it has bound to, but a single receptor can only communicate this information across the single transmembrane helix, which functions as a stiff rod and is poorly suited to such a task.

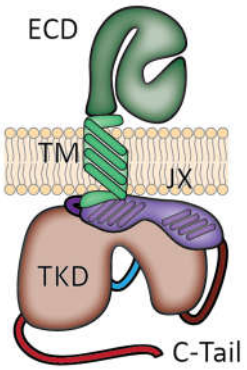

Figure 1.4: Structural representation of EGFR. The EGFR consists of an extracellular ligand binding and dimerization domain (ECD), a single transmembrane helix (TM), a semi-helical amphipathic juxtamembrane domain (JX), a tyrosine kinase domain (TKD), and a flexible C-terminal tail.

Instead, ligand binding results in a conformational change of the extracellular domain and reveals a dimerization domain. This domain can induce a similar conformational change in a neighboring EGFR and force the receptors to dimerize. This dimerization provides the key to differential signal transduction (Figure 1.5).

Following dimerization of the extracellular domains, the intracellular JX and TKD regions also form dimers. The TKDs from each receptor join to form an asymmetric TKD dimer and N-C lobe contact between the TKDs forces an inhibitory loop out of the active site of the "receiving" TKD and activates it[5]. However, the modulatory activity of different ligands appears to depend on the JX dimer formed between the TKDs and the membrane. It has been shown that different ligands binding to EGFR result in distinct JX rotamers and may serve as the physical basis for differential signaling[24].

Once the TKD is activated, the activated EGFR *trans*-autophosphorylates tyrosine residues in the terminal tail of the activating receptor, with a limited capacity for self, *cis*-autophosphorylation[25]. The phosphorylated residues then recruit proteins to drive signaling down key cellular axes like PI3K/Akt/mTOR, Ras/MAPK, Nck, and PLC/PKC. EGFR activation produces immediate cellular effects through these signaling pathways as well as long term effects through the mobilization of transcription factors. The study and understanding of EGFR structure and function is a key step towards understanding these systems and developing therapeutics to combat EGFR- and other RTK-related diseases.

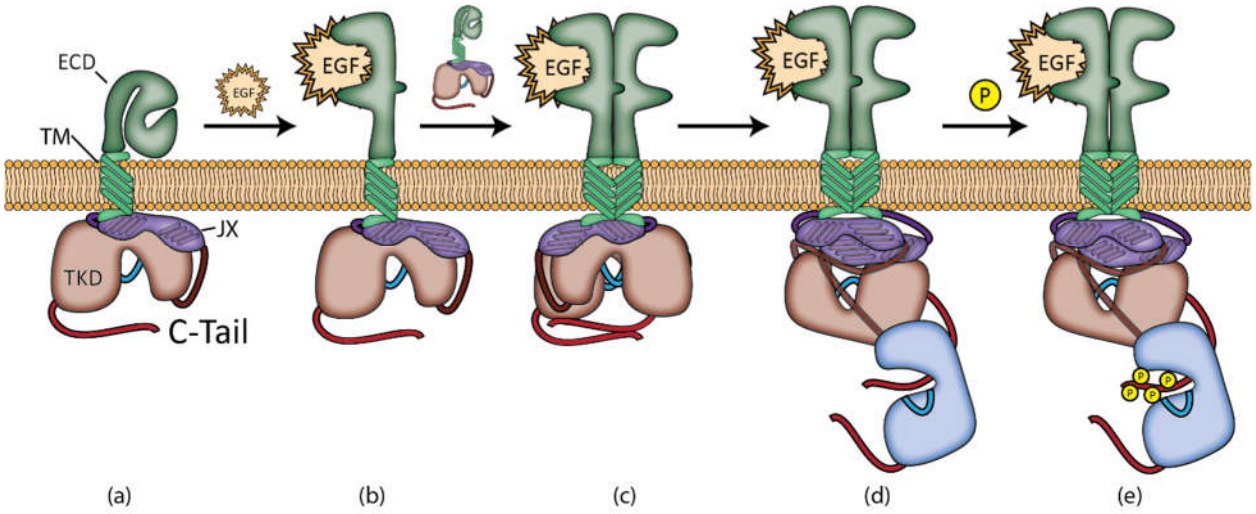

Figure 1.5: Activation scheme of EGFR. (a) EGFR exists as a monomer in the plasma membrane with its ECD tethered to the membrane prior to ligand binding. (b) Ligand binding reorganizes the ECD and reveals a dimerization domain. (c) Another receptor can bind EGFR to form a receptor dimer. (d) ECD dimerization is followed by dimerization of the intracellular domains into the asymmetric TKD dimer and pushes out the inhibitory loop from the active site of the receiving (blue) TKD. (e) The receiving TKD then phosphorylates the terminal tail of the activating EGFR.

1.3 IgE FcεRI receptor mediated signaling, actin, and lipid phases

Overview of the FcεRI Signaling Cluster

The immunoglobulin E (IgE) FcεRI receptor on the surface of mast cells is the principal instigator of the allergic response and is also a model for immunoreceptor signaling. Many of its signaling components are shared between B-cell and T-cell receptors (TCR)[26,27] and thus findings in one system can often provide insight into the other systems. As such, studying FcεRI provides not only the opportunity for advances in our understanding of allergic signaling, but also in B-cell and T-cell biology.

FcεRI consists of four polypeptide chains: the antibody binding α subunit, and the regulatory β and two γ subunits[6]. The α-subunit contains the Fcε binding region which gives the receptor its specificity to the IgE antibody. IgE in turn is specific to a single antigen and serves as an adaptor to allow a single type of cell surface receptor to interface with many different antigens, based on which IgE is bound to it. This is distinct from typical ligand binding receptors which tend to recognize a small subset of similar ligands.

Most IgE is pre-bound to FcεRI on the surface of cells with very little present in the bloodstream[28]. Interactions between multivalent antigens and multiple IgE molecules results in the FcεRI clustering and the formation of a stable ordered lipid domain, which leads to Lyn-mediated phosphorylation of immunoreceptor tyrosine-based activation motifs (ITAMs) on the β and γ subunits. This leads to the recruitment of cytoplasmic Syk-kinase, which is activated by Lyn-mediated phosphorylation (Figure 1.6). pSyk then goes on to phosphorylate LAT (linker for activation of T-cells), SLP-76 (SH2 domain-containing leukocyte protein of 76 kDa, also referred to as LCP2) and PLCγ (phospholipase C-γ)[6].

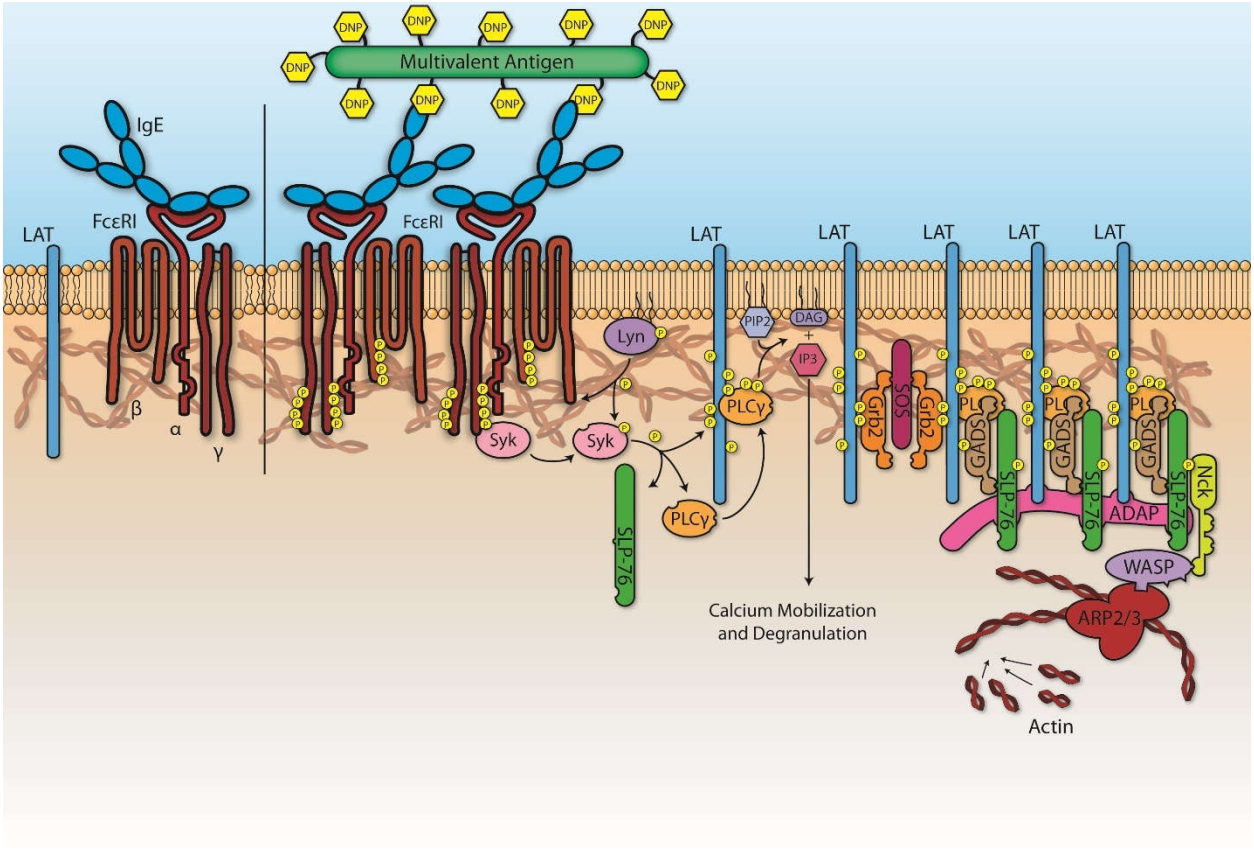

Figure 1.6: Schematic representation of FcεRI signaling emphasizing Ca^{2+} mobilization and Arp2/3 recruitment. FcεRI clustering driven by multivalent antigen binding leads to the recruitment of Lyn-kinase, phosphorylation of ITAMs on the β and γ subunits of FcεRI. This in turn recruits Syk which phosphorylates LAT, SLP-76, and PLCγ. This phosphorylation step leads to the creation of a LAT-centric signaling complex.

LAT serves as a central scaffolding protein in both TCR and FcεRI signaling. Phosphotyrosine residues on LAT provide recruitment sites for SH2 (Src homology 2) domain-containing proteins, like Grb2 (growth factor receptor-bound protein 2), Gads (Grb2 related adaptor protein), and PLCγ. Localization of PLCγ to the plasma membrane by pLAT allows it access to its substrate PIP_2 (phosphatidylinositol 4,5-bisphosphate), which it rapidly hydrolyzes into DAG (diacylglycerol) and IP_3 (inositol 1,4,5-trisphosphate). IP3 then diffuses from the membrane to IP3 receptors in the endoplasmic reticulum (ER) where they initiate store-operated calcium entry (SOCE). The cytoplasm of the cell then undergoes periodic oscillations in cytoplasmic Ca^{2+} levels that lead to the mobilization and release of vesicles containing pre-formed chemical mediators via fusion with the plasma membrane. These mediators, like histamines and cytokines, are ejected into the extracellular environment where they communicate with the surrounding tissues[6] and translate the allergic response from a cellular response into an organismal response.

The recruitment of Grb2 to pLAT connects FcεRI signaling to son-of-sevenless (SOS), like what is observed in EGFR signaling. Gads is also recruited to pLAT and serves to bridge pLAT to pSLP-76. pSLP-76 has been shown *in vitro* to recruit to the Arp2/3 (actin regulatory protein) actin assembly complex through the sequential recruitment of Nck (non-catalytic region of tyrosine kinase adaptor protein), WASP (Wiskott-Aldrich syndrome protein), and Arp2/3 to pSLP-76[29].

Actin and the FcεRI Signaling Complex

The use of actin-polymerizing inhibitors like Cytochalasin D (Cyto D) and Latrunculin have demonstrated a clear link between the actin cytoskeleton and FcεRI signaling. Treatment

with either Cyto D or Latrunculin enhances receptor phosphorylation, duration of phosphorylation[30,31], whole-population Ca^{2+} responses[31], increases sensitivity to antigen[32], and enhances degranulatory release of chemical mediators[31]. In these regards, it appears that the actin cytoskeleton plays a key role in downregulating FcεRI signaling. However, many questions remain. How does actin downregulate FcεRI? Where does this actin come from?

There are two primary enzyme systems in eukaryotic cells that compete to regulate actin polymerization. We hypothesize that one or both systems are responsible for the roles of actin observed in FcεRI signaling. Actin branching is mediated by Arp2/3 and linear actin extensions is mediated by the formins[33]. Arp2/3 is a particularly attractive candidate for further studies because of the high likelihood that it is recruited to FcεRI based on *in vitro* studies of LAT[29]. To the best of our knowledge, there is little evidence in the literature of formins being involved in FcεRI signaling, though it is unclear if this is simply because they have yet to be investigated or are unpublished.

Several hypotheses exist to explain the mechanism behind the different observed effects of actin polymerization inhibitors. In the case of degranulation, it appears that inhibiting actin polymerization reduces the translocation barrier the vesicle must overcome to release its contents[30,31,34], whereas at the signaling complex, cortical actin plays key roles in regulating membrane protein diffusion and lipid domains[30,35] and stabilizing LAT[16,29] complexes.

Lipid domains and the FcεRI Signaling Complex

FcεRI has a particularly novel method of initiating signal transduction compared to classic receptors. FcεRI clustering doesn't significantly affect the receptor's conformation, so there is no signal at the protein-level to indicate to the cell that the receptor has bound antigen. Instead,

FcεRI, and its lipid liquid ordered (Lo) phase preferring transmembrane helix, creates a puddle of Lo phase lipids around the receptor cluster[9,10]. We hypothesize this lipid puddle[36] then selectively recruits Lyn-kinase to FcεRI[7] and simultaneously excludes transmembrane phosphatases. Thus, the phosphorylation state shifts in favor of phosphorylated receptors leading to activation. This domain also favorably recruits LAT and is likely the true driving force behind the formation of the signaling cluster.

There is some evidence to support that actin plays a role in facilitating the formation of nano-domains of Lo and Ld (liquid disordered) domains through an underpinning picket fence model of the plasma membrane[10,37]. Thus, disrupting the cortical actin comprising this underpinning will affect the lipid phases it is in contact with.

1.4 Scope of this thesis

This thesis seeks to address two main questions:

1. What is the mechanism by which electrostatic neutralization of the EGFR's amphipathic JX domain induces constitutive activation?
2. What roles do formins and Arp2/3 play in FcεRI signaling?

Kirsten Bryant demonstrated that electrostatic neutralization of charged residues in the JX domain causes constitutive activation of EGFR[38]. However, it is unclear how this partial charge reduction actually induces EGFR activation. In the next chapter, we show that this reduction in charge leads to the formation of phosphorylated dimers. Furthermore, we show that these dimers likely follow the traditional path of *trans*-autophosphorylation observed in traditional EGFR activation. We propose that the electrostatic residues in the JX domain play an important role in preventing spontaneous intracellular dimerization leading to active dimers.

In the third chapter, we investigate potential roles for Arp2/3 and formins in FcεRI signaling. This work was originally intended as a continuation of Devin Wakefield's findings investigating the effects of Cyto D on FcεRI cluster formation and function[16], but was further inspired by Su *et al*'s *in vitro* demonstration of the recruitment of Arp2/3 to LAT. We set off to confirm this recruitment in RBL-2H3 cells using our patterned ligand features, which we were hopeful could detect this recruitment. At the same time, we became aware of Arp2/3-specific inhibitors and saw an obvious use for them in our research. We initially investigated formins as a negative control to compare to Arp2/3 inhibition, until we saw distinct effects from both inhibitors. Thus, we began charactering the contributions of Arp2/3 and formins using the CK666 Arp2/3 inhibitor and the SMIFH2 (small molecular inhibitor of formin homology 2 domains) formin inhibitor. This work is the first to demonstrate complete recruitment of Arp2/3 to FcεRI in mast cells and to look at the functional effects of different actin polymerizing enzymes in FcεRI signaling.

Chapters 2 and 3 both represent manuscripts in preparation. The supplementary sections include the actual supplements to the manuscripts as well as additional experiments that did not make it into the manuscript but are worth mentioning here.

Lastly, we conclude with a discussion of these findings and potential future directions for these projects to take, both in terms of where to expand upon the current findings and some areas that we were unable to successfully investigate due to time constraints.

REFERENCES

1. Cuatrecasas, P. Membrane Receptors. *Annu. Rev. Biochem.* **43**, 169–214 (1974).
2. Stewart, E. L., Tan, S. Z., Liu, G. & Tsao, M.-S. Known and putative mechanisms of resistance to EGFR targeted therapies in NSCLC patients with EGFR mutations-a review. *Transl. lung cancer Res.* **4**, 67–81 (2015).
3. Herbst, R. S. Review of epidermal growth factor receptor biology. *Int. J. Radiat. Oncol. Biol. Phys.* **59**, 21–6 (2004).
4. Singh, B., Carpenter, G. & Coffey, R. J. EGF receptor ligands: recent advances. *F1000Research* **5**, 2270 (2016).
5. Endres, N. F., Barros, T., Cantor, A. J. & Kuriyan, J. Emerging concepts in the regulation of the EGF receptor and other receptor tyrosine kinases. *Trends Biochem. Sci.* **39**, 437–446 (2014).
6. Rivera, J. & Gilfillan, A. M. Molecular regulation of mast cell activation. *J. Allergy Clin. Immunol.* **117**, 1214–1225 (2006).
7. Shelby, S. A., Veatch, S. L., Holowka, D. A. & Baird, B. A. Functional Nanoscale Coupling of Lyn Kinase with IgE-FcεRI is Restricted by the Actin Cytoskeleton in Early Antigen-Stimulated Signaling. *Mol. Biol. Cell* **27**, 3645–3658 (2016).
8. Sengupta, P., Hammond, A., Holowka, D. & Baird, B. Structural determinants for partitioning of lipids and proteins between coexisting fluid phases in giant plasma membrane vesicles. *Biochim. Biophys. Acta - Biomembr.* **1778**, 20–32 (2008).
9. Sengupta, P., Baird, B. & Holowka, D. Lipid rafts, fluid/fluid phase separation, and their relevance to plasma membrane structure and function. *Semin. Cell Dev. Biol.* **18**, 583–590 (2007).

10. Holowka, D. & Baird, B. Roles for lipid heterogeneity in immunoreceptor signaling. *Biochim. Biophys. Acta - Mol. Cell Biol. Lipids* **1861**, 830–836 (2016).

11. Wilson, B. S., Pfeiffer, J. R. & Oliver, J. M. FcεRI signaling observed from the inside of the mast cell membrane. *Mol. Immunol.* **38**, 1259–1268 (2002).

12. Betzig, E. *et al.* Imaging Intracellular Fluorescent Proteins at Nanometer Resolution\r10.1126/science.1127344. *Science (80-.).* **313**, 1642–1645 (2006).

13. Zhuang, X. Nano-imaging with STORM. *Nat. Photonics* **3**, 365–367 (2009).

14. Brodoceanu, D., Bauer, C. T., Kroner, E., Arzt, E. & Kraus, T. Hierarchical bioinspired adhesive surfaces—a review. *Bioinspir. Biomim.* **11**, 051001 (2016).

15. Mohr, J. D., Ramezani, M., Holowka, D. & Baird, B. A. Micropatterned Ligand Arrays to Investigate Spatial Regulation of Cellular Signaling Initiated by Clustered Fc Receptors. *Methods Mol. Biol.* **In Press**, (2019).

16. Wakefield, D. L., Holowka, D. & Baird, B. The FcεRI signaling cascade and integrin trafficking converge at patterned ligand surfaces. *Mol. Biol. Cell* **28**, 3383–3396 (2017).

17. Torres, A. J., Vasudevan, L., Holowka, D. & Baird, B. a. Focal adhesion proteins connect IgE receptors to the cytoskeleton as revealed by micropatterned ligand arrays. *Proc. Natl. Acad. Sci.* **105**, 17238–17244 (2008).

18. Richter, R. P., Him, J. L. K. & Brisson, A. Supported lipid membranes. *Mater. Today* **6**, 32–37 (2003).

19. Singhai, A. *et al.* Spatially defined EGF receptor activation reveals an F-actin-dependent phospho-erk signaling complex. *Biophys. J.* **107**, 2639–2651 (2014).

20. Orth, R. N., Wu, M., Holowka, D. A., Craighead, H. G. & Baird, B. A. Mast cell activation on patterned lipid bilayers of subcellular dimensions. *Langmuir* **19**, 1599–1605

(2003).

21. Wu, M., Holowka, D., Craighead, H. G. & Baird, B. Visualization of plasma membrane compartmentalization with patterned lipid bilayers. *Proc. Natl. Acad. Sci.* **101**, 13798–13803 (2004).

22. Lemmon, M. A. & Schlessinger, J. Cell signaling by receptor tyrosine kinases. *Cell* **141**, 1117–1134 (2010).

23. Zhang, H. *et al.* ErbB receptors: from oncogenes to targeted cancer therapies. *J. Clin. Invest.* **117**, 2051–8 (2007).

24. Doerner, A., Scheck, R. & Schepartz, A. Growth Factor Identity Is Encoded by Discrete Coiled-Coil Rotamers in the EGFR Juxtamembrane Region. *Chem. Biol.* **22**, 776–784 (2015).

25. Kancha, R. K., von Bubnoff, N. & Duyster, J. Asymmetric kinase dimer formation is crucial for the activation of oncogenic EGFRvIII but not for ERBB3 phosphorylation. *Cell Commun. Signal.* **11**, 39 (2013).

26. Latour, S. & Veillette, A. Proximal protein tyrosine kinases in immunoreceptor signaling Sylvain Latour * † and André Veillette * ‡. *Curr. Opin. Immunol.* 299–306 (2001).

27. Activation, F. C. *et al.* The Same TyrosineBased Inhibition Motif , in the Intra-cytoplasmic Domain of FcyRIIB , Regulates Negatively. *Cell* **3**, 635–646 (1995).

28. Krystel-Whittemore, M., Dileepan, K. N. & Wood, J. G. Mast Cell: A Multi-Functional Master Cell. *Front. Immunol.* **6**, 1–12 (2016).

29. Su, X. *et al.* Phase separation of signaling molecules promotes T cell receptor signal transduction. *Science (80-.).* **352**, 595–599 (2016).

30. Holowka, D., Sheets, E. D. & Baird, B. Interactions between FcεRI and lipid raft

components are regulated by the actin cytoskeleton. *J. Cell Sci.* **113 (Pt 6**, 1009–19 (2000).

31. Frigeri, L. & Apgar, J. R. The role of actin microfilaments in the down-regulation of the degranulation response in RBL-2H3 mast cells. *J. Immunol.* **162**, 2243–50 (1999).

32. Oka, T., Sato, K., Hori, M., Ozaki, H. & Karaki, H. FcεRI cross-linking-induced actin assembly mediates calcium signalling in RBL-2H3 mast cells. *Br. J. Pharmacol.* **136**, 837–846 (2002).

33. Goode, B. L. & Eck, M. J. Mechanism and Function of Formins in the Control of Actin Assembly. *Annu. Rev. Biochem.* **76**, 593–627 (2007).

34. Nishida, K. *et al.* FcεRI-mediated mast cell degranulation requires calcium-independent microtubule-dependent translocation of granules to the plasma membrane. *J. Cell Biol.* **170**, 115–126 (2005).

35. Ostrowski, P. P., Grinstein, S. & Freeman, S. A. Diffusion Barriers, Mechanical Forces, and the Biophysics of Phagocytosis. *Dev. Cell* **38**, 135–146 (2016).

36. Mitra, E. D., Whitehead, S. C., Holowka, D., Baird, B. & Sethna, J. P. Computation of a Theoretical Membrane Phase Diagram and the Role of Phase in Lipid-Raft-Mediated Protein Organization. *J. Phys. Chem. B* **122**, 3500–3513 (2018).

37. Honigmann, A. *et al.* A lipid bound actin meshwork organizes liquid phase separation in model membranes. *Elife* **3**, e01671 (2014).

38. Bryant, K. L., Antonyak, M. A., Cerione, R. A., Baird, B. & Holowka, D. Mutations in the polybasic juxtamembrane sequence of both plasma membrane- and endoplasmic reticulum-localized epidermal growth factor receptors confer ligand-independent cell transformation. *J. Biol. Chem.* **288**, 34930–34942 (2013).

CHAPTER TWO

BASIC AMINO ACIDS WITHIN THE JUXTAMEMBRANE DOMAIN OF THE EPIDERMAL GROWTH FACTOR RECEPTOR REGULATE RECEPTOR DIMERIZATION AND AUTO-PHOSPHORYLATION.

2.1 Abstract

Dysregulation of EGF Receptor (EGFR) has been observed in many human cancers and can serve as both a cause of oncogenesis and a target for chemotherapy. We have previously determined that partial charge neutralization of the juxtamembrane (JX) region of the EGFR can induce constitutive receptor phosphorylation and activation that leads to transformation of NIH 3T3 cells for both plasma membrane and ER-retained mutant constructs. We use chemical crosslinking and immunoblotting to show that these mutant constructs form constitutive, phosphorylated dimers, and they require both intra- and extracellular dimerization interactions to maintain this activity. These findings suggest that the electrostatic charge of the JX region is critical for the negative regulation of the EGFR receptor in the absence of EGF.

2.2 Introduction

Receptor tyrosine kinases are master regulators of extensive and complex cellular signaling networks[1]. The epidermal growth factor receptor (EGFR or ErbB1) is the most studied member of this family. EGFR presides over a system of tightly regulated pro-survival signaling pathways within the cell. Numerous mutations in EGFR cause spontaneous receptor activation and have been observed in human cancers[2]. However, it is unclear how many of these mutations drive receptor activation. Thus, we must develop a deeper understanding of the relationship

between structure and function within EGFR.

Structurally, EGFR contains an extracellular ligand binding domain, a single transmembrane helix, and an intracellular region composed of the juxtamembrane (JX) semi-helical domain, the catalytic tyrosine kinase domain (TKD), and a C-terminal tail sequence[1,3] (Figure 2.1A.a). EGFR is activated when ligand binds to the extracellular domain (Figure 2.1A.b), which initiates a conformational change that exposes the extracellular dimerization arm of the receptor and enables the formation of stable, EGFR homodimers or heterodimers with other members of the ErbB family[3,4] (Figure 2.1A.c). Some evidence also suggests that a small population of EGFRs exist as inactive dimers prior to ligand binding[5]. Ligand-bound dimers release their JX and TKD domains from association with the inner leaflet of the plasma membrane, allowing them to rearrange to form an activated, asymmetric kinase dimer, in which the C lobe of the activating receptor contacts the N lobe of a receiving receptor[6] (Figure 2.1A.d). These rearrangements result in allosteric activation of the receiving TKD. The receiving receptor then primarily *trans*-phosphorylates tyrosine residues in the C-terminal tail of the activating receptor (Figure 2.1A.e), providing binding sites for downstream signaling proteins[3,7–10]. There is also evidence for a limited degree of *cis*-autophosphorylation of the receiving kinase in EGFR heterodimers[11].

The JX domain is a critical regulator of EGFR function, with established roles in activation and signal transduction,[12] and it is conserved across human RTKs[13]. Replacement of the JX domain with an unstructured peptide sequence results in phosphorylation-incompetent receptors[14], indicating that the endogenous sequence plays a necessary role in activation. We previously demonstrated that alanine charge silencing of the electrostatic polybasic sequence within the JX domain leads to constitutive activation of the receptor[15]. This suggests a specific

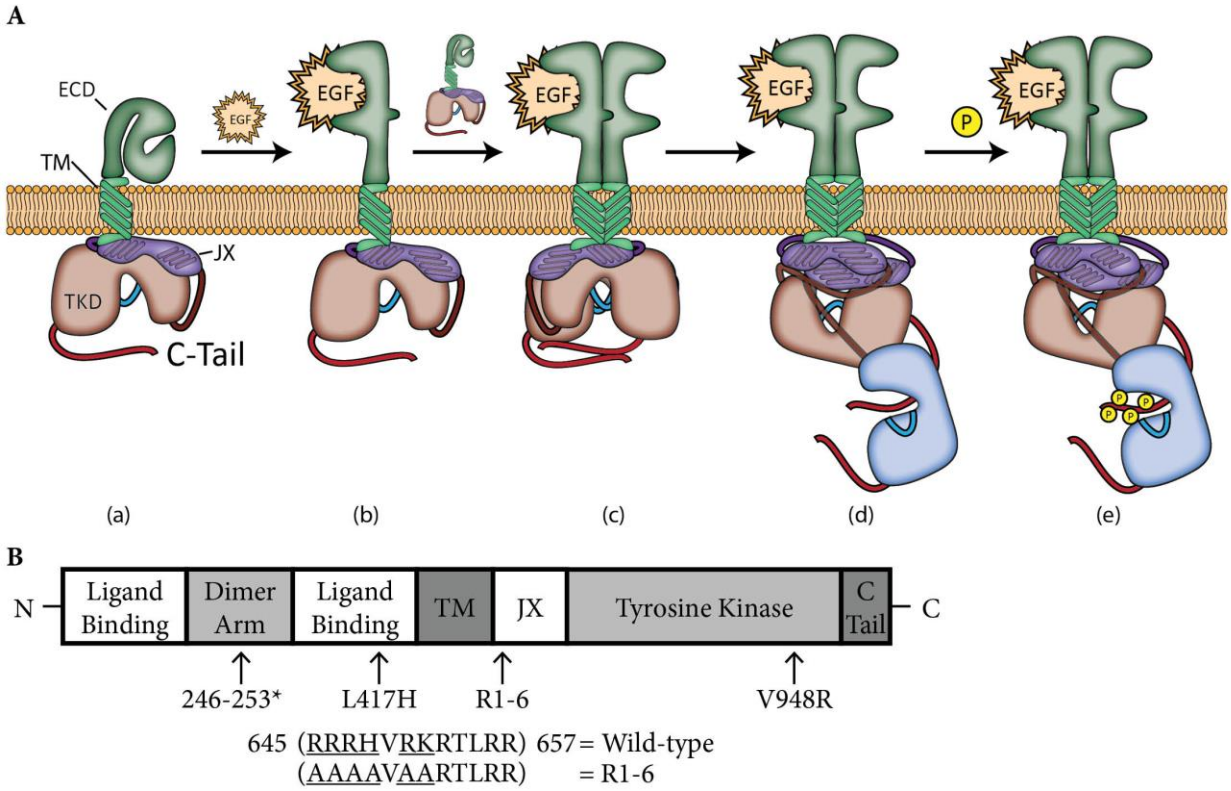

Figure 2.1: Schematic diagrams of EGFR signaling and structure. *A.* Canonical EGFR activation pathway. Ligand binding (a) exposes the dimerization arm (b) and allows for the formation of EGFR dimers (c). These dimers rearrange into an active, asymmetric conformation (d) characterized by dimerized extracellular and intracellular domains with anti-parallel arrangement of the JX domains and N-C lobe contact between the TKDs of the receiving receptor (blue TKD) and the activating receptor (red TKD). The TKD of the receiving receptor phosphorylates the C-terminal tail of the activating receptor (e). *B.* Schematic representation of EGFR with mutagenesis sites and R1-6 sequence. Mutated residues are underlined. The 246-253* mutant blocks extracellular dimerization, L417H mutant blocks exit from the ER, R1-6 is the electrostatic neutralization mutant, and V948R prevents allosteric activation by prevent the N-C lobe contact of the TKDs.

structural role for the JX domain in the regulation of receptor activation. Recently, it has been reported that the JX domain may also participate in receptor multimerization and consequent phosphorylation[16].

Despite our increasing understanding of the complex roles played by the JX domain, the relationship between its structure and function is still poorly understood. Structurally, the JX domain is composed of two electrostatically charged, conjoined amphipathic semi-helices. It begins as a continuation of the single transmembrane helix and is located immediately adjacent to the plasma membrane. In inactive receptors, the JX domain interacts with the plasma membrane through electrostatic interactions between its positively charged polybasic residues (Figure 2.1B) and negatively charged membrane phospholipids[17,18] as well as hydrophobic interactions via hydrophobic residue insertions[19]. Similarly, the adjacent TKD domain associates with the membrane through the insertion of hydrophobic residues. Together, these interactions tightly bind the intracellular domains to the membrane in an inactive conformation. During activation, both the TKD and JX domains are released from the membrane. The JX domains in EGFR homodimers form anti-parallel helices that are stabilized by mutual interactions of their hydrophobic residues[19,20]. Additionally, the JX polybasic region has been shown to interact with an acidic region within the TKD to stabilize the active dimer conformation[21]. Thus, the polybasic region not only prevents activation through membrane interactions in the basal state, but may also promote dimer stability in activated receptors.

Previously, we have demonstrated that the conserved polybasic region within the JX domain is responsible for maintaining EGFR in an inactive basal state. Charge neutralizing mutagenesis of this region, referred to as EGFR R1-6 (Figure 2.1B), results in the constitutive activation of EGFR and induces cellular transformation as determined by anchorage-independent

growth *in vitro*[15]. Due to the varied regulatory roles of this region, the question remains how electrostatic silencing leads to constitutive activation of EGFR.

We further expand upon the regulatory roles of the polybasic region of the JX domain by providing evidence that this region prevents the formation of active dimers in the absence of ligand. The polybasic region has been previously implicated in both preventing basal dimerization by tethering the JX and TKD domains to the plasma membrane, while simultaneously stabilizing the activated dimer. These competing roles of the polybasic region, combined with our previous study demonstrating receptor activation, suggest that the primary role of the polybasic region is inhibitory in nature. We use chemical crosslinking and western blotting to suggest that this region plays a dominant role in preventing spontaneous receptor activation, while its neutralization has little impact on receptor dimerization.

2.3 Methods

Materials:

All cell culture reagents, EGF, and precast gels for blotting were from Invitrogen unless indicated otherwise. Gentamicin sulfate was from VWR. FuGENE HD was from Roche Applied Sciences. Mirus TransIT 2020 was from Mirus Bio. All chemical crosslinkers, BS3 (bis(sulfosuccinimidyl)suberate), DSS (disuccinimidyl suberate), and DSG (disuccinimidyl glutarate) were from CovaChem. PVDF membranes for blotting were from Millipore. The phospho-Y1173-specific EGFR antibody and anti-EGFR antibodies (used for blotting) were from Cell Signaling Technology. Anti-actin antibody was from LabVision/Thermo. HRP-conjugated secondary antibodies were from GE Healthcare. Phusion High-Fidelity DNA Polymerase, restriction enzymes (Xba1 and EcoN1), and other cloning materials were from New

England Biolabs. All chemicals were from Sigma-Aldrich unless otherwise stated.

Expression Plasmids:

The human EGFR and EGR R1-6 constructs in pkH3 vectors have been described previously[15]. The EGFR 246-253* was provided by Dr. Mark Lemmon in a pAc5.1/V5-HisA vector[22]. We cloned into our pkH3 vector by cutting out the native extracellular domain using Xba1 and EcoN1 restriction sites and then cloning in the EGFR 246-253* extracellular domain using In-Fusion® HD Cloning (Clontech® Laboratories, Inc.) with GCAGGTCGACTCTAGA-TGCGACCCTCCGGGACG and TGTTCATGGCCTGAGGCAGG as primers.

The EGFR V948R and EGFR R1-6 V948R constructs were generated by site directed mutagenesis from their parent plasmids using Phusion High-Fidelity DNA polymerase and a forward primer of TGTACCATCGATGTCTACATGATCATGCGCAAGTGC and a reverse primer of CTATCTGCGTCTATCATCCAGCACTTGCGCATGATC. All cloning described was performed by Alice Wagenknecht-Wiesner.

Cell Culture:

NIH 3T3 cells for transient transfections were cultured in Dulbecco's modified Eagle's medium (DMEM) containing 5% (v/v) FBS and 5% NBCS (Atlanta Biologicals) and 1 U/mL Pen/Strep. NIH 3T3 cells were transfected with Mirus TransIT 2020 as per the manufacturer's directions and allowed to express for 24 hours prior to experiments. NIH 3T3 cells stably expressing EGFR constructs[15] were cultured in DMEM containing 5% FBS and 5% NBCS, 1 U/mL Pen/Strep, and 2 µg/mL puromycin. RBL-2H3 cells were cultured in Modified Eagle's media containing 20% FBS and 10 µg/mL gentamicin sulfate as described previously[23].

Chemical Crosslinking:

$5x10^5$ cells were plated and transfected, if necessary, in 6 well, 35 mm plates as described above. All cells expressing EGFR constructs were starved in their respective serum-free media for 12-16 hours prior to chemical crosslinking. All PBS in this section refers to a PBS stock supplemented with 1 mM Mg^{2+} pH 7.5. Prior to the experiment, cells were washed once with PBS containing 1 mM Mg^{2+} pH 7.5 and then treated with 1 mL of 100 ng/mL EGF in PBS/ Mg^{2+} for 5 minutes. 1 mL of PBS/Mg^{2+} containing either 2 mM BS^3 or DSS crosslinker or 10 µL of DMSO vehicle control was then added to the 1 mL of PBS already on the cells (1 mM final crosslinker concentration). The plates containing the cells were cooled to 4°C and allowed to incubate for 30 minutes. Unreacted crosslinker was then quenched with 40 µL 1 M glycine pH 7.2 in PBS for 15 minutes. Cells were then washed once with PBS containing 1 mM Mg^{2+} and then incubated with cold lysis buffer (25 mM Tris, pH 7.4, 100 mM NaCl, 1 mM EDTA, 1% (v/v) Triton, 1 mM sodium orthovanadate, 1 mM β-glycerol phosphate, 1 µg/mL leupeptin, and 1 µg/mL aprotinin). Supernatants were retained following 10 minutes of microfuge centrifugation at 4°C. Protein concentrations of whole cell lysates were measured using the Bio-Rad Protein Assay.

Immunoblot Analysis:

Whole cell lysates (20 µg/lane) were resolved by SDS/PAGE, and the proteins were transferred to PVDF membranes. The membranes were blocked in 5% BSA diluted in 20 mM Tris, 135 mM NaCl, and 0.02% Tween 20, and incubated with primary antibodies in the same buffer overnight. Primary antibodies were detected with HRP-conjugated secondary antibodies

and a Bio-Rad VersaDoc MP 5000 imager.

Densitometry Quantification:

Immunoblots were analyzed using Bio-Rad's Image Lab with a rolling disc background subtraction method to obtain density values for each band. pEGFR bands were normalized by dividing through by the total amount of EGFR present. These values were then compared using a Tukey's comparison of means in conjunction with ANOVA.

2.4 Results

Partial charge silencing of the JX domain leads to constitutive dimerization and phosphorylation of both plasma membrane and ER-retained EGFR constructs:

We sought to determine whether EGFR R1-6 signals as a constitutive dimer, in part because EGF stimulation causes wt EGFR to form phosphorylated dimers, and in part because of a growing body of evidence that constitutively active EGFR mutants signal as dimers[24–27]. For this purpose we used the technique of covalent chemical crosslinking and immunoblotting to detect high molecular weight species[28]. Briefly, NIH 3T3 cells stably expressing EGFR or EGFR R1-6 were incubated with either PBS supplemented with 1 mM Mg^{2+} (unstimulated) or EGF (stimulated) and either chemically cross-linked with the, non-membrane permeable crosslinker, bis-sulfosuccinimidyl-suberate (BS^3) or incubated in PBS (uncrosslinked). The cells were then lysed and immunoblotted to detect phosphorylated tyrosine at position 1173 (EGFR pY1173) that is present in active receptors but not inactive receptors, in addition to detection of total EGFR and actin.

Monomeric EGFR migrates as a ~170 kDa band while dimeric EGFR migrates as a ~340

kDa band. As shown in Figure 2.2A, lane 4, chemical crosslinking of wt EGFR yields an EGFR pY1173 dimer that is dependent on EGF stimulation, as well as chemical crosslinking. Consistent with our earlier findings[15], EGFR R1-6 exhibits basal EGFR phosphorylation in the absence of stimulating ligand (Figure 2.2A, lanes 5 and 7). Importantly, EGFR R1-6 forms a cross-linked phosphorylated dimer in the absence of EGF stimulation (Figure 2.2A, lane 7). Thus, we conclude that EGFR R1-6 forms a constitutively phosphorylated dimer in NIH 3T3 cells, whereas wt EGFR does not (Figure 2.2A, lane 3). Total EGFR and actin were used as measures of EGFR expression and protein loading, respectively.

Densitometry of multiple experiments indicates that EGFR R1-6 constitutively phosphorylated dimers are intermediate in quantity between EGF-stimulated and unstimulated wt receptors (Figure 2.2B, $p < 0.05$). This is consistent with other observations that activating EGFR mutations, like the clinically observed L858R and EGFR ΔL747-P753insS mutations[29], are only weakly active compared to EGF-stimulated receptors. Additionally, both wt EGFR and EGFR R1-6 form similar amounts of EGF-stimulated PEGFR Y1173 dimers (Figure 2.2B), suggesting that mutation of the positively charged residues in the JX domain does not affect the stability of the dimers under these conditions.

Similar methods were used with the membrane-permeable crosslinker, disuccinimidyl suberate (DSS), to assess dimer formation by the ER-retained L417H mutants. Cells stably expressing EGFR L417H and EGFR R1-6 L417H were stimulated or not, crosslinked or not, and immunoblotted as described earlier. As we reported previously[15], EGFR L417H and EGFR R1-6 L417H do not respond to ligand stimulation because they are intracellularly located (Figure 2.3A). We observed basal phosphorylation of EGFR R1-6 L417H (Figure 2.3A, lanes 2 and 4).

Chemical crosslinking of EGFR R1-6 L417H results in the detection of pEGFR dimers,

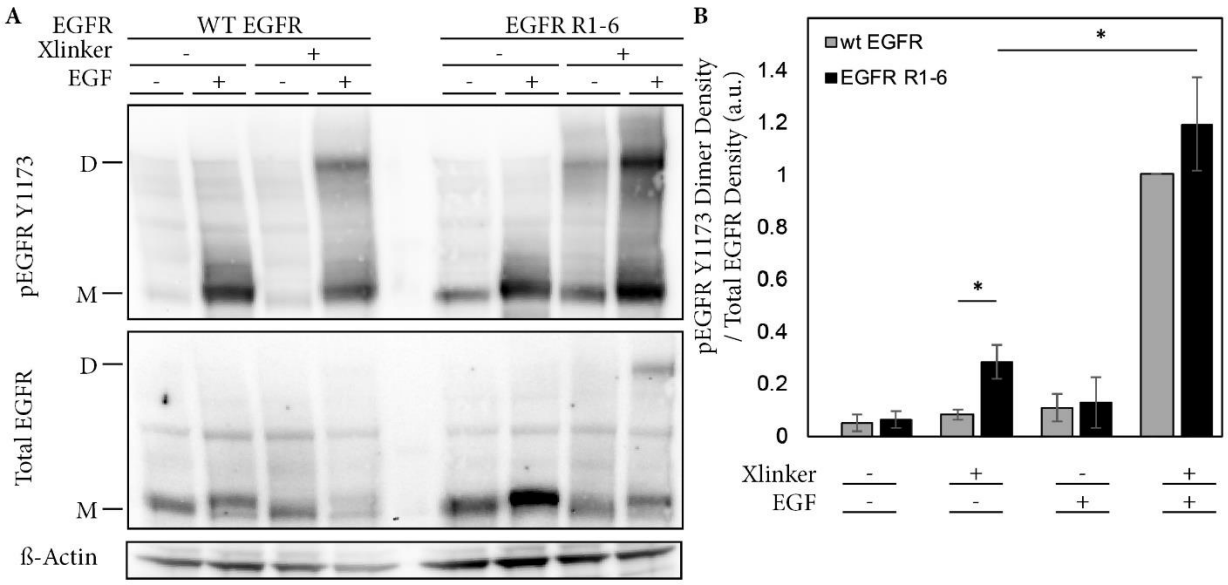

Figure 2.2: EGFR R1-6 forms phosphorylated dimers in the absence of ligand. *A.* Whole cell lysates from NIH 3T3 cells stably expressing either EGFR or EGFR R1-6 and stimulated with EGF or not, then chemically crosslinked with BS^3 prior to lysis. Analysis by western blotting with the indicated antibodies. M and D indicate monomeric and dimeric EGFR, respectively. *B.* Densitometry quantification of multiple experiments as in A, where error bars indicate ± S.D. of three independent experiments (*, $p<0.05$). Data were normalized to the total EGFR present and compared using stimulated and crosslinked wt-EGFR as a baseline.

but dimers of crosslinked EGFR L417H are not detected (Figure 2.3A, lane 3 vs lane 4). Thus, we conclude that EGFR R1-6 L417H forms spontaneous dimers in the ER, but EGFR L417H does not.

Densitometry was performed in a similar manner to the results using BS^3. Crosslinked EGFR R1-6 L417H mutants form phosphorylated dimers while EGFR L417H mutants do not, regardless of EGF treatment (Figure 2.3B). This suggests that the R1-6 activating mutation stabilizes the active dimer conformation, regardless of whether it is located at the plasma membrane or in the ER.

Inhibiting the asymmetric dimer conformation of the TKD inhibits EGFR R1-6 constitutive activation:

Next, we sought to determine whether dimerization is necessary for receptor phosphorylation, or if perhaps the receptor can autophosphorylate as a monomer and then form a stable dimer. To address this, we utilized the EGFR V948R mutant[11,26,30]. This mutation inserts a positively-charged residue onto the C-terminal lobe of the tyrosine kinase domain and prevents the N-C lobe contact required for the active, asymmetric, "CDK/Cyclin-like" kinase conformation, and instead forces receptor dimers to assume an inactive, symmetric, "Src/CDK-like" conformation[6]. Thus, a monomeric EGFR R1-6 V948R autophosphorylation event would not be blocked by this mutant, but a dimer-dependent event could be.

NIH 3T3 cells transiently expressing EGFR V948R and EGFR R1-6 V948R were stimulated and chemically crosslinked with BS^3 as described earlier. Both EGFR V948R and EGFR R1-6 V948R failed to phosphorylate regardless of stimulation (Figure 2.4, lanes 5-12), indicating that EGFR R1-6 requires the asymmetric kinase conformation for phosphorylation.

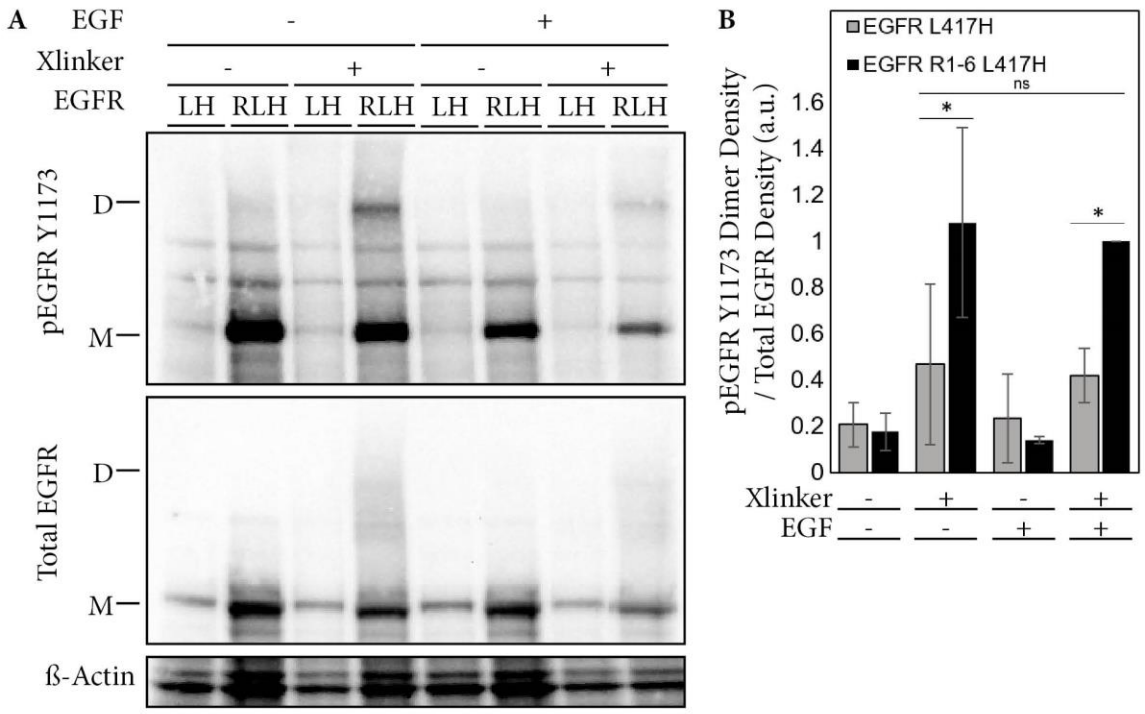

Figure 2.3: EGFR R1-6 forms phosphorylated dimers when combined with the ER-localizing EGFR L417H mutant. *A.* Whole cell lysates from NIH 3T3 cells stably expressing either EGFR L417H (LH) or EGFR R1-6 L417H (RLH) were stimulated with EGF and then chemically crosslinked with DSS prior to western blotting with the indicated antibodies. M and D indicate monomeric and dimeric EGFR respectively. *B.* Densitometry quantification of multiple experiments as in A, where error bars indicate ± S.D. of three independent experiments (*, $p<0.05$). Data were normalized to the total EGFR present and compared using stimulated and crosslinked R1-6-EGFR as a baseline.

This result rules out the possibility of EGFR R1-6 autophosphorylation as a monomer prior to formation of a stable dimer, since no phosphorylation was detected in any of the V948R mutants. Additionally, non-phosphorylated receptor dimers can be observed with the total EGFR antibody in both EGFR V948R and EGFR R1-6 V948R expressing cells following stimulation and crosslinking (Figure 2.4, lanes 8 and 9). This is reasonable, as ligand binding facilitates dimerization through the extracellular domain, and this provides direct evidence of dimer formation for this mutant. Curiously, these stimulated V948R dimer populations seem more stable than their non-V948R counterparts, as we can reliably detect stimulated, non-phosphorylated V948R dimers, but cannot always detect stimulated EGFR and EGFR R1-6 total EGFR dimers (J. Mohr, unpublished results). Furthermore, we occasionally observe EGFR V948R R1-6 dimers (Figure 2.4, lane 10), but are unable to reliably detect this population. Together, these results indicate that EGFR R1-6 requires dimerization to phosphorylate.

Inhibiting the extracellular dimer conformation inhibits EGFR R1-6 constitutive activation:

The EGFR 246-253* mutant alters key residues along the domain II dimerization arm that normally stabilize the extracellular dimer upon ligand binding. EGFR 246-253* is thus able to bind ligand, but unable to form an extracellular dimer. This mutation has been combined with clinically observed oncogenic EGFR mutants and has been shown to inhibit their constitutive activity[22,29]. We decided to use EGFR 246-253* to investigate if the extracellular dimer conformation was required for EGFR R1-6 phosphorylation.

Transient expression of EGFR in NIH 3T3 cells can lead to overexpression-induced receptor activation[20], which we observed in our cell lines. Transient transfections of NIH 3T3 cells with wild-type EGFR demonstrated basal receptor activation in the absence of ligand

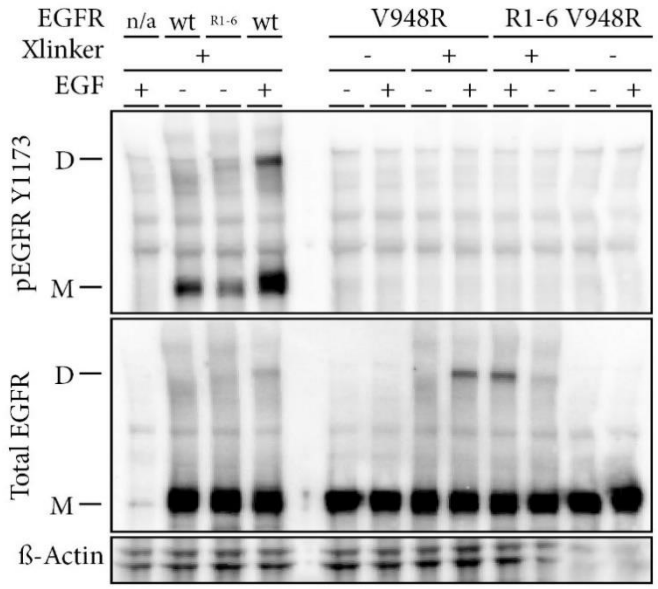

Figure 2.4: The asymmetric kinase conformation is required for EGFR R1-6 phosphorylation. Whole cell lysates from untransfected NIH 3T3 cells (n/a) or NIH 3T3 cells transiently expressing either EGFR, EGFR R1-6, EGFR V948R, and EGFR R1-6 V948R were stimulated with EGF and then chemically crosslinked with BS^3 prior to western blotting with the indicated antibodies. M and D indicate monomeric and dimeric EGFR, respectively.

(Figure 2.5). In our previous experiment, the V948R construct mechanistically prevents receptor phosphorylation, so a lack of phosphorylation is compelling evidence, since it also overcomes this background phosphorylation. However, EGFR 246-253* expressing NIH 3T3 cells demonstrated basal phosphorylation and made it difficult to draw conclusions about EGFR R1-6 246-253* in that context. This result was unexpected and suggests that the EGFR 246-253* mutation is not a dominant inactivator, but instead prevents the release of inhibition imposed by the extracellular domain. Thus, we decided to use RBL-2H3 cells because transient transfections result in lower protein expression with minimal spontaneous phosphorylation (Figure 2.6). We confirmed that RBL 2H3 cells do not exhibit basal wt EGFR phosphorylation (lane 6 vs. lane 1, Figure 2.7), and we detected EGFR R1-6 constitutive dimers (lane 4, Figure 2.5) that were also observed in the NIH 3T3 stables (Figure 2.2).

RBL 2H3 cells transiently expressing EGFR 246-253* or EGFR R1-6 246-253* were stimulated and chemically crosslinked with BS^3 as described earlier. Both EGFR 246-253* and EGFR R1-6 246-253* expressing cells failed to phosphorylate or form dimers, regardless of EGF stimulation and crosslinking (Figure 2.7, lanes 5-12). Wt EGFR exhibited phosphorylated monomers and dimers in response to EGF under these conditions, as expected (Figure 2.7, lane 4). Thus, extracellular domain dimerization is required for EGFR R1-6 phosphorylation and dimerization.

2.5 Discussion

The role of the JX domain in EGFR activation is complex and multi-faceted[12,14]. The JX domain is required for receptor activation[14], but the polybasic region within this domain is necessary to maintain basal receptor autoinhibition[15]. EGFR R1-6 demonstrates this property by using charge-

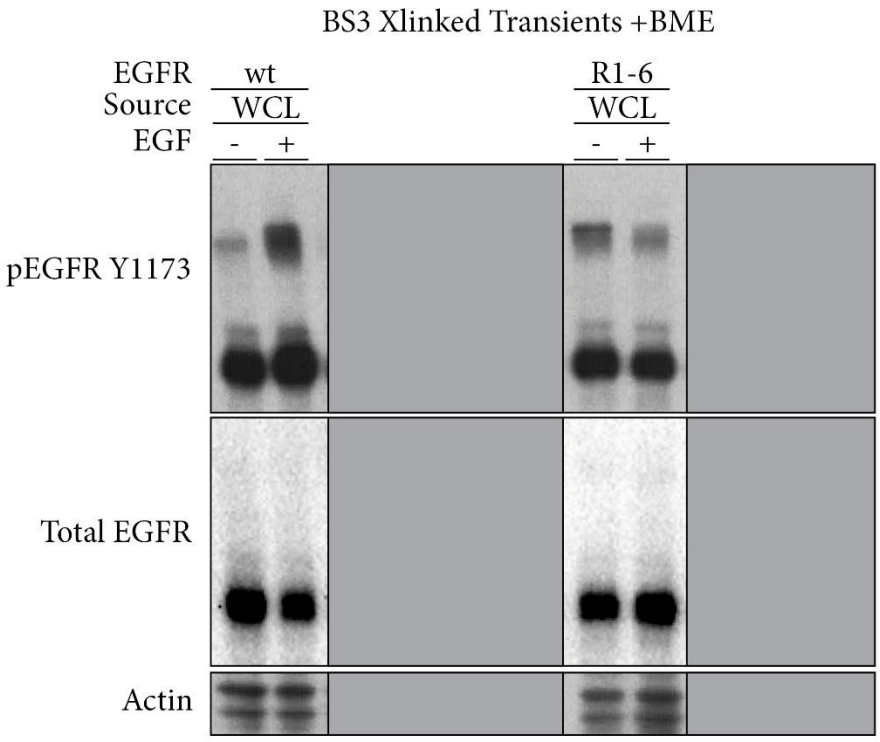

Figure 2.5: NIH 3T3 cell transiently expressing wt-EGFR are constitutively active. NIH 3T3 cells transiently expressing wt-EGFR demonstrate constitutive activation in the absence of ligand (left), likely due to overexpression.

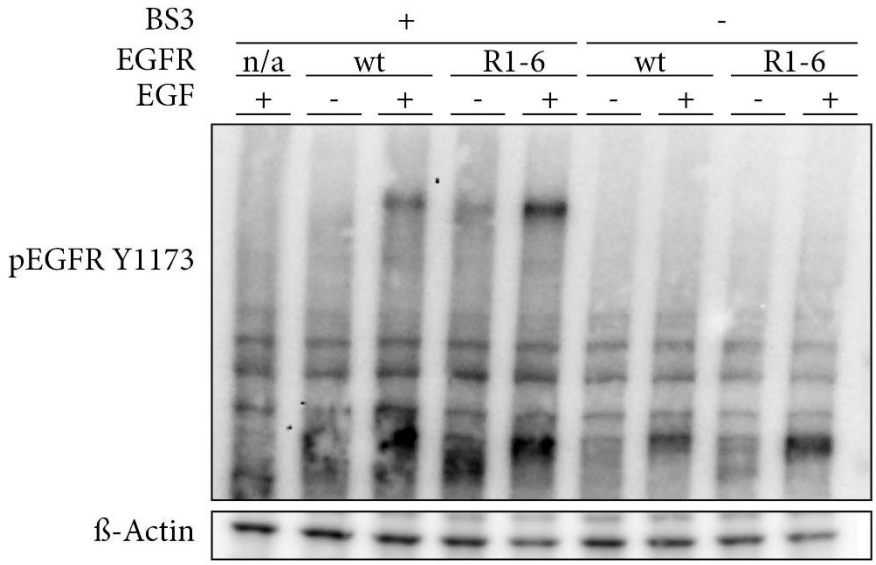

Figure 2.6: RBL-2H3 cells transiently expressing wt EGFR do not demonstrate consitutive activation.

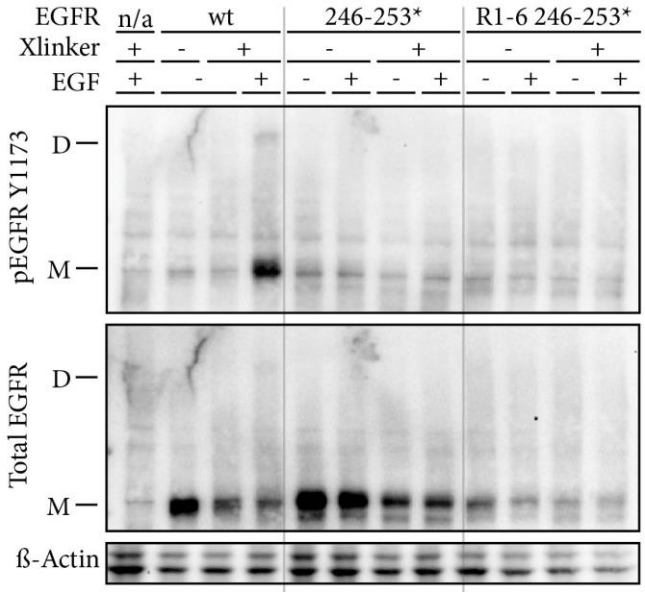

Figure 2.7: EGFR R1-6 requires an extracellular dimer in order to phosphorylate. Whole cell lysates from untransfected NIH 3T3 cells (n/a) or NIH 3T3 cells transiently expressing either EGFR, EGFR R1-6, EGFR 246-253*, and EGFR R1-6 246-253* were stimulated with EGF and then chemically crosslinked with BS^3 prior to western blotting with the indicated antibodies. M and D indicate monomeric and dimeric EGFR, respectively.

silencing alanine mutagenesis to reduce the overall charge of the polybasic region, which results in constitutive activation of the receptor[15]. Yet, how does charge neutralization result in receptor activation? We propose that the loss of the polybasic domain allows EGFR to bypass the initial ligand binding step and proceed directly to spontaneous receptor dimerization and activation. The results of this study support this conclusion.

Canonical receptor dimerization is initiated by ligand binding, which releases the dimerization arm and enables an outside-in mode of dimerization in which extracellular interactions drive the initial steps of dimerization (Figure 2.1A (a))[11,22]. In the case of EGFR L858R and EGFR ΔL747-P753insS, it has been shown that the functionality of the dimerization arm is necessary to maintain phosphorylation and dimerization. Thus, in these mutants, which bypass ligand binding, the dimer-stabilizing effects of the extracellular region are still required to maintain receptor activity. Therefore, we suspect these mutants may be signaling via an inside-out dimerization mechanism in which activation of the TKD drives dimerization of the intracellular components and then forces the extracellular domain into the dimer conformation, resulting in activated receptor dimers.

This inside-out model (Figure 2.8) is well suited for explaining EGFR activation due to charge-neutralization of the polybasic region. The electrostatic charge of the native sequence facilitates tight contact between the JX domain and negatively charged lipids in the plasma membrane[17,19]. Thus, loss of this electrostatic character would decrease the affinity of the JX domain for plasma membrane lipids in unstimulated receptors. We propose that this decrease in affinity enables a subset of receptors to spontaneously release their JX domains, and subsequently their TKDs, from the plasma membrane. Upon contacting another receptor, the JX and TKDs could progress through a series of reversible conformational changes until they form

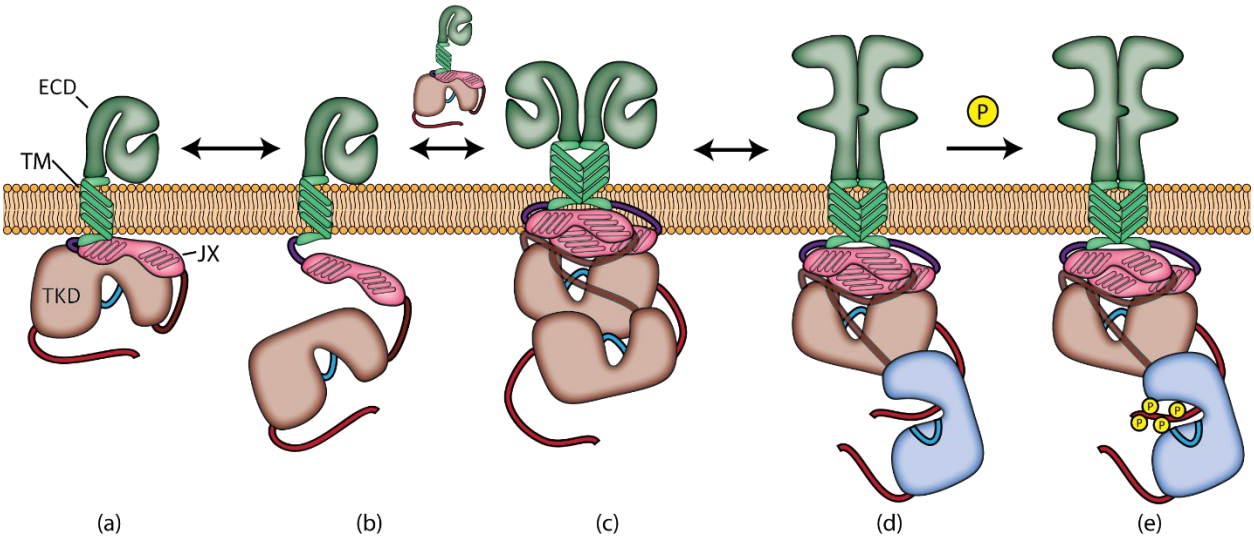

Figure 2.8: Proposed EGFR R1-6 activation scheme. Partial charge silencing of the JX domain (a) leads to spontaneous release of the TKD from the plasma membrane (b). This receptor can encounter another receptor and form an unstable intermediate dimer (c) with the capacity to rearrange into an active dimer (d). The active dimer can then stabilize itself by through phosphorylation (e) and recruitment of other signaling proteins.

an activated dimer, which stabilizes itself through autophosphorylation.

Our findings provide support for this model of inside-out activation. We directly observe phosphorylated dimers of EGFR R1-6 in unstimulated cells (Figure 2.2A), thus confirming the existence of the species proposed in Figure 2.8 (e). EGFR R1-6 forms constitutive dimers in unstimulated receptors (Figure 2.2A). Thus, there exists a mechanism that causes dimerization and phosphorylation of the receptor in the absence of ligand. Additionally, BS^3 crosslinks proteins over a distance of 11.4 Å, suggesting that the extracellular domains of the EGFR R1-6 are within this distance of each other. This provides evidence for possible interactions between the extracellular domains of the receptors and corroborates the data obtained from the EGFR 246-253* mutants (Figure 2.7). Thus, the extracellular domains are in putative contact and disrupting their ability to form dimers inhibits receptor phosphorylation and dimerization.

The EGFR R1-6 V948R asymmetric TKD mutants demonstrate a similar phenotype to 246-253*, but still form dimers in response to ligand stimulation. The EGFR R1-6 V948R data also negates the possibility of autophosphorylating monomers, since it showed no evidence of phosphorylated monomers. Thus, dimerization likely occurs prior to phosphorylation. Additionally, we demonstrated that both intact intracellular (Figure 2.4) and extracellular (Figure 2.5) regions are required for receptor activation (transition from Figure 2.7 (c) to (d)). In light of our data and the observations of other groups, we believe that EGFR requires dimerization of both intracellular and extracellular domains in order to form a functional receptor (Figure 2.8 (d)).

The methods employed in this study primarily characterize ensemble averages of EGFR, with a binary readout for dimerization and activity. They allow insight into, but not precise determination of, receptor conformations. Thus, EGFR R1-6 signals like wt EGFR that has

bypassed the first step of ligand binding and behaves similarly to other observed activating EGFR homodimers. We conclude that the loss of electrostatic charge in the polybasic region of the JX domain allows the receptor to initiate reversible conformational changes that culminate in irreversible receptor phosphorylation. We hypothesize this is due to spontaneous release of the TKD from the membrane and subsequent release of that autoinhibitory mechanism.

Homo- and hetero- receptor dimerization within the ErbB family of receptor tyrosine kinases has emerged as a major component of oncogenic signaling[26]. Heterodimers, in particular, have been implicated as a means of chemoresistance in many cancers as they are often able to compensate for weaknesses and dysfunctions in the component receptors that a homodimer may not[31]. In response, recent advances in chemotherapy have demonstrated that mixed therapies which simultaneously target multiple members of the ErbB family have greater efficacy than therapies targeting single receptors[24]. An improved understanding of receptor activation, structure, and function is necessary to continue advancing these strategies. This study contributes to this understanding by linking the polybasic region of the JX domain to EGFR receptor activation and function and providing a better understanding of the mechanism by which this segment regulates EGFR activation.

2.6 Supplementary Information

In addition to the previous findings, we investigated several other methods for assessing dimerization of EGFR receptors, but was unable to obtain definitive results in these endeavors.

Measuring receptor dimerization using a probability model and immunoprecipitation of

heterolabeled receptors.

One metric of interest we pursued was trying to address the question of "what fraction of EGFR are in dimers?" in a cell. This question is difficult to assess because it requires an accurate measurement of both monomeric and dimeric EGFR. To address this, NIH-3T3 cells were transiently co-transfected with HA- and FLAG-tagged EGFR constructs (wt or R1-6 EGFR-HA and EGFR- FLAG), immunoprecipitated for FLAG, and immunoblotted for HA and FLAG. These blots were measured using densitometry to generate a relative ratio of HA to FLAG to identify the proportion of hetero-dimers pulled down.

Proof of concept:

EGFR-HA can only be pulled down is if it is in a dimer with EGFR-Flag. This information can then be combined in a probabilistic model to calculate the fraction of the EGFR population that has dimerized. Briefly, the total FLAG and HA are measured with the whole cell lysate, and, since the co-IP can only pull-down HA as a dimer, it is possible to determine how much EGFR had to be dimerized to generate the observed co-IP HA signal, after normalizing to the observed FLAG in the co-IP. This can be expressed mathematically as the following.

Assume that there is no significant preference for homodimer formation over heterodimer formation, that antibody signal intensity responses are similar, and that HA can only be pulled down as a heterodimer in the anti-flag precipitation. The latter two assumptions can be accounted for with appropriate controls. Given the total expression levels from whole cell lysates intensities from an immunoblot, WCL_{FLAG} and WCL_{HA}, and the pull-down intensities from an anti-FLAG IP immunoblot, IP_{FLAG} and IP_{HA}. Then, from a binomial distribution we can calculate the expected fraction of HA-FLAG heterodimers out of all possible dimers as,

$$Expected\ Fraction\ of\ Heterodimers = \frac{2WCL_{FLAG}WCL_{HA}}{(WCL_{FLAG} + WCL_{HA})^2}.$$

For a fully dimerized population, then the maximum number of dimers would be

$$Maximum\ heterodimers = \frac{Expected\ Fraction \times Total}{2}$$

$$= \frac{\frac{2WCL_{FLAG}WCL_{HA}}{(WCL_{FLAG} + WCL_{HA})^2} \times (WCL_{FLAG} + WCL_{HA})}{2}$$

$$= \frac{WCL_{FLAG}WCL_{HA}}{WCL_{FLAG} + WCL_{HA}}.$$

Note that the above is divided by 2 because each dimer consists of two units from the original population.

We know from the IP the actual number of heterodimers observed in the population through the HA signal since we have assumed that HA can only be pulled down as a heterodimer with FLAG. Thus,

$$Observed\ Heterodimers = IP_{HA}$$

If we assume all the FLAG was pulled down in the IP, then we can normalize to the WCL with a normalizing factor of,

$$Normalizing\ Factor = \frac{WCL_{FLAG}}{IP_{FLAG}}.$$

Thus we can normalize the observed heterodimers as,

$$Normalized\ observed\ heterodimers = \frac{WCL_{FLAG}}{IP_{FLAG}} \times IP_{HA}.$$

Then the extent of dimerization will simply be the normalized observed heterodimers divided by the maximum possible heterodimers,

$$Relative\ Dimerization = \frac{Normalized\ observed\ heterodimers}{Maximum\ heterodimers}$$

$$Relative\ Dimerization = \frac{\frac{WCL_{FLAG}}{IP_{FLAG}} \times IP_{HA}}{\frac{WCL_{FLAG}WCL_{HA}}{WCL_{FLAG} + WCL_{HA}}}$$

$$= \frac{IP_{HA}}{WCL_{HA}} \times \frac{WCL_{FLAG} + WCL_{HA}}{IP_{FLAG}}$$

In reality, this analysis will capture all EGFR oligomers, but the analysis is robust in that it will still accurately quantitate the amount of oligomerization present since the ratio of HA to FLAG dictates the binomial distribution in a dimerized population and similarly it will dictate the combinatorial distribution of an oligomeric population. Probabilistically this boils down to accounting for the average values and will yield the same result in the presence of dimers or oligomers but will be unable to resolve dimers versus oligomers.

Unfortunately, transient expression of the wt-EGFR constructs led to over-expression based constitutive activation and we were unable to proceed further with this experiment.

Measuring EGFR R1-6 dimer conformations with FRET Probes

We attempted to create FRET probes of EGFR-AcGFP and EGFR-mRFP to measure conformational states of R1-6 compared to wt receptors. However, we were unable to create an EGFR-mRFP construct with plasma membrane localization. All of our attempts produced constructs that appeared to be trapped in the endoplasmic reticulum or other intracellular stores.

Comparing EGFR R1-6 to electrostatic treatments of wt-EGFR

Early on, we wanted to investigate whether electrostatic treatments of wt-EGFR could induce monomeric receptor activation. Part of this was based on a report that high molarity NaCl treatment could induce EGFR activation in the absence of ligand[32]. We used 1 M KCl to shock

the cells and measured pEGFR Y1173 via immunoblotting. We managed to observe monomeric phosphorylation of wt-EGFR in our first experiment (Figure 2.8) but were unable to replicate this result. All subsequent replicates showed no effect of KCl treatment in the absence of ligand. It is also possible that we were simply unable to detect dimers. The high salt concentration may have had some unpredicted effect on the chemical crosslinking, which we did not attempt to control for at the time. Eventually we answered this question by ruling out monomeric activation of R1-6 using EGFR V948R.

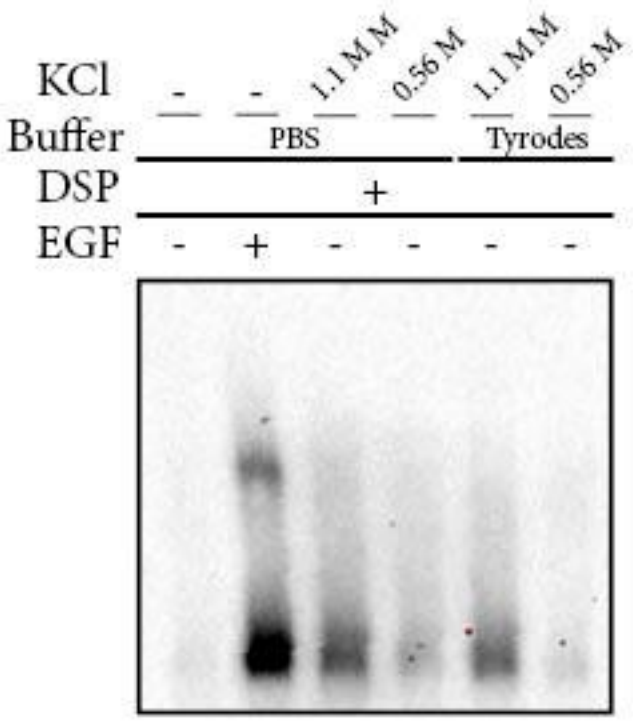

Figure 2.8: KCl electrostatic shock can induce monomeric receptor activation. A13 NIH 3T3 cells stably expressing wt-EGFR were treated with KCl or EGF as indicated in the indicated buffers and chemically crosslinked with DSP to trap receptor dimers.

REFERENCES

1. Lemmon, M. A. & Schlessinger, J. Cell signaling by receptor tyrosine kinases. *Cell* **141**, 1117–1134 (2010).
2. Zhang, H. *et al.* ErbB receptors: from oncogenes to targeted cancer therapies. *J. Clin. Invest.* **117**, 2051–8 (2007).
3. Endres, N. F., Barros, T., Cantor, A. J. & Kuriyan, J. Emerging concepts in the regulation of the EGF receptor and other receptor tyrosine kinases. *Trends Biochem. Sci.* **39**, 437–446 (2014).
4. Sliwkowski, M. X. *et al.* Coexpression of erbB2 and er6B3 proteins reconstitutes a high affinity receptor for heregulin. *J. Biol. Chem.* **269**, 14661–14665 (1994).
5. Moriki, T., Maruyama, H. & Maruyama, I. N. Activation of preformed EGF receptor dimers by ligand-induced rotation of the transmembrane domain. *J. Mol. Biol.* **311**, 1011–1026 (2001).
6. Zhang, X., Gureasko, J., Shen, K., Cole, P. A. & Kuriyan, J. An Allosteric Mechanism for Activation of the Kinase Domain of Epidermal Growth Factor Receptor. *Cell* **125**, 1137–1149 (2006).
7. Huse, M. & Kuriyan, J. The Conformational Plasticity of Protein Kinases. *Cell* **109**, 275–282 (2002).
8. Jura, N. *et al.* Catalytic Control in the EGF Receptor and Its Connection to General Kinase Regulatory Mechanisms. *Mol. Cell* **42**, 9–22 (2011).
9. Hubbard, S. R. & Till, J. H. Protein Tyrosine Kinase Structure and Function. *Annu. Rev. Biochem.* **69**, 373–398 (2000).
10. Lemmon, M. a, Schlessinger, J. & Ferguson, K. M. The EGFR family: not so prototypical

receptor tyrosine kinases. *Cold Spring Harb. Perspect. Biol.* **6**, a020768 (2014).

11. Kancha, R. K., von Bubnoff, N. & Duyster, J. Asymmetric kinase dimer formation is crucial for the activation of oncogenic EGFRvIII but not for ERBB3 phosphorylation. *Cell Commun. Signal.* **11**, 39 (2013).
12. Doerner, A., Scheck, R. & Schepartz, A. Growth Factor Identity Is Encoded by Discrete Coiled-Coil Rotamers in the EGFR Juxtamembrane Region. *Chem. Biol.* **22**, 776–784 (2015).
13. Hedger, G., Sansom, M. S. P. P. & Koldsø, H. The juxtamembrane regions of human receptor tyrosine kinases exhibit conserved interaction sites with anionic lipids. *Sci. Rep.* **5**, 1–10 (2015).
14. He, L. & Hristova, K. Consequences of replacing EGFR juxtamembrane domain with an unstructured sequence. *Sci. Rep.* **2**, 854 (2012).
15. Bryant, K. L., Antonyak, M. A., Cerione, R. A., Baird, B. & Holowka, D. Mutations in the polybasic juxtamembrane sequence of both plasma membrane- and endoplasmic reticulum-localized epidermal growth factor receptors confer ligand-independent cell transformation. *J. Biol. Chem.* **288**, 34930–34942 (2013).
16. Huang, Y. *et al.* Molecular basis for multimerization in the activation of the epidermal growth factor receptor. *Elife* **5**, 1–27 (2016).
17. Abd Halim, K. B., Koldsø, H. & Sansom, M. S. P. P. Interactions of the EGFR juxtamembrane domain with PIP2-containing lipid bilayers: Insights from multiscale molecular dynamics simulations. *Biochim. Biophys. Acta - Gen. Subj.* **1850**, 1017–1025 (2015).
18. Gambhir, A. *et al.* Electrostatic sequestration of PIP2 on phospholipid membranes by

basic/aromatic regions of proteins. *Biophys. J.* **86**, 2188–207 (2004).

19. Arkhipov, A. *et al.* Architecture and membrane interactions of the EGF receptor. *Cell* **152**, 557–69 (2013).
20. Endres, N. F. *et al.* Conformational coupling across the plasma membrane in activation of the EGF receptor. *Cell* **152**, 543–56 (2013).
21. Jura, N. *et al.* Mechanism for Activation of the EGF Receptor Catalytic Domain by the Juxtamembrane Segment. *Cell* **137**, 1293–1307 (2009).
22. Dawson, J. P. *et al.* Epidermal Growth Factor Receptor Dimerization and Activation Require Ligand-Induced Conformational Changes in the Dimer Interface. *Mol. Cell. Biol.* **25**, 7734–7742 (2005).
23. Gosse, J. J. a, Wagenknecht-Wiesner, A., David Holowka, Baird, B. & Holowka, D. Transmembrane Sequences Are Determinants of Immunoreceptor Signaling. *J. Immunol.* **175**, 2123–31 (2005).
24. Pines, G., Köstler, W. J. & Yarden, Y. Oncogenic mutant forms of EGFR: Lessons in signal transduction and targets for cancer therapy. *FEBS Lett.* **584**, 2699–2706 (2010).
25. Chakraborty, S. *et al.* Constitutive and ligand-induced EGFR signalling triggers distinct and mutually exclusive downstream signalling networks. *Nat. Commun.* **5**, 5811 (2014).
26. Wang, Z. *et al.* Mechanistic insights into the activation of oncogenic forms of EGF receptor. *Nat. Struct. Mol. Biol.* **18**, 1388–93 (2011).
27. Poger, D. & Mark, A. E. Activation of the epidermal growth factor receptor: a series of twists and turns. *Biochemistry* **53**, 2710–21 (2014).
28. Cochet, C. *et al.* Demonstration of epidermal growth factor-induced receptor dimerization in living cells using a chemical covalent cross-linking agent. *J. Biol. Chem.* **263**, 3290–5

(1988).

29. Valley, C. C. *et al.* Enhanced dimerization drives ligand-independent activity of mutant EGFR in lung cancer. *Mol. Biol. Cell* **26**, (2015).

30. Coban, O. *et al.* Effect of Phosphorylation on EGFR Dimer Stability Probed by Single-Molecule Dynamics and FRET/FLIM. *Biophys. J.* **108**, 1013–1026 (2015).

31. Shan, Y. *et al.* Oncogenic mutations counteract intrinsic disorder in the EGFR kinase and promote receptor dimerization. *Cell* **149**, 860–70 (2012).

32. King, C., Borrello, I., Porter, L., Comoglio, P. & Schlessinger, J. Ligand-independent tyrosine phosphorylation of EGF receptor and the erbB-2/neu proto-oncogene product is induced by hyperosmotic shock. *Oncogene* **4**, 13–18 (1989).

CHAPTER 3

FORMINS AND ARP2/3 EXHIBIT DIFFERENTIAL ROLES IN FcεRI SIGNALING

3.1 Abstract

We examined potential roles for the actin regulatory protein (Arp2/3) and formins in immunoglobulin E (IgE) receptor (FcεRI) signaling in RBL-2H3 mast cells. We used microfabricated 2,4-dinitrophenyl (DNP) ligand-patterned features to observe the recruitment of Arp2/3 and other proteins to FcεRI signaling complexes. Pharmacological inhibition of Arp2/3 or formins revealed differential roles in FcεRI signaling. Arp2/3 and formins cooperate to recruit F-actin to patterned ligand features and then demonstrate differential roles in phosphotyrosine labeling, Ca^{2+} signaling, and degranulation. We also present a novel use of ligand-patterned features to demonstrate the exclusion of a model transmembrane phosphatase from FcεRI clusters. Together, our results reveal new roles for actin polymerization in FcεRI signaling.

3.2 Introduction

The principal mechanism underlying the allergic response is antigen-mediated clustering of the high-affinity receptor for immunoglobulin E (IgE), FcεRI, receptor in mast cells leading to the release of preformed chemical mediators through degranulation[1,2]. FcεRI also serves as a model immunoreceptor due to its many similarities with B-cell and T-cell signaling pathways.

FcεRI activation requires mobilization and reorganization of the plasma membrane, receptors, enzymes, and vesicles within the cell. Activation begins when IgE bound to FcεRI is crosslinked by multivalent antigen, leading to recruitment of Lyn tyrosine kinase, which is anchored to the membrane by saturated fatty acid chains. This results in phosphorylation by Lyn

of ITAMs (immunoreceptor tyrosine-based activation motifs) in the β and γ subunits of the receptor. The phosphorylated γ-ITAMs recruit Syk kinase (spleen tyrosine kinase) which in turn phosphorylates LAT (linker for activation of T-cells), SLP-76 (SH2 domain-containing leukocyte protein of 76 kDa, also referred to as LCP2) and PLCγ-1 (phospholipase Cγ-1). LAT and SLP-76 go on to form key structural components of the FcεRI signaling complex while PLCγ-mediated hydrolysis of hydrolysis of PIP_2 (phosphatidylinositol 4,5-bisphosphate) into DAG (diacylglycerol) and IP_3 (inositol 1,4,5-trisphosphate) initiates the Ca^{2+} response and degranulation[1].

Prior to antigen stimulation, FcεRI probably exists in a dynamic state of phosphorylation via Lyn kinase and dephosphorylation via a transmembrane phosphatase. This delicate balance maintains receptor homeostasis in the absence of ligand and is thought to be mediated by lipid domains[3] – receptor clustering stabilizes an ordered lipid (Lo-like) domain that preferentially recruits Lyn kinase[4] and excludes transmembrane phosphatases leading to sustained receptor phosphorylation. PTPα (protein tyrosine phosphatase α) has been used as a proxy for a transmembrane phosphatase in FcεRI signaling[5].

In addition to its structural function, the cytoskeleton is involved in mobilizing the cell and plasma membrane to engage antigen, fuse granular vesicles, and reorganize membrane proteins. Due to these functions, the actin cytoskeleton appears to play a prominent role in FcεRI activation. Past studies have used the actin-polymerization inhibitors cytochalasin D (Cyto D – binds the barbed end of F-actin to prevent polymerization) and latrunculin (binds monomeric g-actin to prevent polymerization) to investigate receptor phosphorylation, duration[6] and kinetics[7] of phosphotyrosine signaling, assembly of the signaling complex[8], antigen sensitivity[9], organization of functional lipid domains[6,10,11], degranulation[12], and many other facets of FcεRI

signaling. It is clear from these studies that the actin cytoskeleton plays a key role in targeting and regulating FcεRI signaling.

While many of the functional aspects of F-actin roles have been identified, the underlying mechanisms are still poorly defined. Actin polymerization in eukaryotic cells is predominantly catalyzed through either F-actin filament branching via Arp2/3 (actin regulatory proteins 2 and 3) or filament extension via the formins family of enzymes[13]. These two mechanisms of actin polymerization are competitive and are temporally exclusive in macrophage immune cell signaling[14], in which activation of the Fcγ receptor in macrophages activates Arp2/3 and inhibits formins. Furthermore, perturbations in one system can lead to compensatory effects in the other[15]. In contrast, it has been shown in T cells that Arp2/3 and formins cooperate to form spatially distinct actin networks[16,17] to transport T cell receptor (TCR) clusters along the immunological synapse[18]. Arp2/3 has been shown *in vitro* to be recruited to LAT through a multi-protein complex of LAT, Gads (Grb2 related adaptor protein), SLP-76, Nck (non-catalytic region of tyrosine kinase adaptor protein), and WASP (Wiskott-Aldrich syndrome protein)[19].

Antigen-stimulation of FcεRI creates signaling receptor nanoclusters[20], the majority of which exist below the diffraction limit of conventional microscopy. To overcome this limitation, we have previously demonstrated the use of micron-scale, ligand-patterned features to investigate membrane receptor signaling[7,8,21–23]. These features, when presented to IgE-sensitized cells, allow us to observe non-diffraction limited, micron-sized clusters of IgE-FcεRI and allow quantitative assessment of protein recruitment with greater sensitivity than traditional approaches because large complexes can form and are stabilized.

Here we demonstrate recruitment of the Arp2/3 complex in RBL-2H3 mast cells and investigate the functional roles of Arp2/3 and formins in a model mast cell system using a

combination of pharmacological inhibitors and microfabricated patterned ligand surfaces. Two pharmacological inhibitors of these pathways are commercially available and provide an opportunity for connecting actin polymerization mechanisms to FcεRI signaling. CK666 is an Arp2/3 inhibitor that stabilizes the inactive state of the complex[24] and SMIFH2[25] (small molecular inhibitor of formin homology 2 domains) inhibits the conserved FH2 catalytic domain of formins.

We show that Arp2/3 and its associated proteins co-cluster with activated FcεRI on ligand-patterned features. We also show that Arp2/3 and formins exhibit differential roles in FcεRI activation at the levels of F-actin recruitment, tyrosine phosphorylation, Ca^{2+} signaling, and degranulation. We show how ligand-patterned features can be used to identify exclusion of proteins from sub-feature-size clusters, and we demonstrate that PTPα is selectively excluded from FcεRI signaling clusters. These findings demonstrate recruitment of Arp2/3 to FcεRI and expands the roles of actin polymerization in FcεRI receptor activation.

3.3 Methods

All cell culture reagents as well as Alexa Fluor 488-labeled goat anti-mouse IgG2b (γ2b) antibody and Alexa Fluor 488-labeled phalloidin were purchased from Invitrogen. All chemicals and inhibitors, unless stated otherwise, were purchased from Sigma-Aldrich. The formin inhibitor SMIFH2 was purchased from Millipore. FuGENE HD was purchased from Promega. 4G10 anti-phosphotyrosine antibody was purchased from Millipore. 35 mm CELLSTAR® culture dishes were purchased from Greiner Bio-One North America, Inc. 35 mm No 1.5 coverslip 10 mm glass diameter uncoated culture dishes (MatTEK dishes), and 35 mm 10 mm hole dishes were purchased from MatTEK Corporation. 150 mm culture dishes were purchased

from Corning.

DNP-BSA was made by conjugating DNP sulfonate (Sigma-Aldrich) to BSA[21] (Sigma-Aldrich), for a yield of ~15 DNP per BSA (as determined by UV-vis spectroscopy). Alexa Fluor 488 IgE was made by conjugating Alexa Fluor 488 NHS ester (Invitrogen) to purified mouse monoclonal anti-DNP IgE[26] as previously described[27]. Using a similar method, Alexa Fluor 647 BSA was made by conjugating Alexa Fluor 647 NHS ester to BSA.

The 1,2-dipalmitoyl-sn-glycero-3-phosphoethanolamine-N-[6-[(2,4-dinitrophenyl)amino]hexanoyl] (DNP-cap-DPPE), 1-palmitoyl-2-oleoyl-sn-glycero-3-phosphocholine (POPC), and 1,2-dioleoyl-sn-gly cero-3-phosphoethanolamine-N-(lissamine rhodamine B sulfonyl) (LissRhod DOPE) were purchased from Avanti Polar Lipids.

Expression Plasmids:

The cDNA constructs for Grb2-Emerald GFP[28] (Grb2-EmGFP), EGFP-Gads[28], SLP76-Emerald GFP[28] (SLP-76 EmGFP), YFP-NCK1[29], and ADAP-mCFP[30] were gifts from L. Samelson (NIH). GFP-NWASP[31] and GFP-Arp3[31] were gifts from A. Weaver and D. Webb (Vanderbilt University). GCaMP3 has been described previously[32].
ADAP-EGFP was cloned from ADAP-mCFP into pEGFP-N1 vector (ClonTech) using the BamHI and AgeI restriction sites.

PTPα-EGFP was cloned from a PTPα vector[5] into an mEos3.2[11] (LifeAct) vector provided by Sarah Veatch (University of Michigan) using NheI and XhoI restriction sites to create PTPα-mEos. mEos was then swapped with mCherry using XhoI and NotI restriction sites to create PTPα-mCherry. Then mCherry was swapped with EGFP from the pEGFP-N1 vector using XhoI and NotI to create PTPα-EGFP. PM-PTPα-EGFP was created by using the NheI and

XhoI sites to swap PM-PTPα[5] into the pEGFP-N1 vector. All cloning described was performed by Alice Wagenknecht-Wiesner.

Cell Culture and Transfection:

RBL-2H3 cells were maintained as monolayer cultures in MEM containing 20% (vol/vol) fetal bovine serum (FBS) and 50 µg/mL gentamycin. Cells were harvested near 80% confluence using trypsin-EDTA, as previously described[10].

Grb2-EmGFP, EGFP-Gads, SLP76-EmGFP, and YFP-NCK1 were transfected using chemical transfection. A complex of 1-2.5 µg of cDNA with 8-10 µL FuGENE HD in 100 µL Opti-MEM was added to a 35 mm culture dish of RBL-2H3 cells (~60-75% confluence) in 1 mL of Opti-MEM for 1 h. GCaMP3 was transfected using a larger scale chemical transfection: a 150 mm culture dish of ~60-75% confluent RBL-2H3 cells in 10 mL Opti-MEM was chemically transfected with a complex of 10 µg GCaMP3 cDNA and 80 µL FuGENE HD in 1 mL Opti-MEM for 1 h. In both cases phorbol dibutyrate (0.1 µg/mL) was then added for 3 h to stimulate DNA uptake. Cells were returned to 20% serum medium for overnight expression and used the following day.

ADAP-EGFP, PTPα-EGFP, PM-PTPα-EGFP, GFP-Arp3, and GFP-NWASP were transfected by electroporation[33]. 10 µg of cDNA were added to 1 x 10^7 RBL-2H3 cells in 500 µL cold electroporation buffer (137 mM NaCl, 2.7 mM KCl, 1 mM MgCl2, 1 mg/ml glucose, 20 mM HEPES (pH 7.4)) at 280 V and 950 µF use Gene Pulser X (Bio-Rad). Cells were resuspended in 6 mL full serum media and plated into three separate MatTEK dishes (2 mL/dish). Their media was exchanged after 1 hr and cells were allowed to recover overnight for use the following day.

Pharmacological Inhibitors:

All drug treatments use the following concentrations of inhibitor: Cytochalasin D (Cyto D, actin polymerization inhibitor, IC50: 25 nM): 2 µM. CK666 (Arp2/3 inhibitor, IC50: 4 µM): 10 µM. SMIFH2 (small molecular inhibitor of formin homology 2 domains, formin inhibitor, IC50: 10 µM): 25 µM. The exception is the degranulation assay where a variety of inhibitor concentrations was used to generate a dose-response curve.

Patterned ligand microfabrication and functionalization:

The preparation of microfabricated ligand patterned surfaces by our lab has been previously described[7,8,23,34]. Briefly, fused silica (glass) wafers were coated with a 1-µm-thick layer of parylene-C (diX C parylene dimer [Kisco] and an SCS Labcoter Parylene Deposition System), then an ~40-nm-thick layer of antireflective coating (AR3 DUV Anti-Reflectant, Shipley), and finally, a 1-µm-thick layer of photoresist (UV210; Dow Chemical, and Suss MicroTec Gamma Cluster Tool). Multiple patterned arrays were created in the photoresist layer using a predesigned photomask and exposure to 248-nm light (ASML PAS 5500/300C DUV Stepper). An oxygen-based reactive-ion etch (Oxford 81 Etcher) transferred the features from the patterned photoresist to the underlying parylene layer. Through this etching step, exposed regions of glass masked by the parylene were made available for chemical modification and the presentation of selected biomaterial, including ligands for specific receptors. This fabrication process was performed by Meraj Ramezani.

Parylene-patterned wafers and were stored in a desiccator for long-term storage. Individual patterned segments were then cut from the wafer and rinsed sequentially with DI

water, isopropanol, acetone, and DI water to remove any remaining photoresist. They were then glued to 35 mm 10 mm hole dishes (MatTEK) using NOA 68T UV-curable adhesive (Norland Products, Inc), and then stored in a desiccator until functionalization.

Patterns were functionalized with supported lipid bilayers (SLBs) via small unilamellar lipid vesicle (SUV) fusion[35] immediately prior to use in experiments. The patterns adhered to 35 mm dishes were sequentially washed with DI water, isopropanol, 1:1 methanol:concentrated HCl, and DI water and then oxygen plasma cleaned (Harrick Plasma Basic Plasma Cleaner) twice for 30 sec each. A sufficient volume of SUVs to cover the pattern (~60 µL) was added and incubated for 15 minutes to form the SLB. Excess SUVs were removed by rinsing with DI water. Care was taken during these rinsing to not expose the SLB to air during and after this step to prevent lipid oxidation. The parylene layer was then removed using tweezers and rinsed with 10 mg/mL BSA in PBS and incubated in 1 mg/mL BSA for 10 minutes to reduce non-specific binding around the patterned features. The pattern was then rinsed with buffered saline solution (BSS 135 mM NaCl, 5.0 mM KCl, 1.8 mM CaCl2, 1.0 mM MgCl2, 5.6 mM glucose, and 20 mM HEPES, pH 7.4) for use with cells.

Preparation of small unilamellar lipid vesicles (SUVs) for supported lipid bilayers

Briefly, SUVs were created by mixing chloroform stocks of POPC, DNP-Cap-DPPE, and LissRhod-DOPE in a ratio of 89.9:10:0.1 mol% (DNP-SLB) or 99.9:0:0.1 mol% (SLB no DNP) respectively. The mixture was then dried under a stream of nitrogen gas and further dried under vacuum for 2 h to ensure complete evaporation of the chloroform. The mixture was then resuspended in Tris buffer (50 mM Tris and 200 mM NaCl, pH 8) and vortexed for several minutes to produce a cloudy lipid suspension. The suspension was probe-sonicated (Sonics &

materials) in an ice bath until clear, or ~15 minutes. The clear solution was then briefly centrifuged and filtered through a 0.2 µm pore Acrodisk syringe filter to remove any particulates. This SUV suspension was then stored at 4°C under nitrogen and parafilm for up to two weeks.

Glass surface protein functionalization:

Glass bottom MatTEK dishes were functionalized with DNP-BSA, Alexa Fluor 647 BSA, and unlabeled BSA for Ca^{2+} imaging. MatTEK dishes were rinsed and plasma cleaned as in the initial steps of SLB preparation. After plasma cleaning, dishes were incubated with a 4% (vol/vol) MPTS ((3-mercaptopropyl)trimethoxysilane) solution in ethanol for 30 min, rinsed with ethanol several times and then incubated with 4 mM GMBS (N-γ-maleimidobutyryl-oxysuccinimide ester) in DMF (dimethylformamide) for 30 min. Dishes were then washed with PBS and covered in a sufficient amount (~60 µL) of protein mixture containing 5:25:20 µg/mL DNP-BSA:Alexa Fluor 647 BSA:BSA (50 µg/mL total) for 2 hours at room temperature. This DNP-BSA concentration has been optimized to promote homogeneous IgE recruitment and to maximally stimulate tyrosine phosphorylation, as measured by 4G10 labeling (Figure 3.8), and Ca^{2+} responses (not shown). The dishes were then washed and stored in 1 mg/mL BSA in PBS at 4°C until use.

Cell incubation on patterns, immunolabeling, and fluorescence microscopy:

RBL-2H3 cells were harvested and resuspended in BSS, sensitized with Alexa Fluor 647-IgE for 1 hr at 37°C, and then added to SLB patterns in the presence of drug (DMSO vehicle/Cyto D/CK666/SMIFH2) and allowed to settle for 40 min at 37°C. Cells were then fixed in 4% paraformaldehyde and 0.025% glutaraldehyde in PBS for 10 min, blocked in 10 mg/mL

BSA for 5 min, and rinsed multiple times with 1 mg/mL BSA in PBS.

For 4G10 immunolabeling, cells were labeled with 1 µg/mL 4G10 and 0.1% Triton X-100 in 1 mg/mL BSA in PBS for 1 hour. After additional washing, cells were labeled with 2 µg/mL Alexa Fluor 488 goat anti-mouse IgG2b (γ2b) secondary in 1 mg/mL BSA in PBS for 1 hour. Cells were then washed multiple times and stored at 4°C until imaging.

For phalloidin labeling, cells were labeled with 1 U/µL Alexa Fluor 488 phalloidin and 0.1% Triton X-100 in 1 mg/mL BSA in PBS for 1 hour, washed multiple times, and stored at 4°C until imaging.

Cells were imaged with either a Zeiss LSM i710 confocal microscope or Zeiss LSM i880 confocal microscope. Images of cells on patterned features were taken with a 63x (i710) or 40x (i880) oil Plan-Apochromat objective lens using a DF 488/561/647 filter set. For the Ca^{2+} experiments, time lapses were taken on the i710 using a 40x water immersion objective at 30 frames/s with a DF 488/647 filter set and transmitted light capture.

Patterned feature and cell scoring:

For cases of counting the colocalization of fluorescent probes with patterned ligand features, a cell was considered for scoring if it landed on a pattern and showed IgE recruitment to two patterned ligand features (or 30% of the features in cases where cells dock with 5 or more features). A cell was counted positive if at least two (or 30%, as above) of its patterned features have simultaneous colocalization of IgE, DNP, and probe of interest, and counted negative if not. A slight exception to this is for 4G10 and phalloidin labeling where Triton X-100 permeabilization stripped the supported lipid bilayers. In these cases, the pattern features are inferred from IgE recruitment. The structured nature of the patterns makes this a robust

assumption.

Ca^{2+} Imaging:

RBL-2H3 cells transiently expressing GCaMP3 were pre-treated with drugs (DMSO vehicle/Cyto D/CK666/SMIFH2) for at least 15 minutes. Meanwhile, the focal plane of the microscope was adjusted to detect the BSA-647 functionalized glass. Cells were then added during a time course series to detect when cells first engaged the surface. Cells were imaged for 10 minutes at high gain to capture any Ca^{2+}oscillations and then 10 minutes at a lower gain to detect oscillations in any potentially saturated cells. Cells were then treated with 10 µM ionomycin to release intracellular Ca^{2+} stores to identify transfected cells and measure GCaMP3 expression.

Ca^{2+} lag time Analysis:

Individual cells were masked in NIH ImageJ FIJI and their average GCaMP3 fluorescence per frame was recorded. A baseline for each cell's background was established and the first significant deviation above this baseline was used as a first pass to identify cell-engagement with the surface. This time point was then compared with the transmitted light channel to confirm cell-engagement. If the first pass failed, then an engagement time was manually assigned using the transmitted light channel. Next the first frame of the first Ca^{2+} increase above that cell's baseline was identified. Cells that did not demonstrate any changes in Ca^{2+} levels were excluded from this analysis. The time difference between engagement and this time point was defined as the lag time.

Irregular Ca^{2+}Oscillation Characterization:

The GCaMP3 fluorescence per frame described above was used to characterize Ca^{2+} oscillations as either regular or irregular. Only cells that responded were considered. Regular oscillations were defined as periodic oscillations with narrow bases (typically lasting 10-15 sec). Irregular oscillations were defined as any significant increases in GCaMP3 fluorescence that did not meet the above criteria. This includes non-periodic responses, responses with varying baselines, very broad oscillation bases (typically greater than 30 sec), or cells that increased in fluorescence and failed to oscillate at all.

β-hexosaminidase degranulation assay and analysis:

RBL-2H3 cells were plated onto a 96-well plate at 5 x 10^5 cells/well and allowed to attach overnight. The following day, cells were rinsed with 1 mg/mL BSA in BSS and treated with increasing concentrations of drug (in sextuplicate) for 5 minutes prior to stimulation with 1 ng/mL DNP-BSA. The Cyto D curve ranged from 10 nM -10 μM while CK6666 and SMIFH2 ranged from 0.1-100 μM. Control lanes with no cells (background), unstimulated cells (negative control), and Triton X-100 treated cells (positive control) were included on all plates. β-hexosaminidase release was assessed as described previously[36].

Sextuplicate data were averaged and degranulation was normalized per day by subtracting the background group's fluorescence and dividing through by the Tx-100 treatment group (representing a %-maximal response). Drug curves followed similar trends between days, but the raw values varied from day-to-day. Each day's data was normalized to its untreated, stimulated control to account for this variance.

Colocalization Analysis of PTPμ:

A mask for the patterned feature regions was generated by thresholding the lissamine rhodamine channel in NIH ImageJ FIJI and cleaned to include only on-pattern regions. Masks of individual cells were then combined (AND) with the pattern feature mask to generate single cell collections of patterned features. These features were then analyzed using FIJI's Coloc 2 colocalization plugin to correlate the IgE and fluorescent construct channels. This represents a measure of colocalization of the two channels restricted to areas over the pattern per cell. One Pearson correlation coefficient representing all the patterned features in contact with the cell was recorded per cell.

4G10 Ratiometric Analysis:

The Trition X-100 treatment for 4G10 labeling results in a near complete-loss of the lissamine rhodamine channel for SLB patterned features. We used the IgE channel to infer the location of patterned features by overlaying a grid of patterned features using Aleksandr Mironov's Multiple Circles Grid plugin for ImageJ to generate a "pattern mask". Masks for the IgE and 4G10 channels were generated by thresholding and combined (AND) with the pattern feature mask to generate a mask representing points of colocalization of IgE and 4G10 on patterned features. This mask was deemed the "on-pattern mask" and allows us to focus on bright, stimulated clusters without counting dim, unstimulated pixels. Next, each individual cell was masked and thresholded against background (to generate crisp cell edges and avoid counting dim non-cellular regions). The pattern mask was then subtracted from the cell mask to generate an "off-pattern" mask. Note that this subtraction inherently makes on- and off-pattern masks mutually exclusive, so as to avoid double counting. The on-pattern average fluorescence was

then divided by the off-pattern average fluorescence to generate an on-off ratio.

Ratios demonstrated similar trends between drug treatments each day, but the absolute values of the trends varied due to day-to-day differences in 4G10 labeling. As such, we normalized each day's dataset by dividing through by the average ratio of the control group for that day. This results in a non-intuitive "normalized on-off ratio" near 1 for the controls, but actually represents a 2-6 fold increase in fluorescence depending on the labeling effectiveness.

Statistics:

All counting methods were treated as pooled proportion data sets and analyzed for statistical significance using ANOVA with a Tukey post-hoc multiple comparisons significance test. The exception to this is Figure 3.1b where no comparisons were made because differences between construct localizations likely represent differences in expression and fluorophore efficiency rather than biological differences.

Individual cell data (box plots - Figure 3.3b, Figure 3.4c, Figure 3.6b) were first tested for normality using a Shapiro-Wilkes test, which revealed them to all be non-normally distributed. They were then analyzed for statistical significance with a conservative method using a Kruskal-Wallis non-parametric test followed by a Dunn post-hoc significance test and adjusted with the Benjamini-Hochberg FDR (false discovery rate) for multiple comparisons. Complete statistical comparisons are provided in the supplementary materials.

3.4 Results

The Arp2/3 actin assembly complex is recruited to patterned ligand features.

In T-cells, the Arp2/3 complex is recruited to the T cell receptor (TCR) signaling

complex through the sequential interactions of LAT, Gads, Slp-76, Nck, and WASP[19,37,38], which have also been implicated in FcεRI signaling in mast cells[39–42]. Based on previous evidence of interactions between FcεRI and the actin cytoskeleton[6,7,9,11,12], the broad similarities between FcεRI and T-cell signaling[43,44], and the observed recruitment of Arp2/3 to the TCR signaling complex, we sought to determine if the Arp2/3 actin assembly complex is recruited to FcεRI in a similar manner in RBL-2H3 cells.

We observed the colocalization of the Arp2/3 actin assembly complex of Gads, SLP-76, Nck, N-WASP (Neural Wiskott-Aldrich Syndrome Protein, a commonly used homolog of the immune cell-specific WASP), and Arp3 (a key component of the Arp2/3 complex) to patterned lipid bilayers presenting the DNP ligand (Figure 3.1). Briefly, RBL-2H3 cells were transiently transfected with fluorescent constructs, sensitized with Alexa Fluor 647-labeled anti-DNP IgE, incubated for 40 min with lissamine rhodamine-labeled, DNP-functionalized supported lipid bilayer (DNP-SLB) patterned features, and fixed prior to imaging. Data were collected from at least three independent experiments. The ordered array of patterned ligands enables rapid visual scoring of labeled protein construct recruitment. Cells with visible IgE colocalization to patterns (representing cells that engaged ligand) were considered for scoring, and cells with construct-IgE colocalization were scored positive while cells without construct colocalization were scored negative.

Gads, SLP-76, Nck, N-WASP, and Arp3 all colocalize with IgE and ligand-patterned features (Figure 3.1a). The recruitment of Arp3 suggests that FcεRI clusters in mast cells recruit Arp2/3 and likely represents a link between FcεRI signaling and actin cytoskeleton polymerization. Furthermore, in combination with our previous finding of LAT recruitment to similar patterned features[8], the recruitment of Gads, SLP-76, Nck, and NWASP suggests the

recruitment of Arp2/3 may be similar for mast cells and T-cells.

We also observed recruitment of Grb2 (growth factor receptor-bound protein 2), an adaptor protein involved in FcεRI signaling and other phosphotyrosine signaling pathways[39]. Further, we observed recruitment of ADAP (adhesion and degranulation-promoting adapter protein), a protein involved in TCR signaling[37,45,46], but whose role has not yet been defined in mast cells. Cytoplasmic EGFP and PTPα were included as negative controls, neither of which were detectably recruited to patterned features. PTPα is a transmembrane protein phosphatase, which we showed inhibits FcεRI phosphorylation and used as an experimental proxy for an unidentified phosphatase that acts on Lyn-phosphorylated FcεRI5.

Using our scoring method, we quantified the extent of protein recruitment to patterned features (Figure 3.1b), confirming that Gads, SLP-76, Nck, N-WASP, Arp3, Grb2, and ADAP all colocalize with clustered IgE. Thus, the signaling complex that assembles appears similar to that observed for TCR after engagement of ligands on a surface. Because our ability to detect each of these constructs depends partially on expression levels and fluorescence brightness, we refrain from interpreting any quantitative differences between recruited proteins.

Arp2/3 and formins facilitate actin recruitment to patterned ligand features.

We considered potential functional roles for the Arp2/3 complex in FcεRI signaling and also whether a functional distinction could be made between formin-catalyzed actin extension and Arp2/3-catalyzed actin branching. Normally, formins and Arp2/3 cooperate to maintain actin homeostasis in cells[13,14], and inhibition of one system may lead to compensation by the other[15]. We employed targeted formin or Arp2/3 inhibitors to characterize the role of actin polymerization in signaling downstream of FcεRI clustering to activate cells.

Figure 3.1: The Arp2/3 actin assembly complex and associated proteins are recruited to DNP-SLB patterned features. (a) RBL-2H3 mast cells transiently expressing the indicated constructs (cyan) were sensitized with anti-DNP Alexa Fluor 647 IgE (green), allowed to settle DNP-SLB patterned features (red), incubated for 40 min, and fixed prior to imaging; representative images are shown (scale bar = 5 μm). (b) Plot of fraction of cells with indicated construct localizing to patterned features together with IgE. Total cell counts, collected over 3 independent experiments are listed above bars. (Error bars = SEM).

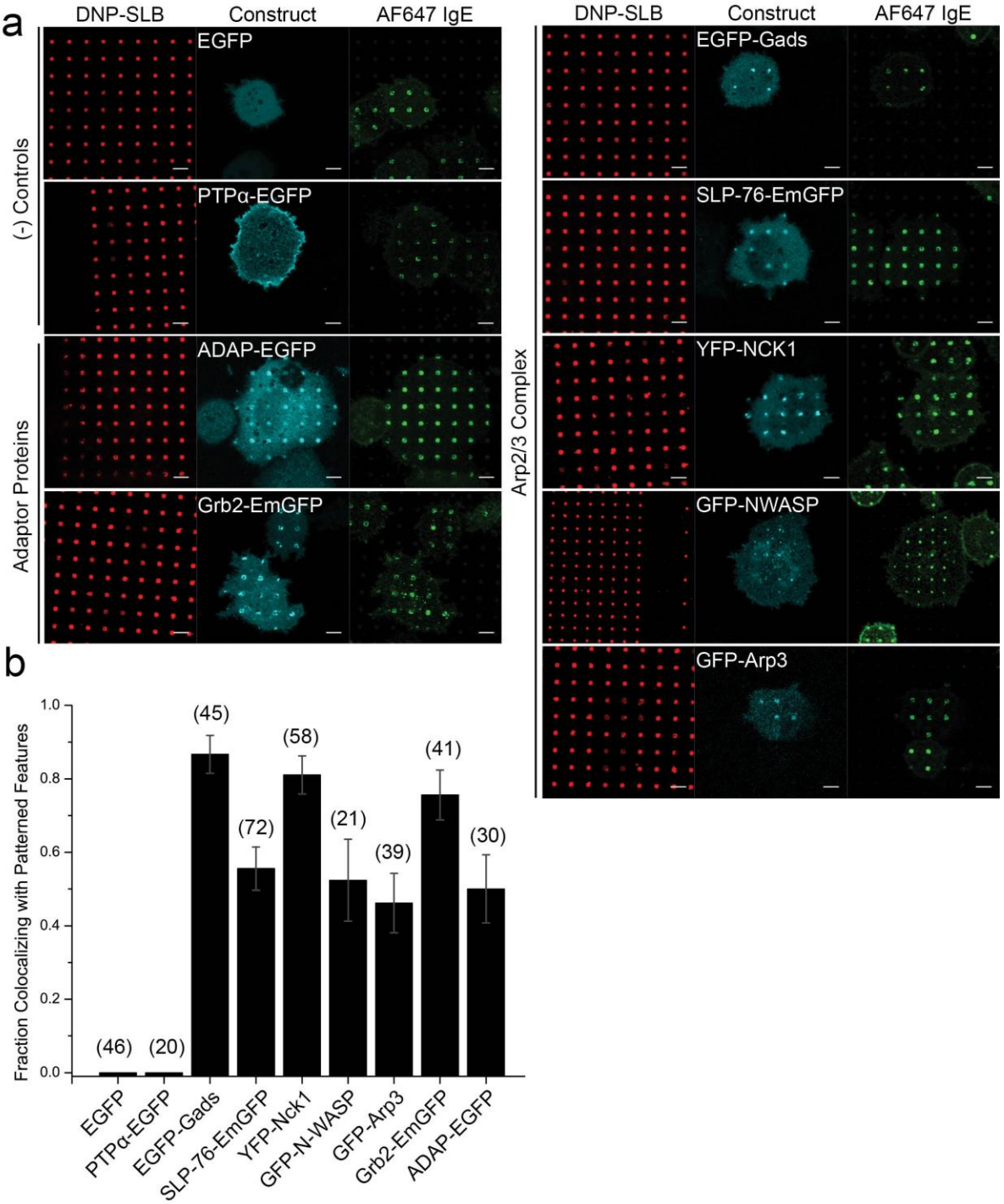
a
DNP-SLB
Construct
AF647 IgE
(-) Controls
EGFP
PTPα-EGFP
Adaptor Proteins
ADAP-EGFP
Grb2-EmGFP
Arp2/3 Complex
EGFP-Gads
SLP-76-EmGFP
YFP-NCK1
GFP-NWASP
GFP-Arp3
b
Fraction Colocalizing with Patterned Features
1.0
0.8
0.6
0.4
0.2
0.0
(46)
(20)
(45)
(72)
(58)
(21)
(39)
(41)
(30)
EGFP
PTPα-EGFP
EGFP-Gads
SLP-76-EmGFP
YFP-Nck1
GFP-N-WASP
GFP-Arp3
Grb2-EmGFP
ADAP-EGFP

To determine whether Arp2/3 activity is necessary to recruit actin to the FcεRI signaling complex we treated RBL-2H3 cells with Cyto D (a general actin polymerization inhibitor), CK666 (an Arp2/3 inhibitor), SMIFH2 (a formin inhibitor), or vehicle (DMSO). We incubated treated cells with DNP-SLB patterned ligand surfaces, then fixed and labeled them with Alexa Fluor 647 phalloidin to identify filamentous F-actin (Figure 3.2a).

Similar to our previous studies[21], 50% of cells treated only with vehicle show F-actin recruitment to patterned ligand-IgE-FcεRI clusters (Figure 3.2b). This recruitment is significantly reduced by treatment with Cyto D. Cyto D treated cells consistently show spindle-like actin formations, do not spread much after contacting the surface, and have small, irregularly shaped ventral surfaces. They also appear fluorescently dimmer relative to the cells treated with the other inhibitors, suggesting that this non-specific polymerization inhibitor yields less F-actin overall. Interestingly, both CK666 and SMIFH2 treatment cause reductions in F-actin recruitment similar to Cyto D (Figure 3.2b), suggesting both formins and Arp2/3 cooperate in the recruitment of actin to patterned features and FcεRI. We also tested the inactive variant CK689 to control for potential off-target effects and found no difference between CK689 treated cells and control cells (supplementary information, Figure 3.9).

We also observed distinct morphological differences between inhibitor-treated cells. One feature of FcεRI activation is spreading of the mast cell after engaging an antigen-presenting surface. SMIFH2 and Cyto D-treated cells fail to spread on surfaces while CK666-treated cells spread normally. SMIFH2-treated cells have smooth, round ventral surfaces compared to the irregular, spindly ventral surfaces of Cyto D-treated cells (Figure 3.2a). Thus, it appears that formins and not Arp2/3 aid in cell spreading in these conditions and that this spreading is independent of F-actin recruitment to FcεRI clusters on patterned features.

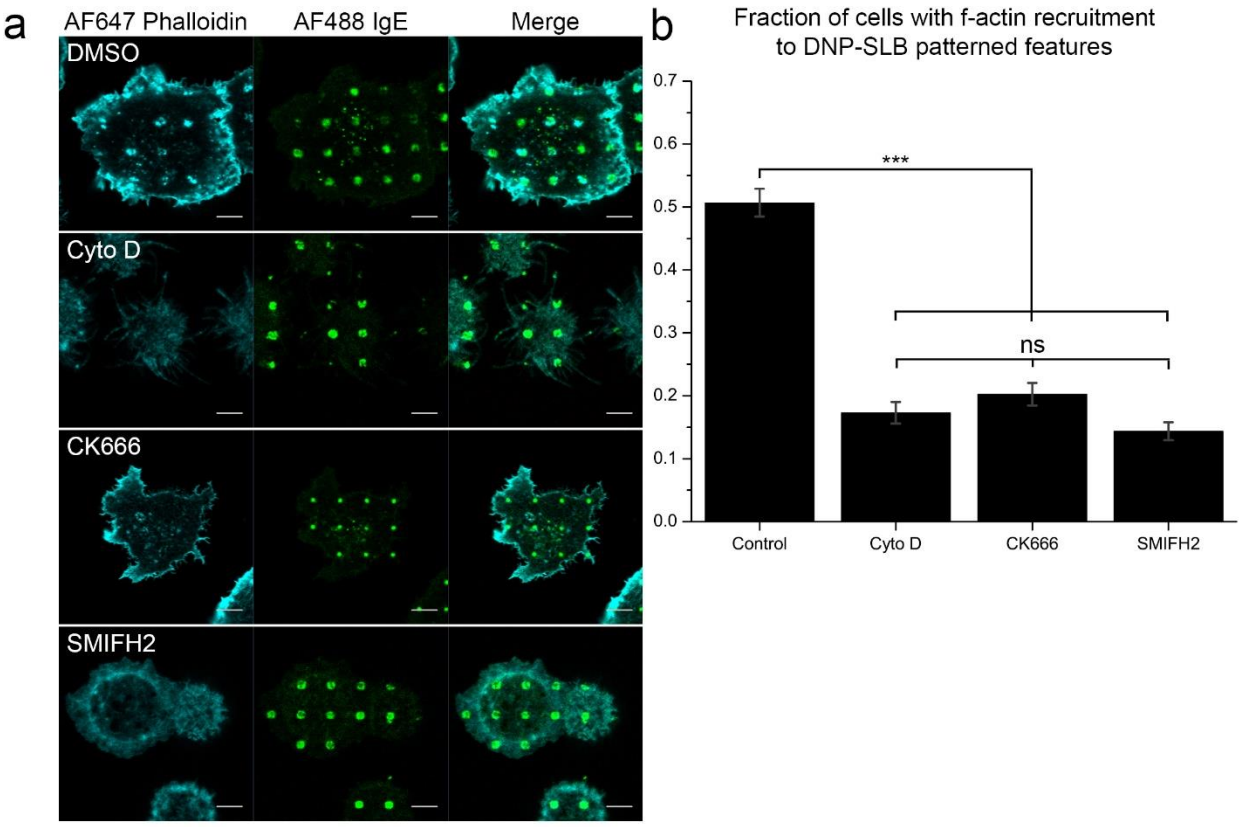

Figure 3.2: Actin polymerization inhibitors block F-actin recruitment to DNP-SLB patterned features. RBL-2H3 cells sensitized with Alexa Fluor 488 IgE were incubated with DNP-SLB patterns for 40 min, then fixed and labeled with Alexa Fluor 647 phalloidin. (a) Representative images of cells treated with DMSO (vehicle) or actin polymerization inhibitors as indicated (scale bar = 5 μm). (b) Scored fractions of cells with f-actin localizing with clustered IgE-FcεRI on patterned features; ~500 cells per treatment over 3 independent experiments. Error bars represents SEM, and *** corresponds to $p < 0.001$ as compared to other treatments.

The reduction of F-actin recruitment to FcεRI clusters by both CK666 and SMIFH2 suggests that both Arp2/3 and formins cooperate in this process. However, it is still unclear what role this recruitment has in FcεRI-mediated signaling. Cyto D treatment has been shown to enhance phosphorylation of receptor clusters, degranulation, and Ca^{2+} signaling[6,12], and we investigated the effects of CK666 and SMIFH2 inhibition on these functional aspects of signaling.

Arp2/3 facilitates formation of phosphorylated clusters while formins enhance phosphorylation within clusters.

Antigen stimulation of FcεRI leads to receptor clustering and tyrosine phosphorylation of multiple proteins within the signaling treated with one of the three actin inhibitors and incubated on DNP-SLB patterned features for 40 minutes prior to labeling with the anti-phosphotyrosine antibody 4G10 (over three independent experiments). Cells were then scored for 4G10 recruitment to patterned features (Figure 3.3a).

76% of untreated control cells showed phosphotyrosine labeling at patterned features persisting after the 40-minute incubation time. Cyto D and CK666 treatment significantly reduced this recruitment to 57% and 51% while SMIFH2 treatment did not significantly affect recruitment. The timepoint at which this measurement was recorded (40 min) is relatively late compared to our previous finding that phosphorylation occurs as early as 5 minutes[7]. Thus, differences between these conditions may reflect changes to the long-term stability of the complex, the cell's capacity to form the initial complex, or a combination of multiple effects. The results suggest that Arp2/3, more than formins, is involved in proximal signaling and the

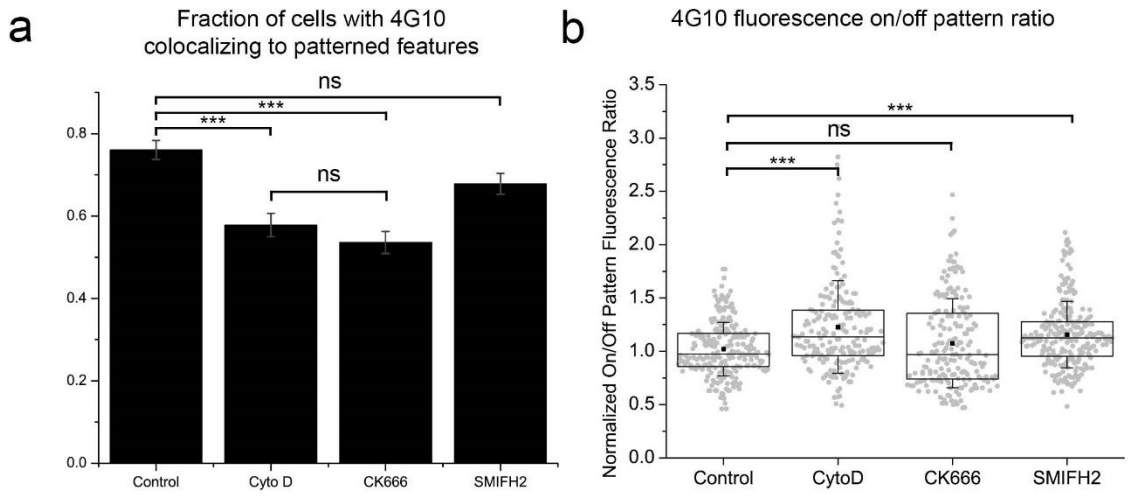

Figure 3.3: Cyto D and CK666 inhibit 4G10 recruitment to patterned features while Cyto D and SMIFH2 enhance 4G10 labeling of clusters. RBL-2H3 cells sensitized with Alexa Fluor 647 IgE, incubated with DNP-SLB patterns for 40 min, then labeled with 4G10 anti-phosphotyrosine antibody and Alexa Fluor 488 secondary antibody. (a) Fraction of cells with 4G10 recruitment to patterned features following treatment with specified inhibitor; ~300 cells per treatment over 3 independent experiments. Statistical comparisons are available in the supplemental materials (error bars = SEM). (b) 4G10 fluorescence colocalizing with IgE on patterns was compared to 4G10 fluorescence off-pattern per cell, and this ratio was normalized to control cells on that day. Control cells had average on/off ratios ranging from 2-6. All comparisons represent significant differences, except where indicated (box = 25-75% range, error bar = SD, line = median, square = average, *** corresponds to $p < 0.001$).

formation of stable FcεRI clusters.

Phosphotyrosine recruitment was also quantitatively measured in positive cells by calculating the fluorescence ratio of on-pattern fluorescent clusters to off-pattern fluorescence. These fluorescence ratios varied between days due to differences in labeling efficiency, so each day's data was normalized to the average of that experiment's untreated control sample. Cyto D and SMIFH2 treatments enhance 4G10 labeling on patterned features by 15-20% per day (Figure 3.3b) while CK666 treatment appears to have no effect. This suggests that formins, more than Arp2/3, are involved in regulating phosphorylation within the signaling cluster.

The actin cytoskeleton has been shown to stabilize signaling clusters and enhance the recruitment of the signaling proteins LAT[8] and PLCγ[8] to patterned features. Conversely, the actin cytoskeleton has also been implicated in inhibiting Lyn recruitment to FcεRI nanoclusters[11]. Although Lyn plays a significant role in FcεRI signaling through initial phosphorylation of Syk and ITAMs to initiate signaling, it also plays a subsequent inhibitory role through the activation of inhibitory molecules and phosphatases[1,47]. Thus, Arp2/3-mediated actin polymerization likely affects the actin structure associated with long-term functional signaling apparatuses, possibly through stabilizing the complex, while formins may be promoting the long-term recruitment and activation of Lyn kinase and facilitating its down regulatory functions.

Formins promote Ca^{2+} signaling and quality

We further investigated the roles of Arp2/3 and formins by measuring single cell Ca^{2+} responses to surface-presented antigen. FcεRI crosslinking by multivalent antigen ultimately leads to the recruitment of PLCγ to the receptor cluster and the hydrolysis of PIP_2 into DAG and IP_3. IP_3 is released into the cytosol where it interacts with the ER-membrane protein

IP_3 receptor to release Ca^{2+} stores and trigger degranulation.

RBL-2H3 cells expressing the cytoplasmic Ca^{2+} indicator GCaMP3 were pre-treated for at least 15 minutes with Cyto D, CK666, SMIFH2, or DMSO (vehicle), then dropped onto glass MatTEK dishes modified with covalently attached DNP-BSA for live imaging over 20 minutes. Then the Ca^{2+} ionophore ionomycin was added to identify GCaMP3 expressing cells.

The fraction of responding cells was calculated by comparing the number of cells demonstrating Ca^{2+} responses to the total number of transfected cells in the field ($n > 50$ cells per treatment over three experiments). We found that 64% of GCaMP3 expressing cells respond to surface ligand presentation in the vehicle control group (Figure 3.4a). Cyto D treatment enhances the number of responding cells, which is consistent with Cyto D enhancing whole population Ca^{2+} mobilization[12]. CK666 treatment results in a non-significant increase in the number of responding cells while SMIFH2 treatment significantly reduces the number of responding cells. These results suggest that formins and Arp2/3 cooperate in triggering Ca^{2+} responses.

Because some cells exhibited irregular Ca^{2+} responses, we characterized responding cells as having either regular (periodic) oscillatory responses, or irregular (irregular periodicity, broad peaks, or bright fluorescence with no oscillations). We found that a significant number of responding cells treated with Cyto D (33%) and SMIFH2 (77%) generated irregular, periodic Ca^{2+} responses, compared to control (11%) and CK666 (20%) (Figure 3.4b). Combined, these data suggest that formins are involved in initiating Ca^{2+} responses and assuring the quality of these responses.

We also observed the morphology and spreading of these cells to confirm they were healthy and that these irregularities were not due to other effects. All cells demonstrated similar morphologies similar to those described for the phalloidin labeling (Figure 3.2a). Control and

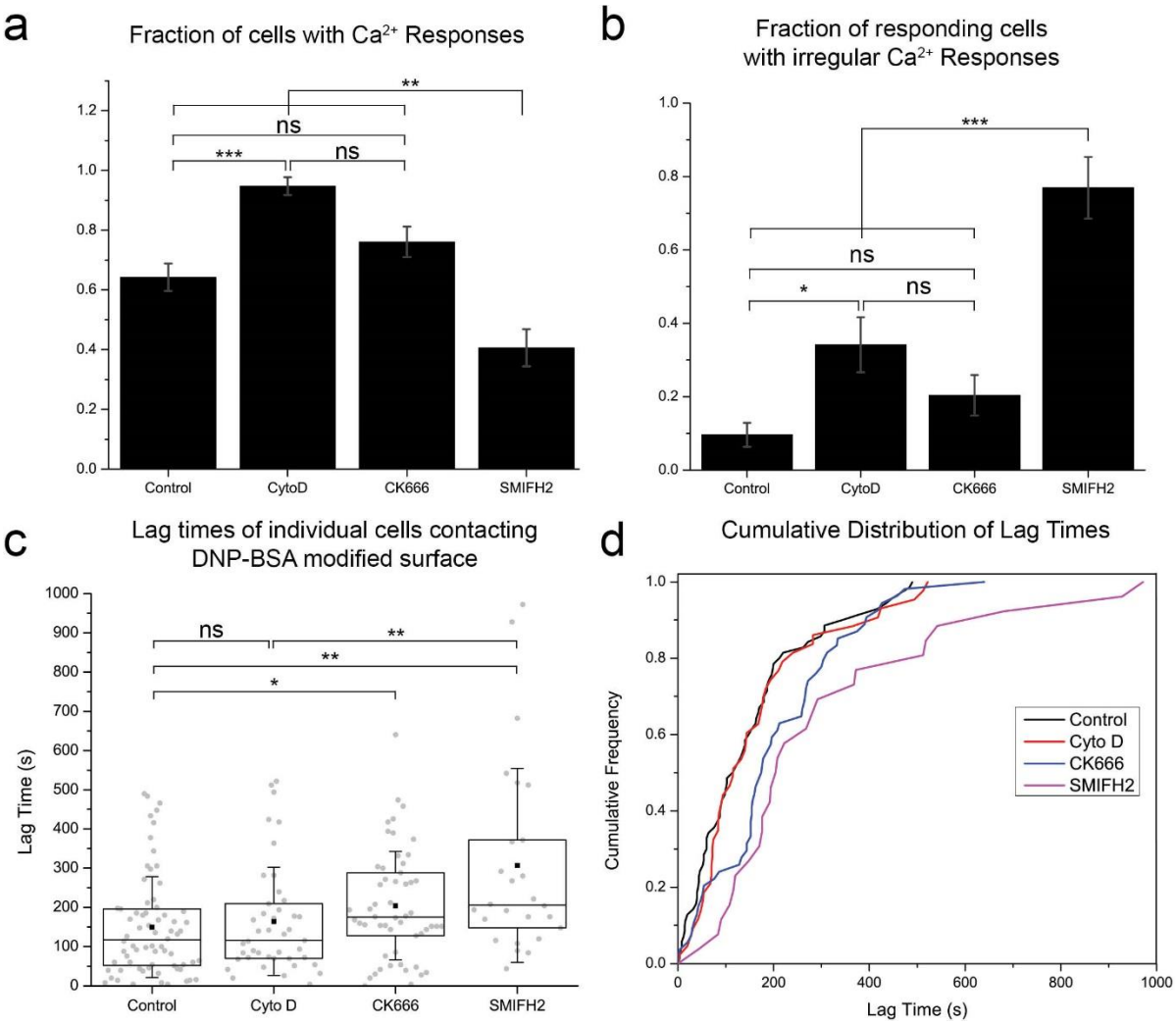

Figure 3.4: SMIFH2 impairs Ca^{2+} signaling. RBL-2H3 cells expressing GCaMP3 were recorded landing on a DNP-BSA modified glass surface using confocal microscopy and imaged for an additional 20 minutes; ~50-100 cells per treatment over 3 independent experiments. (a) Fraction of cells showing Ca^{2+}responses before conclusion of imaging (error bars = SEM, * corresponds to $p < 0.05$, ** to $p < 0.01$, and *** to $p < 0.001$). (b) Fraction of responding cells with irregular Ca^{2+} responses (error bars = SEM). (c) Lag times of Ca^{2+} responses of individual cells (box = 25-75% range, error bar = SD, line = median, square = average). (d) Cumulative distribution of the data in (c).

CK666 cells spread normally and quickly after coming into contact with the surface while Cyto D and SMIFH2 cells spread briefly after contacting the surface but then remain rounded throughout imaging. There were no morphological signs of poor cell health in counted cells.

Arp2/3 facilitates rapid initiation of the Ca^{2+} response

We calculated lag times for each responding cell by determining the time between when a cell landed on the surface and when it showed its first Ca^{2+} increase. Lag time represents the time required for the cell to engage ligand, assemble the FcεRI signaling complex, activate PLCγ, and hydrolyze PIP_2 into IP_3. Control and Cyto D treated cells responded with similar lag times with a median of 116 sec (Figure 3.4c). CK666 and SMIFH2 treatment significantly increased lag time relative to control cells (median lag times of 175 sec and 206 sec respectively).

Conversion of this data to a cumulative frequency (Figure 3.4d) indicates that CK666 treatment results in two populations of cells: one that responds similarly to the control cells (<90 sec), and another that responds much slower (>120 sec). One possibility is that Arp2/3 activity lowers an activation barrier without compromising the ability of cells to mount oscillatory Ca^{2+} responses.

Formins promote degranulation

We investigated potential roles of Arp2/3 and formins in degranulation. Degranulation is the process through which mast cells fuse pre-formed vesicles of chemical mediators to their membranes to release their contents into the extracellular environment. This process is initiated by Ca^{2+} release and represents a complex process of mobilizing vesicles, reorganizing the cytoskeleton, and many other factors. Because of the complexity of the response and how far

downstream it is from FcεRI clustering, it is difficult to assign the effects of an inhibitor to a direct mechanism of action. However, we can look at the dose-response curve of an inhibitor to identify a broad effect on degranulation.

RBL-2H3 cells were treated with increasing concentrations of inhibitors and then stimulated for 1 hour at 37°C with 1 ng/mL DNP-BSA antigen. Untreated, stimulated baseline cells ranged from 20%-50% β-hexosaminidase release relative to Tx-100 treated cells. This day-to-day variance was reflected in all conditions but did not change the day-to-day trends observed by treatments. The data were normalized by dividing each day through by its untreated, stimulated baseline (representing 100% on the plots, (Figure 3.5).

Cyto D treatment enhances degranulation, with maximal enhancement near the 1-2 μM concentration frequently used in the literature (Figure 3.5a). SMIFH2 treatment yielded a linear dose response curve with noticeable inhibition at concentrations ≥50 μM, while CK666 only inhibited at the highest concentration tested (Figure 3.5b). However, it is difficult to ascribe these results to a particular effect due to the complexity of degranulation. It is possible that the disruptions in Ca^{2+} signaling observed with SMIFH2 treatment in turn negatively impact degranulation. However, it is also possible that formin inhibition affects the cortical actin barrier to vesicle fusion. Given the complexity of degranulation, we conclude that formins play a role in promoting degranulation, but we cannot say conclusively what that role may be.

PTPα is excluded from FcεRI Clusters

As described above, PTPα-EGFP does not visibly co-localize with AF647-IgE-FcεRI on patterned DNP-SLBs of micrometer dimensions (Figure 3.3a). However, the PTPα-EGFP distribution is not perfectly uniform, and we investigated whether there may be a sub-micrometer

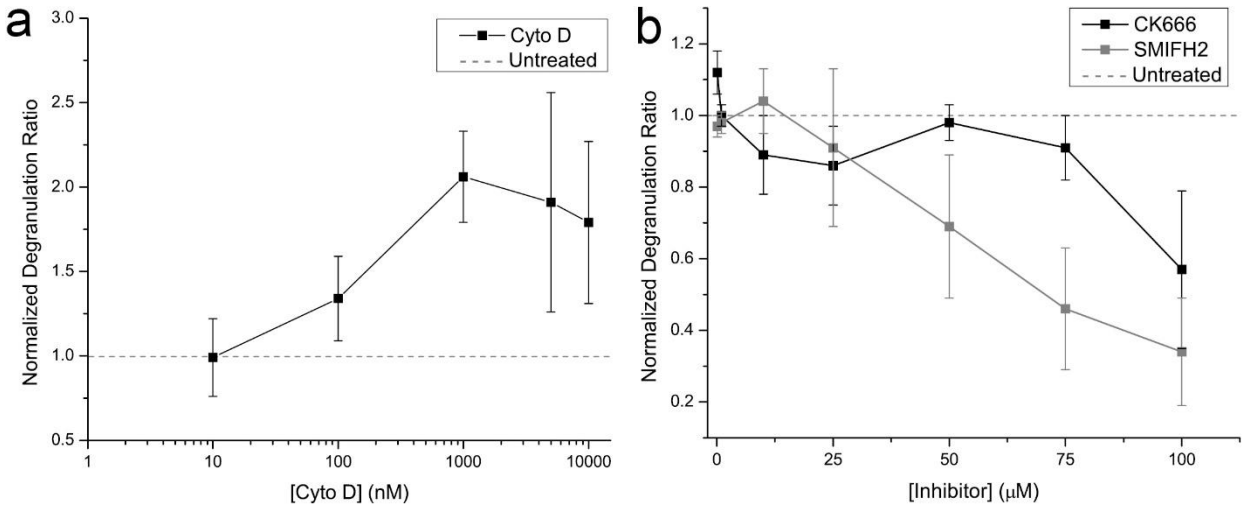

Figure 3.5: SMIFH2 inhibits degranulation. Normalized degranulation response curves of RBL-2H3 cells measuring β-hexosaminidase release in the presence of increasing concentrations of actin polymerization inhibitors. Cells were pre-treated with inhibitor for 5 minutes prior to stimulation and allowed to degranulate for 1 hour. β-hexosaminidase release was measured by fluorimetry as described previously[36]. Within each experimental group, a no-cell background control was subtracted from each condition and then divided through by a Tx-100-permeabilized positive control to assign each cell a raw 'degranulation response' value. These values were then normalized to the untreated, stimulated condition to account for day-to-day variability in the cells. (a) Effect of Cyto D treatment on degranulation. (b) Effect of CK666 or SMIFH2 treatment on degranulation (error bars = SD of at least 3 independent experiments, dotted line represents untreated baseline).

spatial relationship between this transmembrane phosphatase and IgE-FcεRI. For this purpose, we quantified the distribution of each of these two probes, pixel-by-pixel on the patterned features. We found that both PTPα-EGFP and IgE-FcεRI distribute non-uniformly across the features (Figure 3.6a top). However, these two distributions are spatially exclusive (Figure 3.6a top - inlay). This is an intriguing observation, as a current model for FcεRI activation is that FcεRI clustering causes kinase recruitment and transmembrane phosphatase exclusion through the formation of a stable Lo domain around the receptor[3]. We quantified this exclusion by measuring Pearson Correlation Coefficients (PCC) values between IgE and PTPα (or other constructs of interest) on patterned features (Figure 3.6b). We determined that PTPα-EGFP has a median PCC value of -0.13 across the DNP-SLB features, corresponding to weak anticorrelation with FcεRI.

For comparison, we measured the PCC of PTPα-EGFP on patterned features of SLBs with no DNP ligand. Cells incubated with these surfaces show non-uniform distributions of both PTPα-EGFP and AF647-IgE-FcεRI (Figure 3.6a middle). In this case where IgE-FcεRI is not clustered by ligand we found PTPα-EGFP positively cross correlates (PCC = 0.23; Figure 3.6b), suggesting that PTPα more closely associates with FcεRI prior to stimulation. To compare this positive PCC value with a signaling protein that co-localizes with ligand-clustered IgE- FcεRI we evaluated SLP-76 (Figure 3.6a bottom) and determined a positive PCC (PCC = 0.30; Figure 3.6b). The similarities of these PCC values is consistent with PTPα colocalizing with FcεRI prior to stimulation, at this diffraction-limited level of resolution.

To test whether apparent spatial exclusion we observed between PTPα-EGFP and AF647-IgE-FcεRI (PCC = -0.13) is mediated by the liquid disordered (Ld)-preferring transmembrane portion of PTPα, we attached the cytoplasmic portion of PTPα-EGFP to the

Figure 3.6: PTPα is excluded from IgE clusters on DNP-SLB patterned features. RBL-2H3 cells transiently expressing PTPα-EGFP or other constructs were sensitized with Alexa Fluor 647 IgE, incubated with DNP-SLB patterned features for 40 min, fixed, and then imaged. (a) Representative images of transfected cells (scale bar = 5 μm). Inlay sec (right) of patterned feature emphasizes (yellow areas) of IgE-rich and PTPα-deficient regions. Overlap shows whether a pixel is IgE-rich (green), PTPα-rich (blue), deficient in both (white) or rich in both (orange). (b) Pearson Correlation Coefficients (PCC) of AF647-IgE-FcεRI and indicated constructs across all patterned features for individual cells; ~30-50 cells per treatment over 3 independent experiments. All differences not shown are significant (box = 25-75% range, error bar = SD, line = median, square = average, *,**,*** correspond to $p < 0.05$, 0.01, 0.001 respectively).

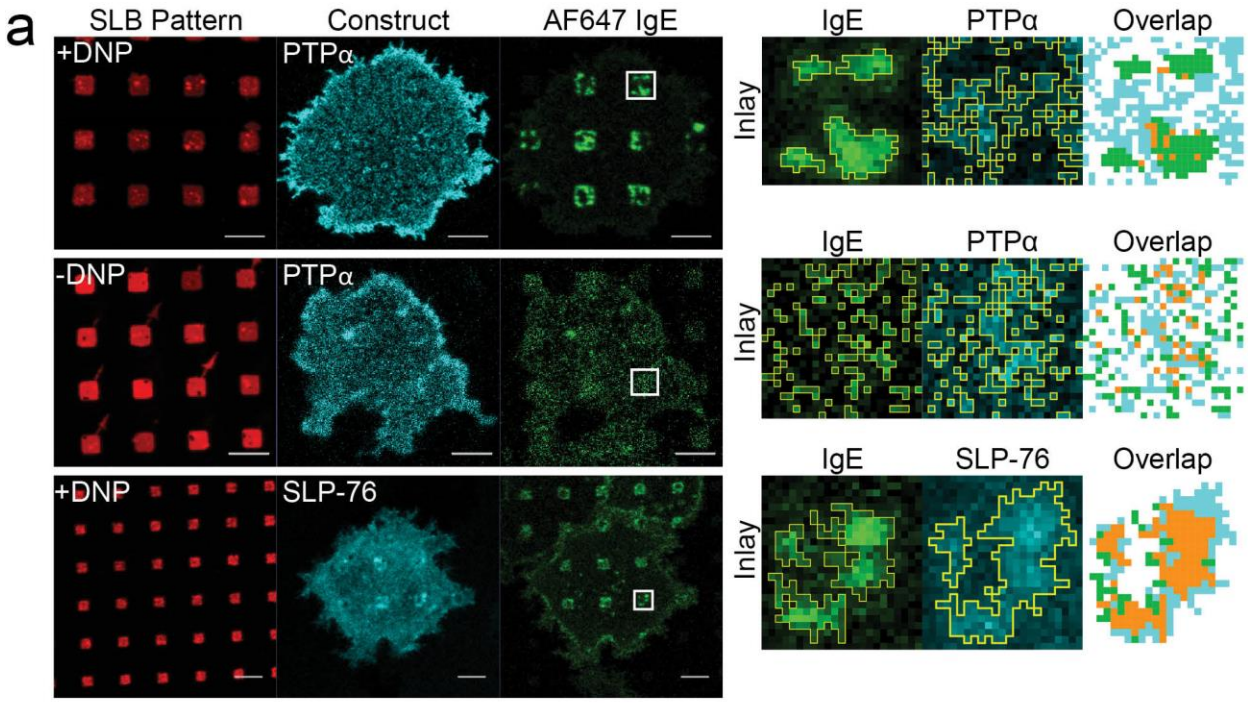
a
SLB Pattern
Construct
AF647 IgE
IgE
PTPα
Overlap
+DNP
PTPα
Inlay
-DNP
PTPα
+DNP
SLP-76

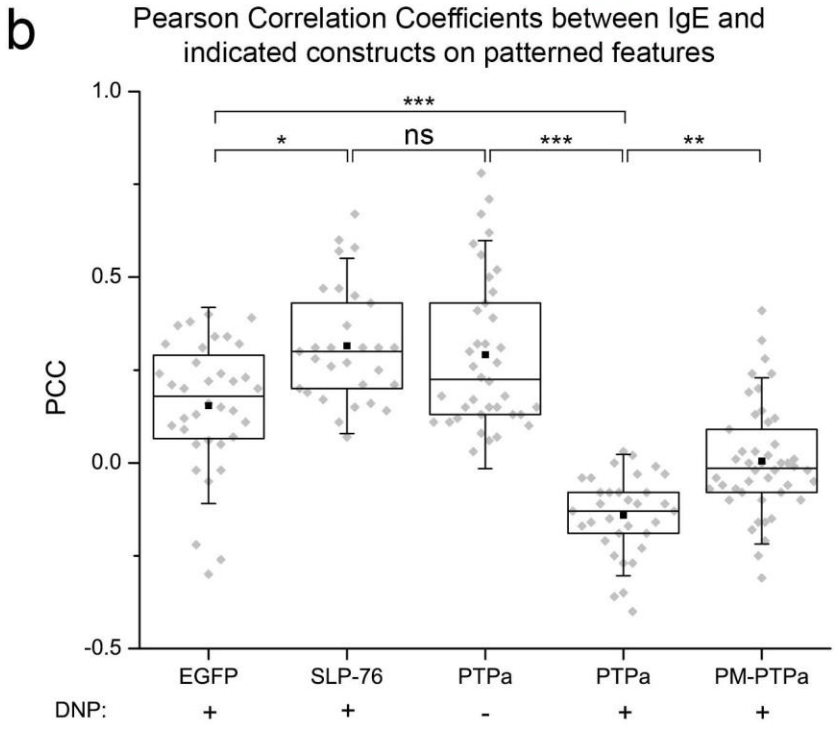
b
Pearson Correlation Coefficients between IgE and indicated constructs on patterned features
PCC
1.0
0.5
0.0
-0.5
***
*
ns
***
**
EGFP
SLP-76
PTPa
PTPa
PM-PTPa
DNP:
+
+
-
+
+

plasma membrane anchoring region of Lyn kinase, which is acylated with Lo-preferring lipids palmitate and myristoylate (PM-PTPα- EGFP). We found that this modification significantly increases the cross correlation with AF647-IgE-FcεRI relative to PTPα-EGFP (PCC = -0.01), although not to the level observed in the absence of stimulating ligand (PCC = 0.23; Figure 3.6b). This suggests that the transmembrane region is only partly responsible for antigen-stimulated exclusion of PTPα and that some of the exclusion is mediated by another factor, for instance steric hindrance and exclusion of non-binding proteins from the densely packed signaling cluster.

Together, these data suggest that in the resting state, a transmembrane phosphatase can interact with FcεRI more freely and then become excluded upon ligand-induced FcεRI clustering, which is consistent with the Lo mediated exclusion model. This exclusion apparently depends in part on the transmembrane segment of the phosphatase and also on the cytoplasmic portion, suggesting a combination of lipid- and protein-mediated exclusion.

3.5 Discussion

The Arp2/3 complex is recruited to patterned ligand features.

Micron-scale patterned ligand features allows us to observe diffraction limited clustering of fluorescent probes with FcεRI complexes. While this method does not inform us about the nanoscale assembly of the observed constituents or their direct interactions, it does allow us to observe the localization of interactions that would otherwise be too small or too transient to observe using traditional approaches. Using this method, we were able to observe colocalization of Gads, SLP-76, Nck, N-WASP, and Arp2/3 to patterned ligand surfaces (Figure 3.1). This provides strong evidence that endogenous FcεRI clusters recruit Arp2/3 under stimulating

conditions and points to a physiological role for Arp2/3 in receptor activation.

This is consistent with both macrophages[14] and T-cells[48] where Arp2/3 is recruited in response to ligand stimulation. In macrophages, Arp2/3 recruitment is accompanied by a localized temporal switch from a formin-mediated "resting" cytoskeleton to Arp2/3-mediated actin branching. Our data support a similar role in mast cells, in which Arp2/3 responds to ligand-stimulation to regulate FcεRI activation. This is consistent with other observations in which Arp2/3 has been associated with unique actin dynamics following antigen stimulation[42].

Arp2/3 and formins cooperate to recruit F-actin to FcεRI signaling complexes.

We summarize our key pharmacological findings in Table 3.1. We found that inhibition of Arp2/3 activity significantly reduces F-actin recruitment to ligand patterned features. Furthermore, the reduction of recruitment is similar to that caused by the general actin polymerization inhibitor Cyto D (Figure 3.2). We also found that the formin inhibitor SMIFH2 causes a similar reduction in F-actin recruitment. These data suggest that Arp2/3 and formins cooperate to recruit F-actin to signaling complexes. It is possible the formins maintain an infrastructure required to bring actin to FcεRI complexes following stimulation, and this infrastructure provides a scaffolding for Arp2/3-mediated actin branching. This raises the question of other potential roles for formins and this infrastructure in FcεRI signaling, which has not been studied to the best of our knowledge. One possible connection is through formin-mobilizing Rho-GTPases which are activated during FcεRI signaling[49].

	Cyto D (f-actin)	CK666 (Arp2/3)	SMIFH2 (Formins)
F-actin recruitment	↓	↓	↓
Tyrosine Phosphorylation	↓	↓	-
Phosphotyrosine on/off ratio	↑	-	↑
Ca^{2+} response fraction	↑	-	↓
Ca^{2+} irregular responses	↑	-	↑
Ca^{2+} lag time	-	↑	↑
Degranulation	↑ (≥100 nM)	- (≤75 μM)	↓ (≥50 μM)

Table 3.1: Summary of pharmacological results. Down arrows indicate inhibition, up arrows indicate enhancement, line indicates no significant effect. For degranulation, the general dose-response trends are indicated and the concentrations at which they noticeably deviate from baseline. CK666 demonstrated degranulation inhibition only at 100 μM concentrations.

Arp2/3 facilitates FcεRI activation and rapid kinetics of FcεRI signaling.

We found that Arp2/3 facilitates the formation and activation of receptor clusters. 4G10 labeling of phosphotyrosine residues shows that cells treated with Arp2/3 inhibitor CK666 are less likely to form stabilized phosphorylated clusters that persist over 40 minutes compared to control cells (Figure 3.3a) without affecting the relative amount of phosphotyrosine within these clusters. This suggests that Arp2/3-mediated actin polymerization helps stabilize the signaling complex and may thereby facilitate FcεRI activation.

Arp2/3 activity does not affect the capacity of cells to mount Ca^{2+} responses nor their oscillatory quality, but instead affects when the cells respond, or in other words, the kinetics of Ca^{2+} signaling onset (Figure 3.4). A cumulative probability distribution of the Ca^{2+} lag times (Figure 3.4d) reveals two distinct populations of cells responding to CK666 treatment, suggesting Arp2/3 lowers an activation barrier in FcεRI signaling. This finding is consistent with observations in T cells that Arp2/3 inhibition impairs Ca^{2+} mobilization[48]. The generation of the secondary messenger IP_3 by PLCγ at the membrane is the key initiator of Ca^{2+} responses in FcεRI signaling. Thus, these results may indicate that Arp2/3 facilitates the recruitment of PLCγ to signaling clusters. This is consistent with our previous study showing that PLCγ recruitment is enhanced by the actin cytoskeleton[8].

The results of Cyto D treatment on phosphotyrosine labeling observed here may seem at odds with the Cyto D treatment enhancing phosphorylation of FcεRI in western blot experiments[12], as we saw enhancement of phosphotyrosine labeling of individual clusters, but a decrease in the fraction of cells responding. One possible solution is simply that the fewer cells responding individually possess significantly more phosphotyrosine per cell. However, it is more likely we are observing the effect of destabilized signaling complexes over time. We know from

previous studies that the recruitment of LAT, the backbone of the FcεRI signaling cluster, is facilitated by the actin cytoskeleton[8]. Thus, Cyto D treatment, which reduces the recruitment of this key protein, may compromise the capacity of the cluster to persist on our 40 min time scale.

Alternatively, this contradiction of increased labeling per feature and decreased number of responding cells could be caused by the method of antigen presentation. Most reports of Cyto D treatment in combination with phosphotyrosine labeling use soluble antigen stimulation, rather than surface-attached ligand stimulation. It has been shown that mast cells are more responsive to soluble ligands than surface-attached ligands[50]. Thus the actin cytoskeleton may play a greater role in forming receptor clusters when engaging surface ligands, which is consistent with what is seen in T-cell responses to surface presented antigens[3]. For a more direct comparison, our laboratory previously investigated tyrosine phosphorylation on similar DNP-SLB patterned ligand features with and without Cyto D treatment[7]. Phosphotyrosine labeled cells were scored using a similar scoring method at various time points spanning 30 minutes. Under those conditions, there was an increase in phosphotyrosine labeling in Cyto D treated cells relative to untreated control cells in the first ten minutes of signaling. This agrees with the literature suggesting that Cyto D treatment enhances the early stages of phosphorylation. After 10 minutes, responses plateaued and reached similar values for both treated and untreated cells.

Our data was recorded at 40 minutes, or 10 minutes later than Min's latest time point. This could simply mean that perhaps there is a significant loss of phosphorylation in that 10-minute window due to Cyto D treatment. We also observed a larger fraction of control cells with 4G10 labeling under our conditions: we observed 76% of cells with recruitment compared to the peak 60% observed previously[7]. This could simply reflect a longer time span to recruit phosphotyrosine, or it could reflect a difference in sensitivity in our detection methods, a silicon

base for patterned features with a 1.3 NA objective were used previously, compared to the glass base and the 1.6 NA objective in this study.

To use inverted confocal microscopy with a silicon wafer, the patterned surface must be inverted and placed in a dish. This method may lead to increased scattering as the light from the basal membrane must travel a longer distance through water than in our current setup, which minimizes this scattering by imaging the feature through optical glass. Thus, it is possible that we could identify cells with weak 4G10 labeling that could not be detected previously and that Cyto D treatment reduces labeling in that subset of cells.

We also observed that Cyto D treatment does not affect Ca^{2+} lag times while both CK666 and SMIFH2 increases lag times. Thus, inhibiting either system dramatically impacts signaling while globally-inhibiting actin rescues lag times. This may suggest that initiating Ca^{2+} mobilization may require a balance of formin and Arp2/3 activity. However, Cyto D also enhances the number of responding cells unlike both CK666 and SMIFH2, and it is possible that Cyto D is influencing Ca^{2+} signaling through means we do not fully understand.

Formins inhibit FcεRI complex phosphorylation and promote downstream Ca^{2+} oscillations and degranulation.

We found that formin inhibition enhances phosphotyrosine labeling on patterned features relative to controls without affecting the total number of responding cells, significantly disrupts Ca^{2+} signaling, and inhibits degranulation in a dose-dependent manner (Table 3.1). These data suggest a complex role for formins in FcεRI function. At the receptor complex, formins downregulate receptor phosphorylation, similar to what is observed with Cyto D treatment. This may be through enhancing the recruitment of Lyn kinase, which down regulates signaling after

its initial role in phosphorylating FcεRI[47].

Downstream of signal initiation, formins enable Ca^{2+} oscillations and facilitate degranulation. SMIFH2 treatment negatively affects all measured aspects of Ca^{2+} signaling and inhibits degranulation in a dose-dependent manner. However, the molecular mechanisms behind these observations remain unclear. This may indicate the importance of the basal state of the actin cytoskeleton, which is primarily maintained by formins. Disruptions to the actin infrastructure may cumulatively affect downstream functions that integrate multiple cellular processes, possibly explaining the large effects of SMIFH2 on Ca^{2+} mobilization and degranulation. Alternatively, formins could be affecting an upstream component that is critical to Ca^{2+} mobilization, like PLCγ recruitment or activation.

PTPα is excluded from FcεRI clusters on patterned ligand features.

A current model is that FcεRI activation is driven by a local shift in lipid phase due to formation of a stable Lo-like domain around FcεRI clusters that selectively recruits kinases and excludes phosphatases. Here we demonstrated using the transmembrane tyrosine phosphatase PTPα that such an exclusion is physiologically possible and can be observed in mast cells (Figure 3.6). Furthermore, this exclusion partially depends on the transmembrane portion of PTPα, which prefers Ld-like domains. When swapped with an Lo-preferring anchor, the PM-PTPα construct lost its apparent antilocalization, but was not restored to unstimulated levels of colocalization. These experiments demonstrate how the functionality of our patterned ligand system may be extended to study not only colocalization of transient interactions on the scale of the patterned features, but also co- or anti-localization of labeled proteins on the sub-micrometer scale.

Contrasting roles for formins and Arp2/3 in FcεRI signaling.

Combined, these results suggest that formins and Arp2/3 play distinct roles in FcεRI signaling in mast cells, although both types of actin-polymerizing enzymes cooperate to bring F-actin to the signaling cluster. Our phosphotyrosine labeling experiments (Figure 3.3) suggest that Arp2/3 stabilizes the signaling cluster while formins regulate phosphorylation, perhaps through enhanced recruitment of Lyn and its multiple substrates. Downstream of FcεRI-initiated signaling, Arp2/3 promotes the rapid mobilization of Ca^{2+} in response to antigen stimulation, possibly by enhancing PLCγ recruitment to FcεRI-mediated signaling complexs[8]. Formins appear necessary to generate normally oscillating Ca^{2+} responses and may be involved to onset similarly to Arp2/3, but this is harder to demonstrate given the complex effects of SMIFH2 treatment on Ca^{2+} signaling.

These responses can be compared to Cyto D treatment, which in many cases resembles one, both, or a mixed phenotype of the Arp2/3 and formin inhibitors. This suggests varying roles of each type of inhibition compared to global inhibition represented by CytoD. We observed only two exceptions to this: Cyto D enhanced the fraction of cells with Ca^{2+} responses and enhanced degranulation These results suggest that Cyto D is acting in other ways we have not anticipated, or that cooperation and competition between Arp2/3 and formins play key roles in some aspects of FcεRI signaling.

Our data suggest differential roles for actin polymerizing enzymes in FcεRI signaling and are consistent with roles observed in other immunoreceptor signaling systems. Arp2/3 has been shown to play a role in activating TCR in T cells[48] and the Fcγ receptor in macrophages, in which inhibition of Arp2/3 via pharmacological or genetic approaches inhibits TCR and Fcγ

receptor activation. However, in T cells, CK666-inhibited cells still form TCR macroclusters and demonstrate inhibited PLCγ activation and Ca^{2+} signaling downstream. Meanwhile, formins are considered to maintain homeostasis and the basal actin cytoskeleton in macrophages[14], while in T cells, formins are considered responsible for generating concentric actin rings in the immunological synapse and aiding in trafficking of TCR as the synapse matures[16,18].

A similar model likely applies to FcεRI signaling: Arp2/3 responds to antigen-stimulation via the assembly of LAT, Gads, SLP-76, Nck, WASP, and Arp2/3 to aid in the assembly of functional signaling complexes, while formins cooperate in the activation process and participate in basic cellular processes to ensure signaling quality (Figure 3.7). However, the molecular mechanisms underlying this model remain unclear. It has been shown that the arrangement of cortical actin depends on a balance of Arp2/3 and formin activity[51]. Thus, disrupting actin polymerization may restrict a cell's ability to rearrange cortical actin and thus impact the diffusion and accessibility of proteins near the plasma membrane. Actin has also been shown to regulate the composition of lipids and lipid domains in local environments[52,53], which can affect receptor signaling. We note that inhibition of one system can induce compensation or other adjustments in another, so it is possible that we have measured not only the effect of inhibition of one enzyme, but also the simultaneous effect of enhancement of associated systems.

These data suggest novel roles for Arp2/3 and formin-mediated actin polymerization in FcεRI signaling and show that use of CK666 and SMIFH2 provide an easily accessible means for researchers to investigate these roles. However, we caution that drug-based approaches also have drawbacks including the risk of off-target effects and require that dosages between different types of experiments be carefully considered.

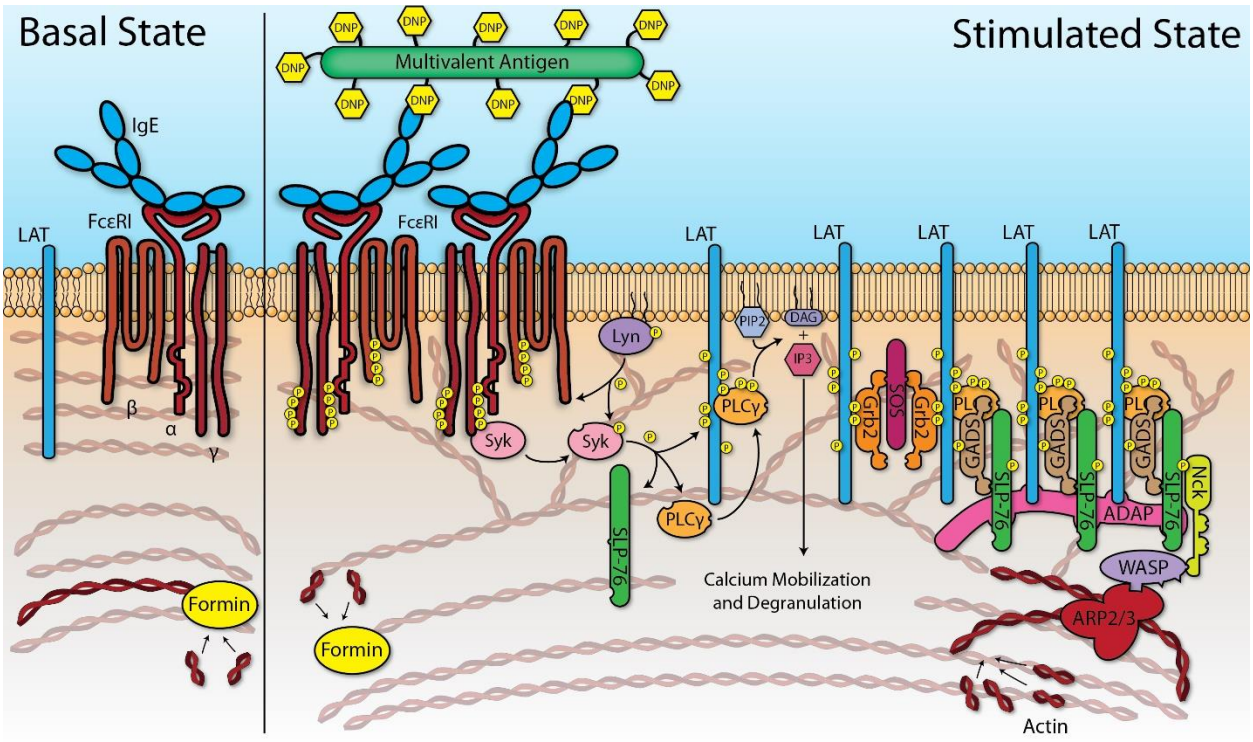

Figure 3.7: Model for Arp2/3 and formins in FcεRI signaling. In the basal state, formins maintain a linearly extended basal actin cytoskeleton. Antigen stimulation of FcεRI leads to recruitment of LAT, GADS, SLP-76, Nck, WASP, and Arp2/3 to the signaling cluster resulting in the localized branching of actin in the cluster. Arp2/3-mediated actin branching facilitates formation and stabilization of the receptor cluster formation and may utilize the underlying formin-mediated actin cytoskeleton as a scaffold. Emanating from the cluster, downstream processes, including regulated Ca^{2+} oscillations and consequent degranulation are enhanced by the formin-mediated actin cytoskeleton, and this likely requires PLCγ recruitment to hydrolyze PIP2 and generate secondary messengers IP3 and DAG.

3.6 Supplementary Information

Optimizing DNP-BSA patterned ligand feature recruitment and function.

Previously, we used a 25 μg/mL prep of DNP-BSA to study protein recruitment in mast cells to patterns[8]. We observed in many cases that IgE and protein recruitment often recruit as a concentrated "ring" around the feature.

We suspected this was caused by highly concentrated receptor engagement leading to a diffusion barrier that prevented receptors from migrating to the interior of the feature. To test this, we compared a range of DNP-BSA concentrations to DNP-SLB in mast cells. DNP-SLB patterns showed a mix of uniform and non-uniform IgE recruitment, but few cases of well-defined ring recruitment (Figure 3.8). Further, we wanted to compare functional recruitment to non-functional recruitment, so we labeled cells with the 4G10 anti-phosphotyrosine antibody. We found that 5 μg/mL DNP-BSA demonstrated similar IgE recruitment phenotypes to DNP-SLB and had maximal 4G10 responses compared to other DNP-BSA concentrations. A lower concentration (1 μg/mL) showed both weak IgE recruitment and less phosphorylation. The original 25 μg/mL showed strong ring-like recruitment and minimal 4G10 labeling.

Figure 3.8: Optimizing DNP-BSA patterned ligand feature recruitment and function. RBL-2H3 cells were sensitized with AF647-IgE, incubated for 40 min with the indicated DNP-patterned feature surfaces, fixed, and then labeled with the 4G10 anti-phosphotyrosine antibody. Cells were scored for 4G10 and IgE recruitment (similar to Figure 3.3). The distribution of IgE recruitment was also qualitatively scored as uniform, non-uniform, or ring-like. Uniform recruitment corresponds to a homogeneous distribution of IgE across the patterned feature, non-uniform corresponds to heterogeneous clustering of IgE across the patterned feature, and ring-like recruitment corresponds to the formation of a concentric "ring" of IgE around the edge of the cluster.

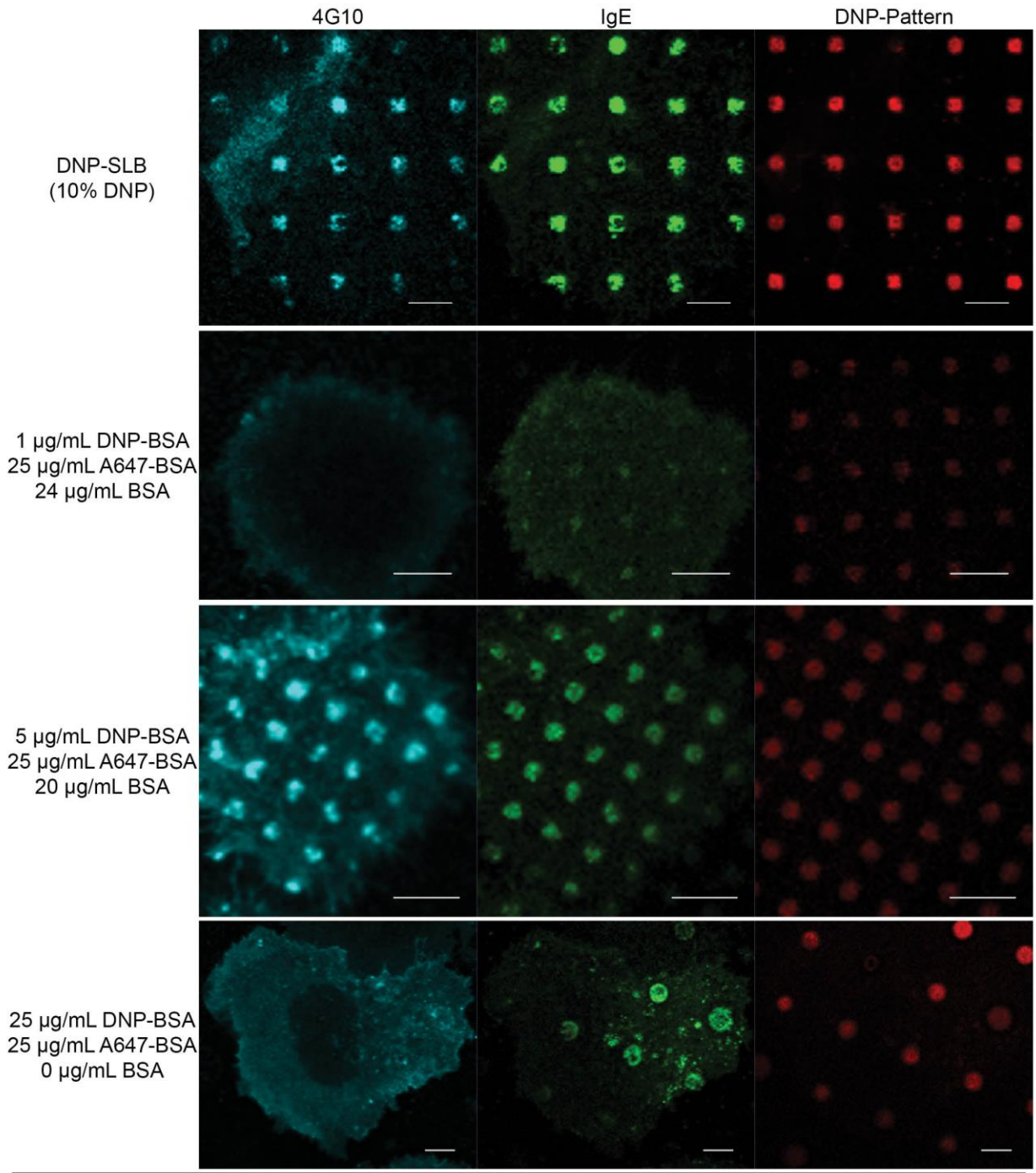

	n	4G10 Recruitment	IgE Recruitment	Uniform IgE Recruitment	Non-Uniform IgE Recruitment	IgE Ring-Like Recruitment
SLB (10% DNP)	31	90%	100%	51%	41%	6%
1 µg/mL DNP-BSA	27	22%	52%	100%	0%	0%
5 µg/mL DNP-BSA	39	66%	100%	48%	43%	5%
25 µg/mL DNP-BSA	25	4%	100%	22%	18%	59%

The inhibitory activity of CK666 is required to block f-actin recruitment to patterned ligand features

As a control, CK666 was tested alongside CK689, an inactive homolog of CK666 that does not affect Arp2/3 activity, to show that Arp2/3 inhibition is responsible for our observed effects (Figure 3.9). Briefly, RBL-2H3 cells were incubated for 40 minutes on DNP-SLB patterned features in the presence of CK689, CK666, or a vehicle control (DMSO) for 40 minutes before being fixed, labeled with the F-actin label phalloidin, and scored for recruitment. This is identical to the phalloidin labeling described in the main body of the text (error bars = SE).

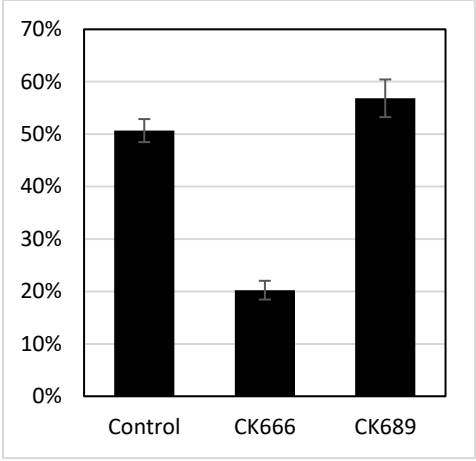

Figure 3.9: Fraction of cells showing phalloidin recruitment following CK666 or CK689 treatment. RBL-2H3 cells were incubated for 40 minutes on DNP-SLB patterned features in the presence of CK689, CK666, or a vehicle control (DMSO) for 40 minutes before being fixed, labeled with the F-actin label phalloidin, and scored for recruitment. This is identical to the phalloidin labeling described in the main body of the text (error bars = SE).

p values for all comparisons presented in Results section 3.4:

Figure 3.10 – Figure 3.13 present *p* values for all possible comparisons made in Results section 3.4. These are presented in a table where each value represents the p-value comparing the corresponding row and column. *p* values for pooled proportions were calculated using ANOVA with a Tukey post-hoc multiple comparisons significance test. Individual cell data (box plots) were first tested for normality using a Shapiro-Wilkes test, which revealed them to all be non-normally distributed. They were then analyzed for statistical significance with a conservative method using a Kruskal-Wallis non-parametric test followed by a Dunn post-hoc significance test and adjusted with the Benjamini-Hochberg FDR (false discovery rate) for multiple comparisons.

In the *p* value tables, only one comparison is shown for each pair (thus why half the table is empty, to avoid reflexive comparisons). The initial row and final column have also been omitted from each table since these would be entirely blank, which is why there are always $(n - 1)$ rows and columns when comparing n variables. This also explains why there are values along the diagonal, since this method of presentation removes identity pairings. (* corresponds to $p < 0.05$, ** corresponds to $p < 0.01$, *** corresponds to $p < 0.001$)

Figure 3.10: *p* values for Figure 3.2b phalloidin labeling.

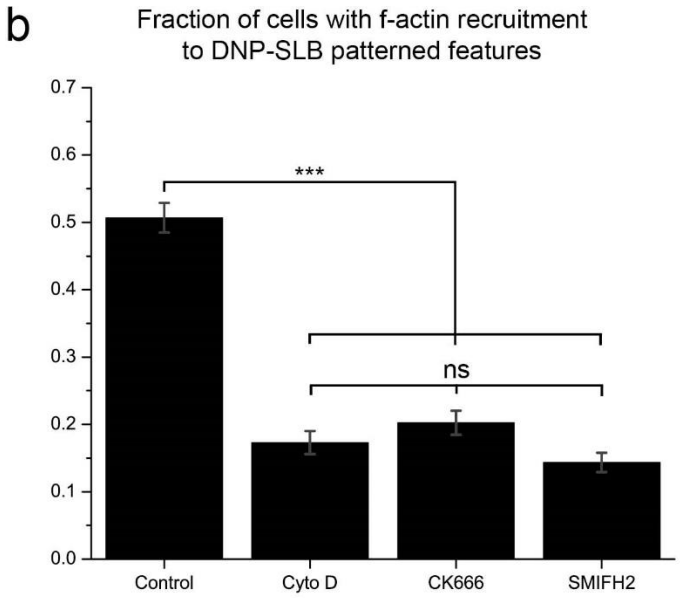

Comparison *p*-values			
	Control	CK666	Cyto D
CK666	<0.001		
Cyto D	<0.001	0.674	
SMIFH2	<0.001	0.084	0.640

Figure 3.11: *p* values for Figure 3.3a-b 4G10 labeling.

a

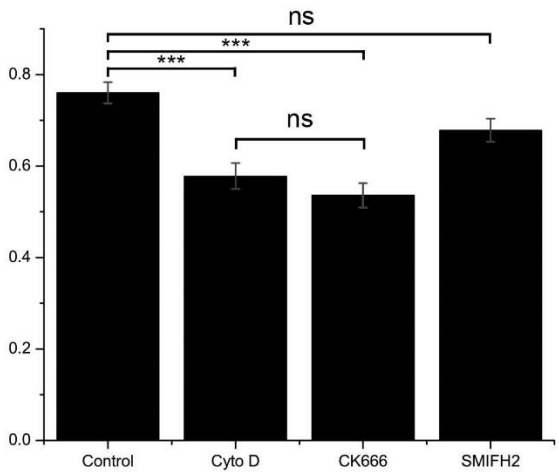

Comparison *p*-values			
	Control	CK666	Cyto D
CK666	<0.001		
Cyto D	<0.001	0.667	
SMIFH2	0.105	<0.001	0.037

b

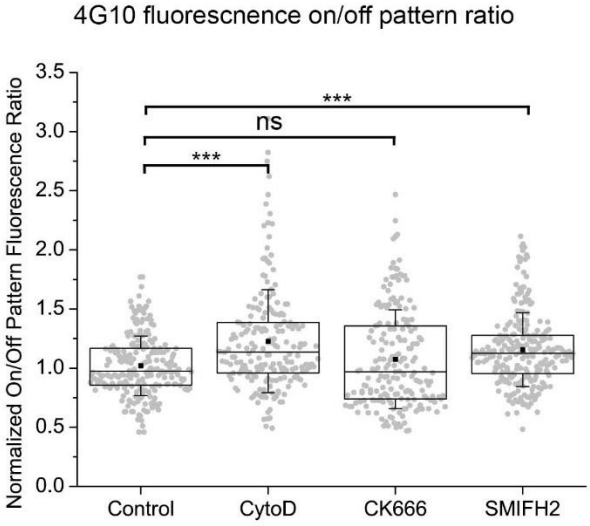

Comparison *p*-values			
	Control	CK666	Cyto D
CK666	0.6333		
Cyto D	<0.001	<0.001	
SMIFH2	<0.001	0.0003	0.4795

Figure 3.12: *p* values for Figure 3.4a-c Ca^{2+} experiments

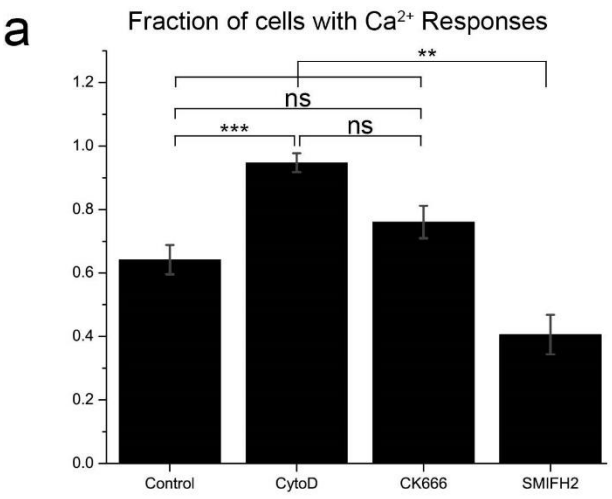

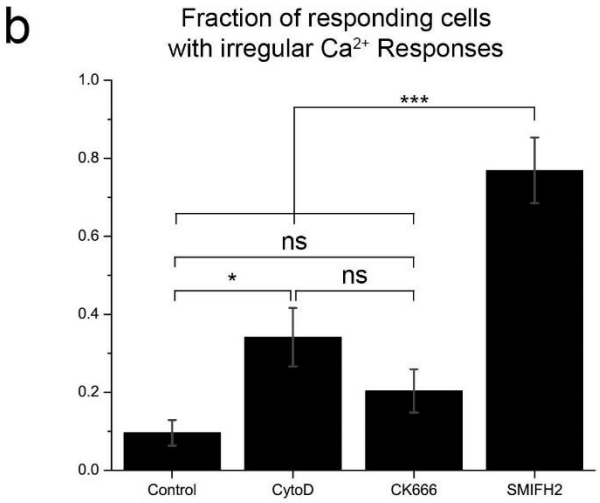

Comparison *p*-values			
	Control	CK666	Cyto D
CK666	0.283		
Cyto D	<0.001	0.077	
SMIFH2	0.004	<0.001	<0.001

Comparison *p*-values			
	Control	CK666	Cyto D
CK666	0.602		
Cyto D	0.034	0.440	
SMIFH2	<0.001	<0.001	<0.001

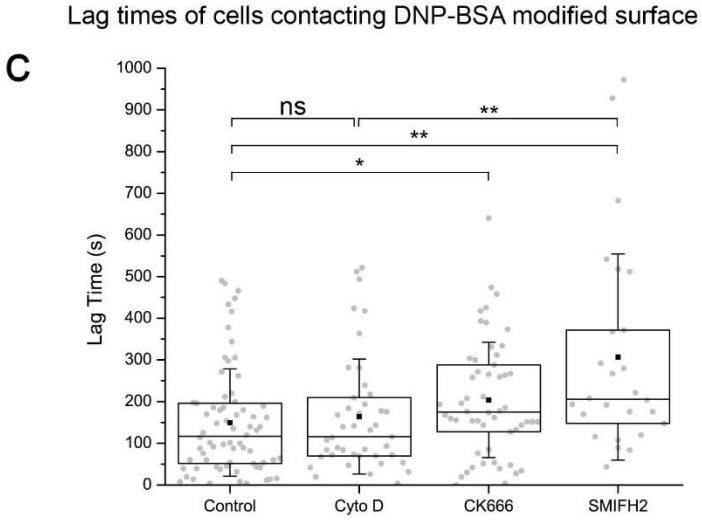

Comparison *p*-values			
	Control	CK666	Cyto D
CK666	0.030		
Cyto D	0.592	0.119	
SMIFH2	0.002	0.119	0.009

Figure 3.13: *p* values for Figure 3.6b PTPα PCC values comparison.

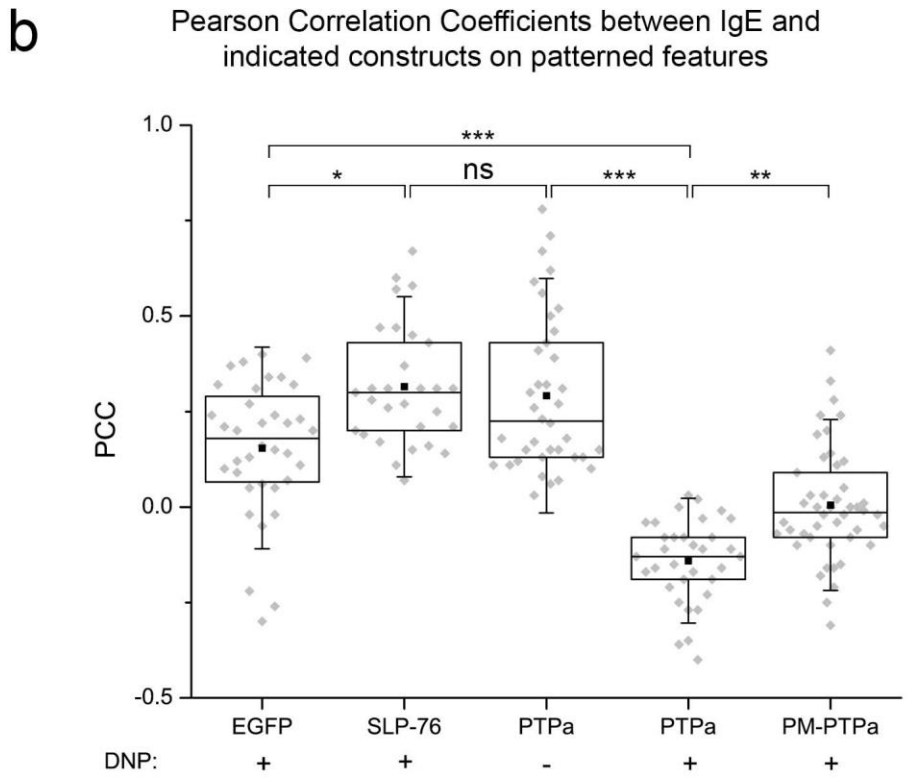

Comparison *p*-values				
	EGFP +DNP	PM-PTPα +DNP	PTPα +DNP	PTPα -DNP
PM-PTPα +DNP	<0.001			
PTPα +DNP	<0.001	0.005		
PTPα -DNP	0.098	<0.001	<0.001	
SLP-76 +DNP	0.025	<0.001	<0.001	0.451

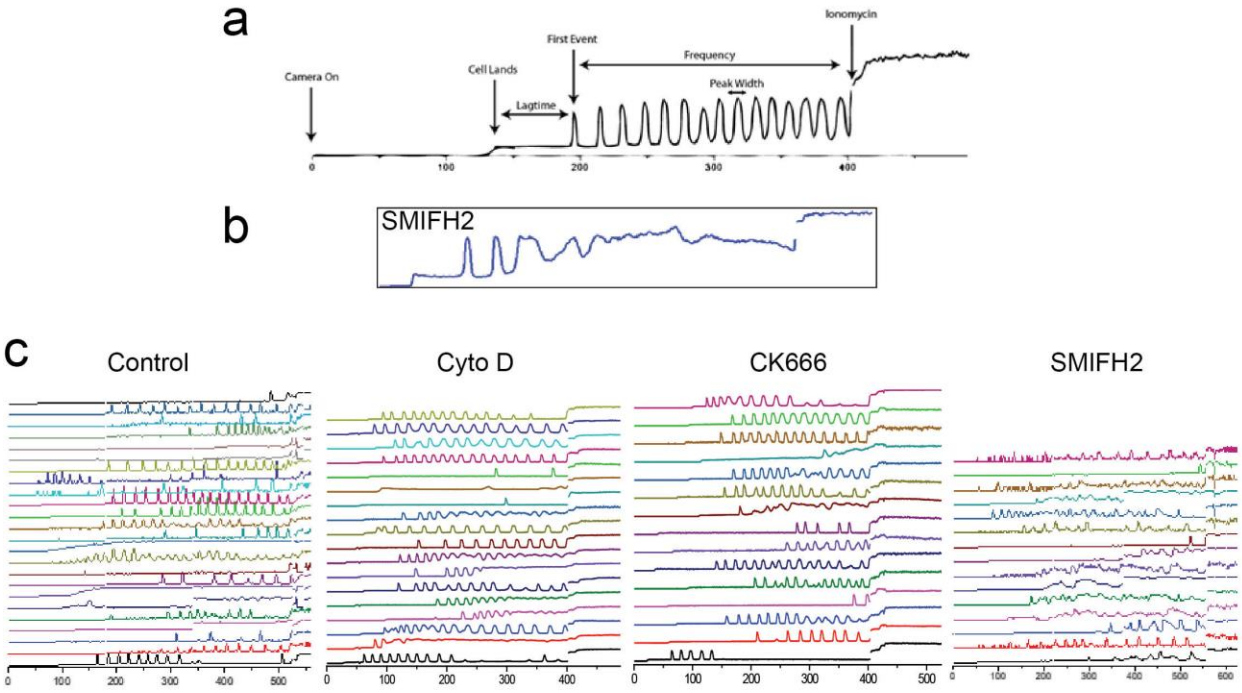

Figure 3.14: Sample Ca^{2+} Oscillations. (a) Sample Ca^{2+} oscillation of an untreated control cell with key features labeled. (b) Sample SMIFH2 cell with impaired caclium oscillations (as in Figure 3.4b). (c) Sample of multiple Ca^{2+} oscillations from a single experiment.

Preliminary Fluorimetry Studies of CK666:

We carried out preliminary fluorimetry experiments to evaluate large cell populations using the RGECO1 Ca^{2+} indicator. Arianna Gagnon initially looked at GCaMP3 fluorescence in combination with CK666 and SMIFH2, but she was unable to finish her investigation. She found that SMIFH2 treatment resulted in a strange and irregular increase of GCaMP3 fluorescence in the absence of antigen. This was not observed in our confocal studies of GCaMP3, however cells were pre-treated with SMIFH2 in that case while SMIFH2 is added during the measurement of the cells in this case. We tested RGECO1 to see if this result was specific to GCaMP3.

Breifly, 1.8 mL of RBL-2H3 cells transiently expressing RGECO1 at 1 x 10^6 cells/mL were added to a fluorimeter tube with a stir bar. Baseline RGECO1 fluorescence was measured for 100 sec, prior to adding inhibitor. A new baseline was recorded for 100 sec and then cells were stimulated with antigen. Fluorescence was recorded for 300 sec and then the cells were permeabilized with Tx-100 and fluoresence was recorded for an additional 100 sec. The Tx-100 permeabilization was defined as a 100% maximal response. Then the cells were quenched with EGTA and fluorescence was recorded for a final 100 sec.

Using RGECO1, we were still unable to analyze SMIFH2 treatments. The response to SMIFH2 treatment was similar to what was observed using GCaMP3. We also did not see drastic differences between treatments, except maybe decreased decay rates in inhibited cells. We were unable to obtain data for SMIFH2 because SMIFH2 treatment results in a huge spike in fluorescence independent of antigen (which was not observed in the single cell microscopy measurements). However, the Cyto D curve does not match previous results, so we suspect this may reflect problems in the cells themselves rather than a real experimental result. As such, we did not make any specific conclusions regarding this experiment, but this experiment is worth

further investigation. This data would be particularly interesting to compare to Kumari et al's findings in T-cells, where they observed a decrease in Ca^{2+} responses following CK666 treatment[48]. I would recommend using 100 μM CK666 in a followup experiment.

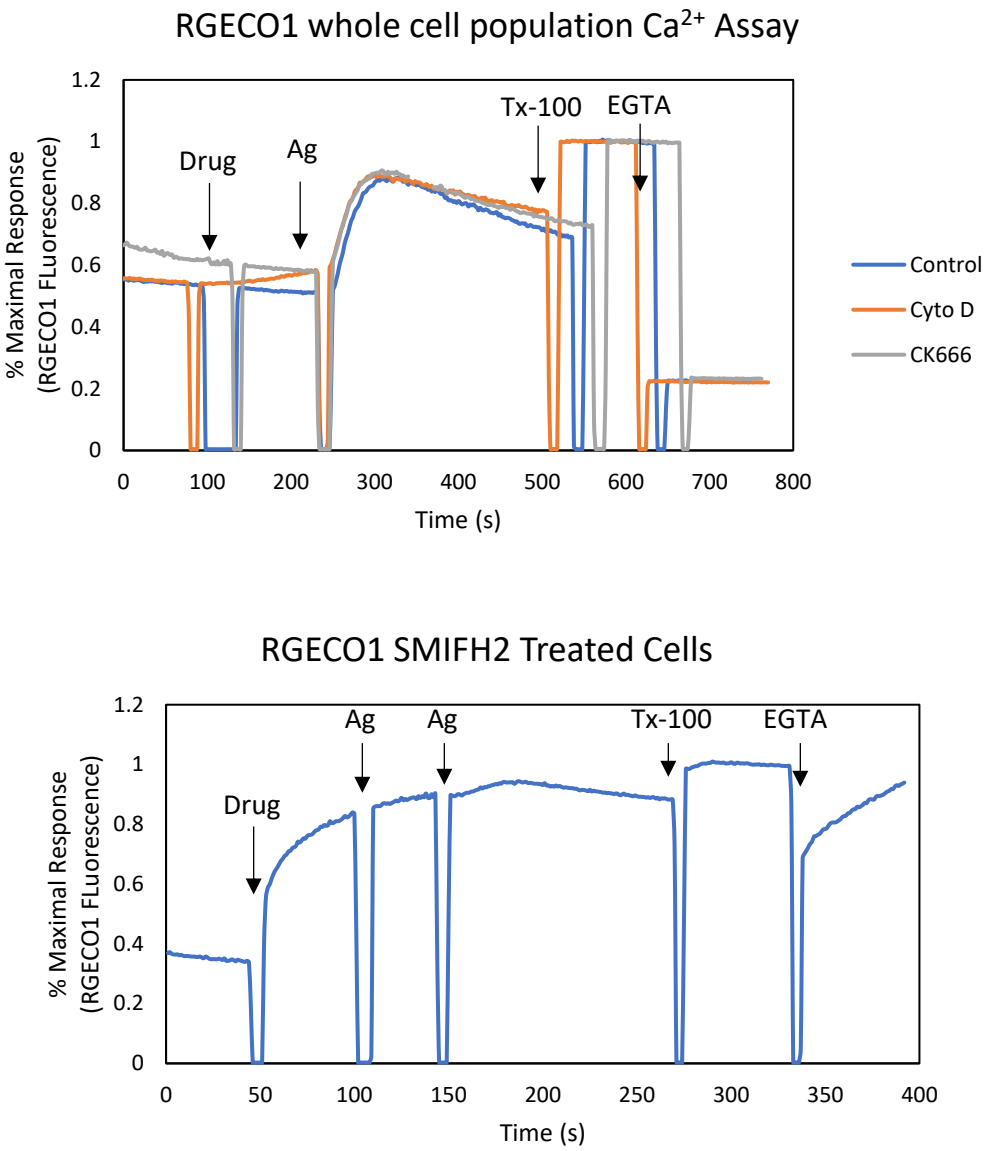

Figure 3.15: Fluorimetry of RBL-2H3 cells transiently expressing RGECO1. Live RBL-2H3 cells transiently expressing the RGECO1 Ca^{2+} indicator had their fluorescence measured in real time with a fluorimeter. (Top) Normalized RGECO1 fluorimetry data of cells treated with Cyto D, CK666, or vehicle control (DMSO). (Bottom) Normalized RGECO1 fluorimetry data of cells treated with SMIFH2.

Degranulation antigen dose-response curve.

While optimizing the degranulation conditions, we generated an antigen dose-response curve to identify the dose-response region. We wanted a region with high sensitivity so we could avoid a case where a weak effect was obscured beneath a strong dose. We identified ~0.6 ng/mL as the 50% response. We chose to use 1 ng/mL for our experiments so we would have a little more signal to work with while still being in the dose-response range.

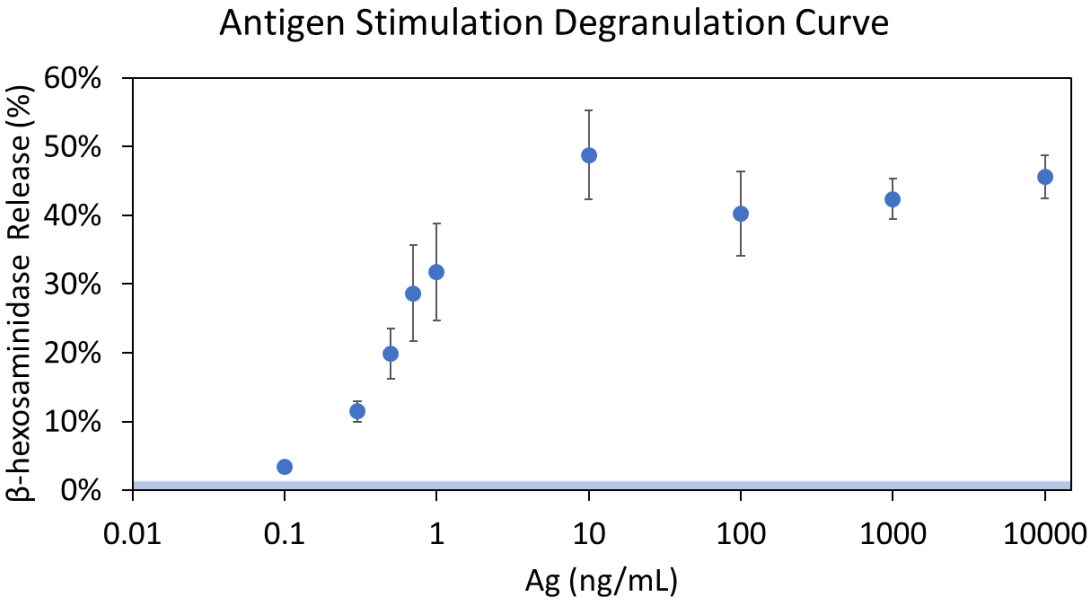

Figure 3.16: Degranulation DNP-BSA dose response curve in RBL-2H3 cells. RBL-2H3 cells were stimulated with varying concentrations of DNP-BSA and β-hexosaminidase release was measured as previously described[36]. (Error bars = SD. Shaded region represents unstimulated cells.)

REFERENCES

1. Rivera, J. & Gilfillan, A. M. Molecular regulation of mast cell activation. *J. Allergy Clin. Immunol.* **117**, 1214–1225 (2006).
2. Krystel-Whittemore, M., Dileepan, K. N. & Wood, J. G. Mast Cell: A Multi-Functional Master Cell. *Front. Immunol.* **6**, 1–12 (2016).
3. Holowka, D. & Baird, B. Roles for lipid heterogeneity in immunoreceptor signaling. *Biochim. Biophys. Acta - Mol. Cell Biol. Lipids* **1861**, 830–836 (2016).
4. Young, R. M., Holowka, D. & Baird, B. A lipid raft environment enhances Lyn kinase activity by protecting the active site tyrosine from dephosphorylation. *J. Biol. Chem.* **278**, 20746–20752 (2003).
5. Young, R. M., Zheng, X., Holowka, D. & Baird, B. Reconstitution of Regulated Phosphorylation of FcεRI by a Lipid Raft-excluded Protein-tyrosine Phosphatase. *J. Biol. Chem.* **280**, 1230–1235 (2005).
6. Holowka, D., Sheets, E. D. & Baird, B. Interactions between FcεRI and lipid raft components are regulated by the actin cytoskeleton. *J. Cell Sci.* **113 (Pt 6**, 1009–19 (2000).
7. Wu, M., Holowka, D., Craighead, H. G. & Baird, B. Visualization of plasma membrane compartmentalization with patterned lipid bilayers. *Proc. Natl. Acad. Sci.* **101**, 13798–13803 (2004).
8. Wakefield, D. L., Holowka, D. & Baird, B. The FcεRI signaling cascade and integrin trafficking converge at patterned ligand surfaces. *Mol. Biol. Cell* **28**, 3383–3396 (2017).
9. Oka, T., Sato, K., Hori, M., Ozaki, H. & Karaki, H. FcεRI cross-linking-induced actin assembly mediates calcium signalling in RBL-2H3 mast cells. *Br. J. Pharmacol.* **136**,

837–846 (2002).

10. Pierini, L., Holowka, D. & Baird, B. FcεRI-mediated association of 6-μm beads with RBL-2H3 mast cells results in exclusion of signaling proteins from the forming phagosome and abrogation of normal downstream signaling. *J. Cell Biol.* **134**, 1427–1439 (1996).
11. Shelby, S. A., Veatch, S. L., Holowka, D. A. & Baird, B. A. Functional Nanoscale Coupling of Lyn Kinase with IgE-FcεRI is Restricted by the Actin Cytoskeleton in Early Antigen-Stimulated Signaling. *Mol. Biol. Cell* **27**, 3645–3658 (2016).
12. Frigeri, L. & Apgar, J. R. The role of actin microfilaments in the down-regulation of the degranulation response in RBL-2H3 mast cells. *J. Immunol.* **162**, 2243–50 (1999).
13. Goode, B. L. & Eck, M. J. Mechanism and Function of Formins in the Control of Actin Assembly. *Annu. Rev. Biochem.* **76**, 593–627 (2007).
14. Ostrowski, P. P., Grinstein, S. & Freeman, S. A. Diffusion Barriers, Mechanical Forces, and the Biophysics of Phagocytosis. *Dev. Cell* **38**, 135–146 (2016).
15. Isogai, T. *et al.* Initiation of lamellipodia and ruffles involves cooperation between mDia1 and the Arp2/3 complex. *J. Cell Sci.* **128**, 3796–3810 (2015).
16. Murugesan, S. *et al.* Formin-generated actomyosin arcs propel t cell receptor microcluster movement at the immune synapse. *J. Cell Biol.* **215**, 383–399 (2016).
17. Yi, J., Wu, X. S., Crites, T. & Hammer, J. A. Actin retrograde flow and actomyosin II arc contraction drive receptor cluster dynamics at the immunological synapse in Jurkat T cells. *Mol. Biol. Cell* **23**, 834–852 (2012).
18. Ditlev, J. A. *et al.* A composition-dependent molecular clutch between T cell signaling condensates and actin. *Elife* **8**, 1–44 (2019).

19. Su, X. *et al.* Phase separation of signaling molecules promotes T cell receptor signal transduction. *Science (80-.).* **352**, 595–599 (2016).

20. Wilson, B. S., Pfeiffer, J. R. & Oliver, J. M. FcεRI signaling observed from the inside of the mast cell membrane. *Mol. Immunol.* **38**, 1259–1268 (2002).

21. Torres, A. J., Vasudevan, L., Holowka, D. & Baird, B. a. Focal adhesion proteins connect IgE receptors to the cytoskeleton as revealed by micropatterned ligand arrays. *Proc. Natl. Acad. Sci.* **105**, 17238–17244 (2008).

22. Singhai, A. *et al.* Spatially defined EGF receptor activation reveals an F-actin-dependent phospho-erk signaling complex. *Biophys. J.* **107**, 2639–2651 (2014).

23. Orth, R. N., Wu, M., Holowka, D. A., Craighead, H. G. & Baird, B. A. Mast cell activation on patterned lipid bilayers of subcellular dimensions. *Langmuir* **19**, 1599–1605 (2003).

24. Hetrick, B., Han, M. S., Helgeson, L. A. & Nolen, B. J. Small molecules CK-666 and CK-869 inhibit actin-related protein 2/3 complex by blocking an activating conformational change. *Chem. Biol.* **20**, 701–712 (2013).

25. Rizvi, S. A. *et al.* Identification and Characterization of a Small Molecule Inhibitor of Formin-Mediated Actin Assembly. *Chem. Biol.* **16**, 1158–1168 (2009).

26. Liu, F. *et al.* Monoclonal dinitrophenyl-specific murine IgE antibody : preparation , isolation , and Information about subscribing to The Journal of Immunology is online at : MONOCLONAL DINITROPHENYL-SPECIFIC MURINE IgE ANTIBODY : PREPARATION , ISOLATION , AND CHARACTER. *J. Immunol.* **124**, 2728–2737 (1980).

27. Larson, D. R., Gosse, J. A., Holowka, D. A., Baird, B. A. & Webb, W. W. Temporally

resolved interactions between antigen-stimulated IgE receptors and Lyn kinase on living cells. *J. Cell Biol.* **171**, 527–536 (2005).

28. Bunnell, S. C. *et al.* T cell receptor ligation induces the formation of dynamically regulated signaling assemblies. *J. Cell Biol.* **158**, 1263–1275 (2002).

29. Barda-Saad, M. *et al.* Cooperative interactions at the SLP-76 complex are critical for actin polymerization. *EMBO J.* **29**, 2315–2328 (2010).

30. Coussens, N. P. *et al.* Multipoint Binding of the SLP-76 SH2 Domain to ADAP Is Critical for Oligomerization of SLP-76 Signaling Complexes in Stimulated T Cells. *Mol. Cell. Biol.* **33**, 4140–4151 (2013).

31. Wegner, A. M. *et al.* N-WASP and the Arp2/3 Complex Are Critical Regulators of Actin in the Development of Dendritic Spines and Synapses. *J. Biol. Chem.* **283**, 15912–15920 (2008).

32. Tian, L. *et al.* Imaging neural activity in worms, flies and mice with improved GCaMP calcium indicators. *Nat. Methods* **6**, 875–881 (2009).

33. Wilkes, M. M., Wilson, J. D., Baird, B. & Holowka, D. Activation of Cdc42 is necessary for sustained oscillations of Ca2+ and PIP2 stimulated by antigen in RBL mast cells. *Biol. Open* **3**, 700–710 (2014).

34. Singhai, A., Bryant, K. L., Hammes, S. R., Holowka, D. & Baird, B. Spatially defined EGF receptor activation reveals an F-actin-dependent phospho-Erk signaling complex.

35. Richter, R. P., Him, J. L. K. & Brisson, A. Supported lipid membranes. *Mater. Today* **6**, 32–37 (2003).

36. Naal, R. M. Z. G., Tabb, J., Holowka, D. & Baird, B. In situ measurement of degranulation as a biosensor based on RBL-2H3 mast cells. *Biosens. Bioelectron.* **20**,

791–796 (2004).

37. Balagopalan, L., Kortum, R. L., Coussens, N. P., Barr, V. A. & Samelson, L. E. The linker for activation of T Cells (LAT) signaling hub: From signaling complexes to microclusters. *J. Biol. Chem.* **290**, 26422–26429 (2015).

38. Zhang, W. *et al.* Association of Grb2, Gads, and phospholipase C-γ1 with phosphorylated LAT tyrosine residues: Effect of LAT tyrosine mutations on T cell antigen receptor-mediated signaling. *J. Biol. Chem.* **275**, 23355–23361 (2000).

39. Li, W., Hu, P., Skolnik, E. Y., Ullrich, A. & Schlessinger, J. The SH2 and SH3 domain-containing Nck protein is oncogenic and a common target for phosphorylation by different surface receptors. *Mol. Cell. Biol.* **12**, 5824–5833 (1992).

40. Silverman, M. A., Shoag, J., Wu, J. & Koretzky, G. A. Disruption of SLP-76 Interaction with Gads Inhibits Dynamic Clustering of SLP-76 and Fc RI Signaling in Mast Cells. *Mol. Cell. Biol.* **26**, 1826–1838 (2006).

41. Pivniouk, V. I. *et al.* Impaired signaling via the high-affinity IgE receptor in Wiskott-Aldrich syndrome protein-deficient mast cells. *Int. Immunol.* **15**, 1431–1440 (2003).

42. Colin-York, H. *et al.* Cytoskeletal actin patterns shape mast cell activation. *Commun. Biol.* **2**, 1–12 (2019).

43. Kambayashi, T. & Koretzky, G. A. Proximal signaling events in FcεRI-mediated mast cell activation. *J. Allergy Clin. Immunol.* **119**, 544–552 (2007).

44. Gaud, G., Lesourne, R. & Love, P. E. Regulatory mechanisms in T cell receptor signalling. *Nat. Rev. Immunol.* **18**, 485–497 (2018).

45. Geng, L. & Rudd, C. Adaptor ADAP (adhesion- and degranulation-promoting adaptor protein) regulates β1 integrin clustering on mast cells. *Biochem. Biophys. Res. Commun.*

289, 1135–1140 (2001).

46. Geng, L., Pfister, S., Kraeft, S.-K. & Rudd, C. E. Adaptor FYB (Fyn-binding protein) regulates integrin-mediated adhesion and mediator release: Differential involvement of the FYB SH3 domain. *Proc. Natl. Acad. Sci.* **98**, 11527–11532 (2001).

47. Odom, S. *et al.* Negative Regulation of Immunoglobulin E–dependent Allergic Responses by Lyn Kinase. *J. Exp. Med.* **199**, 1491–1502 (2004).

48. Kumari, S. *et al.* Actin foci facilitate activation of the phospholipase C-γ in primary T lymphocytes via the WASP pathway. *Elife* **4**, 1–31 (2015).

49. Dráber, P., Sulimenko, V. & Dráberová, E. Cytoskeleton in Mast Cell Signaling. *Front. Immunol.* **3**, 1–18 (2012).

50. Wu, M., Baumgart, T., Hammond, S., Holowka, D. & Baird, B. Differential targeting of secretory lysosomes and recycling endosomes in mast cells revealed by patterned antigen arrays. *J. Cell Sci.* **120**, 3147–3154 (2007).

51. Bovellan, M. *et al.* Cellular control of cortical actin nucleation. *Curr. Biol.* **24**, 1628–1635 (2014).

52. Sengupta, P., Baird, B. & Holowka, D. Lipid rafts, fluid/fluid phase separation, and their relevance to plasma membrane structure and function. *Semin. Cell Dev. Biol.* **18**, 583–590 (2007).

53. Han, X. *et al.* IgE receptor-mediated alteration of membrane-cytoskeleton interactions revealed by mass spectrometric analysis of detergent-resistant membranes. *Biochemistry* **48**, 6540–6550 (2009).

CHAPTER 4

SUMMARY AND FUTURE DIRECTIONS

4.1 Inhibitory roles for electrostatic residues in the JX domain of the EGFR

Previously, we demonstrated that electrostatic residues in the JX domain play an inhibitory role in EGFR activation[1]. Here, we expanded upon these findings by demonstrating that these charged residues prevent the spontaneous functional dimerization of EGFR receptors. We further showed that these receptors likely signal in a manner similar to ligand-bound wt receptor, requiring both intra- and extracellular domain dimerization to form phosphorylated dimers.

Using immunoblotting in combination with chemical crosslinking to trap receptor dimers, we showed the presence of phosphorylated dimers in the absence of ligand. We hypothesized that these phosphorylated dimers came about through either the traditional pathway of dimerization followed by *trans*-autophosphorylation, or through a novel pathway of *mono*-autophosphorylation followed by dimerization. In order to investigate this possibility, we utilized the V948R mutant which prevents the formation of the active asymmetric kinase conformation of the receptor[2]. We found that EGFR R1-6 V948R receptors lost their constitutive phosphorylation, indicating that the receptor had to progress through a functional asymmetric kinase dimer in order to phosphorylate.

Next, we were curious if dimerization of the extracellular domain was still required in the R1-6 mutants. In the traditional activation pathway, EGF binding induces extracellular dimerization followed by intracellular dimerization, which we have loosely termed “outside-in” activation. In contrast to this, we reasoned that since the observed constitutive activation was

driven by intracellular mutations, that we were inherently starting from some type of "inside" activation. Something had to be occurring in the intracellular domains to lead to receptor activation, which either bypasses extracellular dimerization or forces it to occur later.

In its basal state, the extracellular domain is tethered[3] to the plasma membrane and this conformation hides the dimerization domain and protects the receptor from spontaneous dimerization. Removal of significant portions of the extracellular domain, like in the EGFRvIII[4] mutant, results in constitutive receptor activation, suggesting the extracellular domain plays an inhibitory role in activation. Furthermore, it's been shown in the L858R non-small cell lung cancer mutation that its constitutive activity is dependent on extracellular dimerization[5]. Based on this observation, we believe that activating EGFR mutants may be signaling through an "inside-out" activation mechanism, whereby intracellular dimerization is stabilized by extracellular dimerization. We decided to test this in our R1-6 mutant by combining EGFR R1-6 with the EGFR 246-253* mutant, in which the dimerization arm facilitating extracellular dimerization has been deleted. EGFR 246-253* is still able to bind ligand, but is unable to form dimers[6].

We found the EGFR R1-6 246-253* mutant was constitutively inactive and unable to respond to ligand treatment. This supports our "inside-out" signaling hypothesis. Together, these data suggest that electrostatic residues in the membrane regulate EGFR activation by inhibiting receptor dimerization. We propose that this mechanism is due to tight associations between the JX domain and the plasma membrane, thus preventing the TKD from freely dimerizing with another receptor.

4.2 Future directions for EGFR R1-6 Characterization

EGFR R1-6's value is in studying the role of electrostatic residues in the JX domain because of the shared similarities between EGFR and other RTKs[7]. To that extent, the primary question remaining regarding EGFR R1-6 is, does it actually have a lower affinity for the membrane? While we proposed this as the basis for our observations, we have not directly proven it.

Fluorescence Resonance Energy Transfer (FRET) experiments between a fluorescent EGFR construct and a plasma-membrane lipid label might be one method to address this question. If the JX domain really does result in a decreased affinity for the membrane, then we should be able to observe that as either a decrease in FRET efficiency or a larger fluctuation in FRET efficiency over time for a single molecule. This poses significant technical challenges though. For instance, a FRET probe in the JX region would provide the best information but may not be technically feasible. A fluorescent protein construct between the JX and TKD would likely interfere with receptor activation and conformational dynamics. Targeted organic labeling of the JX domain provides a more attractive option, especially given advances in labeling techniques. However, this method still requires the incorporation of a functional handle into the JX domain. EGFR-EGFP is an attractive candidate, but the C-terminal EGFP may be too far removed from the membrane to measure strong differences in FRET and would not be a direct measure of JX affinity.

Alternatively, it might be possible to show *in vitro* that purified JX and JX R1-6 segments have different affinities for lipid bilayers. Though this would not necessarily translate to the *in vivo* case in the context of the plasma membrane, it would go a long way towards supporting these findings. Either way, I believe this is the primary question remaining in our studies of

EGFR R1-6.

4.3 New roles for Arp2/3 and formins in FcεRI signaling

Previously, we used microfabricated micron-scale patterned ligand features to show the recruitment of proteins to the FcεRI signaling apparatus[8–10]. Here, we use similar methods to show the recruitment of the Arp2/3 actin assembly complex to patterned ligand features of micrometer scale, using the same proteins required for *in vivo* reconstitution[11]. These findings provide direct evidence for the recruitment of Arp2/3 in mast cells. Furthermore, we decided to investigate the role of Arp2/3 activity in FcεRI signaling based on the clear roles that actin plays in FcεRI signaling[9,12–15]. Our goal in doing so was to identify whether Arp2/3 activity could explain the observations of Cyto D and Latrunculin treatments observed in the literature. In doing so, we identified not only roles for Arp2/3 in FcεRI, but also differential roles for formins, the other dominant family of actin polymerizing enzymes in eukaryotes[16].

We found that Arp2/3 and formins differentially affect FcεRI activation. The recruitment of actin to complexes requires both Arp2/3 and formin activity, suggesting cooperativity between these systems. We propose that the formin-mediated basal actin infrastructure provides the initial framework upon which Arp2/3 branching is built. When either Arp2/3 or formins are inhibited, actin is unable to recruit to patterned features.

We concluded that Arp2/3 may stabilize the FcεRI signaling apparatus as CK666 treatment reduces how many cells are able to maintain phosphorylated clusters after 40 minutes (measured by 4G10 anti-phosphotyrosine labeling). We also observed an increase in Ca^{2+} lag times following CK666 treatment, possibly indicating a decrease in PLCγ recruitment to or activation at the signaling complex. This finding is consistent with both T cell literature where

CK666 treatment inhibits Ca^{2+} responses[17] and our previous study showing the recruitment of PLCγ to signaling complexes is enhanced by the cytoskeleton[10]. Thus, Arp2/3 may also play a role in activating or recruiting PLCγ to the cluster.

Formins appear to play a more nuanced role in FcεRI signaling. Like Arp2/3, they are necessary to recruit F-actin to clusters. Our phosphotyrosine labeling suggests that formins may facilitate the negative regulatory role of Lyn kinase, as SMIFH2 treated cells had lower on/off patterned feature fluorescence ratios compared to control cells. Formins help cells mount Ca^{2+} responses, generate regular Ca^{2+} oscillations, rapidly initiate Ca^{2+} signaling, and facilitate degranulation. One explanation is perhaps formins aid in the recruitment or activation of PLCγ. Another possibility is that this may indicate the importance of the basal state of the actin cytoskeleton, which is primarily maintained by formins. Disruptions to the actin infrastructure may cumulatively affect downstream functions that integrate multiple cellular processes.

Based on similar models in T cells[18,19] and macrophages[20], we propose that formins and Arp2/3 cooperate in FcεRI signaling. Formins play a key role in providing a stable framework and facilitating key cellular processes while Arp2/3 builds upon formin-mediated actin to stabilize the signaling cluster.

This work represents the first targeted study of Arp2/3 and formin activity in mast cells. Previous works have utilized actin polymerization inhibitors that function by preventing monomeric G-actin from polymerizing (Latrunculin) or capping the barbed end of f-actin to prevent further polymerization (Cyto D). This effect happens upstream of Arp2/3- or formin-catalyzed actin polymerization and so in a sense represents a global inhibition of all actin polymerizing systems. This work is the first step towards delineating the origins of the regulatory effects of different actin polymerizing enzymes in FcεRI signaling.

4.4 Future directions for patterned ligand features and actin polymerizing enzymes in FcεRI signaling

This work opens several new directions for projects. It is clear now that the effects observed by Cyto D treatment are obscuring the differential effects of Arp2/3 and formins in FcεRI. This is original scope of this project sought to address the question, "How does actin regulate FcεRI signaling?" by using patterned ligand features in combination with Cyto D treatments. Overtime, this question evolved into, "How do Arp2/3 and formins regulate FcεRI signaling?" with the use of CK666 and SMIFH2. The latter question directly provides an immediate area of investigation.

One major question brought about by this study is, "Is a formin recruited to the FcεRI signaling complex?". There is evidence in T cells that concentric actin rings in the TCR signaling cluster are mediated by the formin mDia1[19]. The immunological synapse formed by T cells is magnitudes larger than FcεRI nanoclusters, and this size and complex function likely necessitates a significant contribution from the actin cytoskeleton. Due to the similarities between TCR and FcεRI signaling, there is reason to suspect a role for mDia1 in FcεRI signaling. However, what this role is remains unclear. Thus, it would be enlightening to observe the recruitment of a fluorescent mDia1 construct to patterned features.

Another major question is, do formins and Arp2/3 aid in the recruitment of PLCγ? We have observed this using Cyto D[10], but now the question is: Does one or both systems aid in this recruitment? We posed this as a potential explanation for some of our observations and it is well within the bounds of our experimental setup to test this.

We used a low concentration of 10 μM CK666 in this study, but the literature often uses

up to 100 μM. Under these conditions, we saw some effects of CK666, but they were not as dramatic as we expected. This could simply reflect the biology of the system, or it could reflect the concentration of CK666 used. We initially used this concentration because we observed it was sufficient to block phalloidin recruitment. Near the end, we identified that 100 μM CK666 treatment could inhibit degranulation, so it is likely worthwhile to investigate the effects of stronger CK666 treatments on FcεRI signaling.

Methodologically, pharmacological inhibition with CK666 and SMIFH2 is similar to Cyto D treatments. The flexibility and ease of incorporating Cyto D treatments into experiments made it a powerful tool for study, and that same flexibility applies to CK666 and SMIFH2. Thus, much of the original exploratory work with Cyto D can be repeated with CK666 and SMIFH2 to attempt to delineate their roles in well-studied processes. For instance, these inhibitors could be combined with the classic Cyto D experiments performed Frigeri & Apgar[21] to assess potential roles for each inhibitor in signaling. They could also be used to study differences between surface and soluble presentations of antigens. With regards to Min Wu's work[9], it would be ideal to carry out a time course looking at 4G10 labeling from early in receptor activation to later on for comparison.

One direction we did not explore in this work was a definitive test comparing Cyto D treatment to simultaneous CK666 and SMIFH2 treatment. This would provide direct evidence to our assumption that Cyto D treatment mimics simultaneous inhibition of both systems. We considered this condition early on, but dismissed it for fear of risk of toxicity, but in hindsight this may be valuable information.

One of our hypotheses in this model is that Arp2/3 facilitates membrane protein and lipid diffusion to aid in the rapid assembly of functioning receptor complexes. Thus, fluorescent

correlation spectroscopy (FCS) methods could be paired with CK666 to investigate this role. Ideally, such an experiment would track the diffusion of membrane protein or lipid probes over patterned feature and compare diffusion rates in the presence or absence of CK666.

Lastly, this project did not fully explore the directions presented by Devin Wakefield, and I would refer you to his thesis for a clearer description of those directions. One of our great questions is "Functionally, why does Cyto D treatment enhance FcεRI activation?". We sought to investigate phosphorylated PLCγ (pPLCγ) on patterns in response to Cyto D treatment, to see if Cyto D enhanced the recruitment of pPLCγ to patterns. This would represent a potential mechanism by which we could justify observations like the enhancement of the Ca^{2+} response. However, we were unable to achieve strong, consistent labeling and thus abandoned this approach due to technical limitations. This question still remains though and connecting actin polymerization to functional readouts should remain a high priority going forward. It might also be worthwhile to determine whether the recruitment and phosphorylation of LAT requires Arp2/3 activity, as this would represent a strong readout of Arp2/3's role in the formation of the signaling complex.

REFERENCES

1. Bryant, K. L., Antonyak, M. A., Cerione, R. A., Baird, B. & Holowka, D. Mutations in the polybasic juxtamembrane sequence of both plasma membrane- and endoplasmic reticulum-localized epidermal growth factor receptors confer ligand-independent cell transformation. *J. Biol. Chem.* **288**, 34930–34942 (2013).
2. Wang, Z. *et al.* Mechanistic insights into the activation of oncogenic forms of EGF receptor. *Nat. Struct. Mol. Biol.* **18**, 1388–93 (2011).
3. Nevoltris, D. *et al.* Conformational Nanobodies Reveal Tethered Epidermal Growth Factor Receptor Involved in EGFR/ErbB2 Predimers. *ACS Nano* **9**, 1388–1399 (2015).
4. Gan, H. K., Kaye, A. H. & Luwor, R. B. The EGFRvIII variant in glioblastoma multiforme. *J. Clin. Neurosci.* **16**, 748–54 (2009).
5. Valley, C. C. *et al.* Enhanced dimerization drives ligand-independent activity of mutant EGFR in lung cancer. *Mol. Biol. Cell* **26**, (2015).
6. Dawson, J. P. *et al.* Epidermal Growth Factor Receptor Dimerization and Activation Require Ligand-Induced Conformational Changes in the Dimer Interface. *Mol. Cell. Biol.* **25**, 7734–7742 (2005).
7. Endres, N. F., Barros, T., Cantor, A. J. & Kuriyan, J. Emerging concepts in the regulation of the EGF receptor and other receptor tyrosine kinases. *Trends Biochem. Sci.* **39**, 437–446 (2014).
8. Orth, R. N., Wu, M., Holowka, D. A., Craighead, H. G. & Baird, B. A. Mast cell activation on patterned lipid bilayers of subcellular dimensions. *Langmuir* **19**, 1599–1605 (2003).
9. Wu, M., Holowka, D., Craighead, H. G. & Baird, B. Visualization of plasma membrane

compartmentalization with patterned lipid bilayers. *Proc. Natl. Acad. Sci.* **101**, 13798–13803 (2004).

10. Wakefield, D. L., Holowka, D. & Baird, B. The FcεRI signaling cascade and integrin trafficking converge at patterned ligand surfaces. *Mol. Biol. Cell* **28**, 3383–3396 (2017).
11. Su, X. *et al.* Phase separation of signaling molecules promotes T cell receptor signal transduction. *Science (80-.).* **352**, 595–599 (2016).
12. Holowka, D., Sheets, E. D. & Baird, B. Interactions between FcεRI and lipid raft components are regulated by the actin cytoskeleton. *J. Cell Sci.* **113 (Pt 6**, 1009–19 (2000).
13. Oka, T. *et al.* IgE alone-induced actin assembly modifies calcium signaling and degranulation in RBL-2H3 mast cells. *Am. J. Physiol. Cell Physiol.* **286**, C256–C263 (2004).
14. Pierini, L., Holowka, D. & Baird, B. FcεRI-mediated association of 6-μm beads with RBL-2H3 mast cells results in exclusion of signaling proteins from the forming phagosome and abrogation of normal downstream signaling. *J. Cell Biol.* **134**, 1427–1439 (1996).
15. Shelby, S. A., Veatch, S. L., Holowka, D. A. & Baird, B. A. Functional Nanoscale Coupling of Lyn Kinase with IgE-FcεRI is Restricted by the Actin Cytoskeleton in Early Antigen-Stimulated Signaling. *Mol. Biol. Cell* **27**, 3645–3658 (2016).
16. Goode, B. L. & Eck, M. J. Mechanism and Function of Formins in the Control of Actin Assembly. *Annu. Rev. Biochem.* **76**, 593–627 (2007).
17. Kumari, S. *et al.* Actin foci facilitate activation of the phospholipase C-γ in primary T lymphocytes via the WASP pathway. *Elife* **4**, 1–31 (2015).

18. Murugesan, S. *et al.* Formin-generated actomyosin arcs propel t cell receptor microcluster movement at the immune synapse. *J. Cell Biol.* **215**, 383–399 (2016).

19. Ditlev, J. A. *et al.* A composition-dependent molecular clutch between T cell signaling condensates and actin. *Elife* **8**, 1–44 (2019).

20. Ostrowski, P. P., Grinstein, S. & Freeman, S. A. Diffusion Barriers, Mechanical Forces, and the Biophysics of Phagocytosis. *Dev. Cell* **38**, 135–146 (2016).

21. Frigeri, L. & Apgar, J. R. The role of actin microfilaments in the down-regulation of the degranulation response in RBL-2H3 mast cells. *J. Immunol.* **162**, 2243–50 (1999).